

2012

Development and application of multi-functionalized mesoporous silica nanomaterials in intracellular drug delivery and heterogeneous catalysis

Chih-Hsiang Tsai
Iowa State University

Follow this and additional works at: <https://lib.dr.iastate.edu/etd>

 Part of the [Chemistry Commons](#), and the [Materials Science and Engineering Commons](#)

Recommended Citation

Tsai, Chih-Hsiang, "Development and application of multi-functionalized mesoporous silica nanomaterials in intracellular drug delivery and heterogeneous catalysis" (2012). *Graduate Theses and Dissertations*. 12255.
<https://lib.dr.iastate.edu/etd/12255>

This Dissertation is brought to you for free and open access by the Iowa State University Capstones, Theses and Dissertations at Iowa State University Digital Repository. It has been accepted for inclusion in Graduate Theses and Dissertations by an authorized administrator of Iowa State University Digital Repository. For more information, please contact digirep@iastate.edu.

**Development and application of multi-functionalized mesoporous
silica nanomaterials in intracellular drug delivery and
heterogeneous catalysis**

by

Chih-Hsiang Tsai

A dissertation submitted to the graduate faculty

in partial fulfillment of the requirements for the degree of

DOCTOR OF PHILOSOPHY

Major: Chemistry

Program of Study Committee:

Brian G. Trewyn, Co-Major Professor

Aaron D. Sadow, Co-Major Professor

Marek Pruski

George Kraus

Scott Chumbley

Iowa State University

Ames, Iowa

2012

Copyright © Chih-Hsiang Tsai, 2012. All rights reserved.

TABLE OF CONTENTS

ACKNOWLEDGEMENTS	iv
ABSTRACT	vi
CHAPTER 1. GENERAL INTRODUCTION	1
Dissertation Organization.....	1
Introduction	2
1.1 The evolution of porous materials.....	2
1.2 Synthesis of mesoporous silica materials.....	9
1.3 Functionalization of mesoporous silica materials	14
1.4 Control of particle morphology of mesoporous silica materials (size, shape).....	18
1.5 Recent advance of functionalized mesoporous silica materials	21
a). Applications of MSN materials in drug delivery system	21
b). Applications of MSN materials in heterogeneous catalysis.....	27
Summary	44
Reference.....	44
CHAPTER 2. SURFACTANT-ASSISTED CONTROLLED RELEASE OF HYDROPHOBIC DRUGS USING ANIONIC SURFACTANT TEMPLATED MESOPOROUS SILICA NANOPARTICLES	60
Abstract	60
1. Introduction	61
2. Materials and Methods	64
3. Results and Discussion.....	72
4. Conclusions	95
Acknowledgments.....	96
Reference.....	96
Supporting Information.....	102

CHAPTER 3. RATIONAL CATALYST DESIGN: A MULTIFUNCTIONAL MESOPOROUS SILICA CATALYST FOR SHIFTING THE EQUILIBRIUM REACTION BY REMOVAL OF BYPRODUCT	106
Abstract	106
1. Introduction	107
2. Materials and Methods	110
3. Results and Discussion.....	119
4. Conclusions	127
Acknowledgments	127
Reference.....	128
Supporting Information.....	131
CHAPTER 4. AEROBIC OXIDATIVE ESTERIFICATION OF PRIMARY ALCOHOLS OVER Pd-Au BIMETALLIC CATALYSTS SUPPORTED ON MESOPOROUS SILICA NANOPARTICLES	132
Abstract	132
1. Introduction	133
2. Materials and Methods	136
3. Results and Discussion.....	140
4. Conclusions	151
Acknowledgments.....	152
Reference.....	152
Supporting Information.....	158
CHAPTER 5. GENERAL CONCLUSION	162

ACKNOWLEDGEMENTS

First and foremost, I would like to express my wholehearted appreciation to Prof. Victor Shang-Yi Lin for inspiring me with his wisdom and enthusiasm in chemistry. As a mentor, he showed me how important creativity is, and how to make imagination possible with hard work. His big smile is always encouraging and I will always have that image in mind.

I would like to thank my major professor Dr. Brian Trewyn for his guidance and valuable discussion on my research projects and thesis.

To my co-major professor Dr. Aaron Sadow and my POS committee members, Dr. George Kraus, Dr. Marek Pruski and Dr. Scott Chumbley, I deeply appreciate their valuable time and support.

Also I would like to thank my past and current group members, especially Dr. Tommy Hung-Ting Chen, Dr. Wei Huang, Dr. Juan L. Vivero-Escoto and Dr. Kevin Chia-Wen Wu. It is really nice to work with them and brainstorm together.

My great acknowledgement is given to the Department of Chemistry, Iowa State University for providing a good environment for research.

To my long-time lunch partner and dear roommate Isaac Hong-An Ho, thank you very much for your trash talk during our lunch time. It did fresh my thoughts at most of frustrating days.

Finally, I am deeply grateful to my family, especially my wife Irene Hsiu-Chen Fu, for fully supporting me in all aspects during these years in Ames.

CHAPTER 1. GENERAL INTRODUCTION

Dissertation Organization

This dissertation is composed of five chapters. Chapter 1 is a comprehensive review article focusing on the development of mesoporous silica materials. Topics related to material synthesis, functionalization method, characterization, and applications on both drug delivery system and heterogeneous catalysis are discussed. Recent development of mesoporous silica nanomaterials (MSNs) is also included. Chapters 2 to 4 are journal articles, in which Chapter 2 and 3 have already been published and Chapter 4 is a manuscript ready for submission. Chapter 5 is a general conclusion summarizing the significance of the research done in this dissertation.

Chapter 2 highlights a newly developed surfactant-assistant strategy for hydrophobic drug delivery based on MSNs as the delivery platform. This delivery system was demonstrated efficient for intracellular delivery of resveratrol into human cells. In addition, it also shows great potential on the application of Ca^{2+} -responsive controlled release system. Chapter 3 depicts a rational design of bifunctionalized MSN catalyst for esterification reactions. The incorporated secondary pentafluorophenyl (PFP) groups provide strong hydrophobicity which efficiently expels produced water out of mesochannels, pushing the equilibrium reaction to completion. The synthesis and application of novel bimetallic Pd-Au@MSN catalysts for aerobic oxidative esterification is reported in Chapter 4. A sequential impregnation method is demonstrated to be very efficient on the synthesis of metal nanoparticle supported on MSNs with highly homogenous distribution. Finally in Chapter 5,

the significance and future prospect of the research done in this dissertation is discussed as a general conclusion.

Introduction

Porous materials are of scientific and industrial interest due to their ability to interact with ions and molecules not only at their surfaces, but throughout the bulk of the material. Traditionally, porous materials were applied to fields involving ion-exchange, adsorption, separation and catalysis, and many of them benefit from the large surface area and pore volume.^{1,2} According to the definition from International Union of Pure and Applied Chemistry (IUPAC), the porous materials have been classified as three categories: pore sizes below 2 nm are called micropores, those in between 2 nm to 50 nm are mesopores, and those above 50 nm are macropores. In this dissertation, I will mainly concentrate on the development and applications of mesoporous silica materials.

1.1 The evolution of porous materials

The first porous material was discovered by a Swedish mineralogist Axel F. Cronstedt in 1756, who observed that a large amount of water steam were produced once the material “stilbite” was rapidly heated.^{3,4} He then concluded the water molecules were originally absorbed in the “micropores” of stilbite, and later, he termed this material as “Zeolite”. Up to the 1940s, a group of scientists led by Dr. Richard M. Barrer successfully synthesized the

first artificial aluminosilicate zeolite via a hydrothermal condition, in which they mimicked the natural environment of the growth of zeolite.⁵⁻⁷ As of now, there are more than 190 unique zeolite frameworks have been identified and over two-third of them are man-made, according to the *Database of Zeolite Structures*. Due to their high degree of crystallinity and uniform size of micropores, zeolite materials provide superior properties on the fields of adsorption, separation, ion-exchange and catalysis.^{1,2,8-10} For example, in petrochemical industry synthetic zeolites, such as HY, are widely used as catalysts for catalytic cracking reactions. Zeolites confine molecules in the micropores, providing a high density of solid-state acid sites which can facilitate a host of acid-catalyzed reactions.¹¹ In addition, most of zeolites are thermally stable up to 800 °C as a result of their crystalline structure.¹²

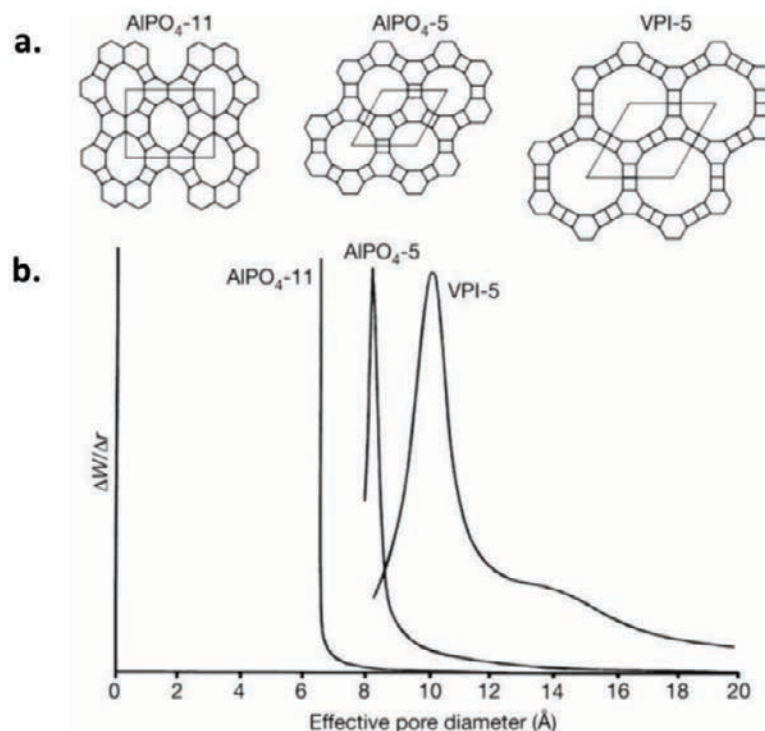


Figure 1-1 Pore characteristics in the aluminophosphates AlPO₄-11, AlPO₄-5, and VPI-5. **a**, Rhomboids indicate the unit cell. **b**, measured pore sizes by argon adsorption technique.¹

Despite the above-mentioned merits, the applications of zeolite materials are often restricted by their small pore size. The demands on the development of porous materials with larger pores were eagerly increased since the 1980s. In 1988, Mark E. Davis *et al.* first reported an aluminophosphate type of zeolite, VPI-5, with uniform pores larger than 10 Å, opening up the area of extra-large porous crystalline materials.¹³ (Figure 1-1) Since then, many attempts to synthesize larger pore zeolites have achieved great success on the basis of the aluminophosphate frameworks (AlPO_{4-n}).¹⁴⁻¹⁶ Very recently, researchers in Spain and Sweden have successfully synthesized a germanosilicate (Ge_xSi_yO_z(OH)_n) zeolite ITQ-37 with crystalline pores as large as 2 nm, which is reportedly the largest pore of crystalline materials at present.¹⁷ The emergence of the extra-large microporous materials has led to a rapid development in the areas of heterogeneous catalysis involving bigger molecules, host-guest chemistry and material science.

Meanwhile, the development of another class of porous materials, which is now known to be mesoporous silica material, was underway. The first successful attempt to synthesize this type of materials has appeared as early as 1971, where a material described as low-bulk density silica was obtained from hydrolyzing and condensing tetraethoxy silicate (TEOS) in the presence of cationic surfactants.¹⁸ This result did not gain much attention at the time it was published because the porosity and structural properties were not reported. However, a reproduced experiment suggested that it may have yielded ordered mesoporous silica materials.¹⁹ It was not until 1992 that the chemistry society started to realize the potential of this field, when scientists in oil giant Mobil Corporation laboratories published a series of ordered mesoporous materials (M41S) with pore sizes ranging from 1.5-10 nm.^{20,21} These

silica materials were synthesized via a liquid-crystal template mechanism under basic aqueous solution, and later denoted as MCM-41 (hexagonal), MCM-48 (cubic) and MCM-50 (lamellar) according to their mesopore arrangements. (Figure 1-2) Among them, MCM-41 type

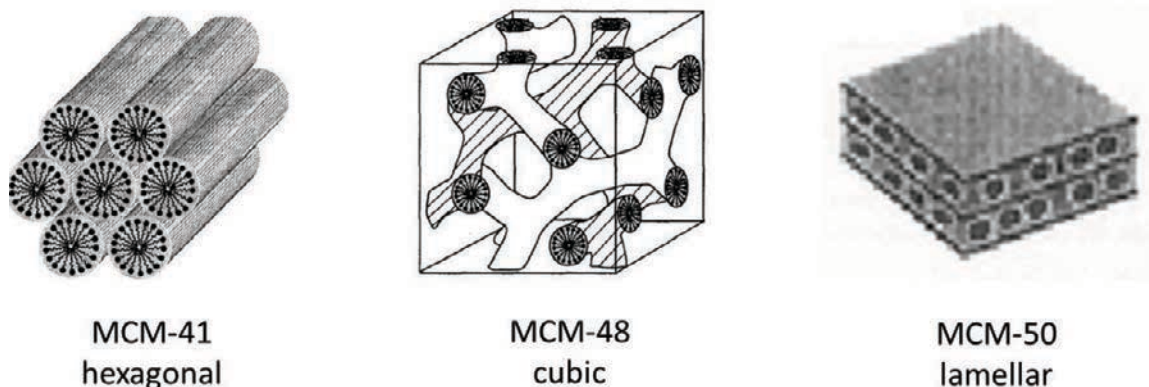


Figure 1-2 Representation of mesostructure of M41S materials.

material, featuring highly ordered 2d-hexagonal porous structure with BET (Brunauer-Emmett-Teller) surface area exceeding $1000 \text{ m}^2 \text{ g}^{-1}$ and pore volumes up to $1 \text{ cm}^3 \text{ g}^{-1}$, has been comprehensively studied and widely applied to many fields such as drug delivery, biosensors and catalysis.²²⁻³¹

In 1998, G. D. Stucky and co-workers successfully synthesized SBA-type (Santa Barbara Amorphous-type) materials, best known for SBA-15, using a triblock co-polymer as the structure-directing agent (SDA) instead of commonly used cationic tetraalkylamine surfactant under acidic condition.^{32,33} The characteristic results showed that this type of material had ordered hexagonal pores with pore sizes over 15 nm in average. In addition, its wall-thickness is around 4-6 nm, around two to three times thicker than that of MCM-41

Table 1-1 Structural diversity of the most common mesoporous silica materials.³⁴

Name	Possible SDA	Type of interaction	Structure	Pore size (nm)
MCM-41	$C_n(CH_3)_3$ N ⁺ Br ⁻ or Cl ⁻ ($8 \leq n \leq 20$)	S^+I^-	2-D hexagonal (<i>p6mm</i>)	1.5-10
MCM-48	$C_n(CH_3)_3$ N ⁺ Br ⁻ or Cl ⁻ ($12 \leq n \leq 20$)	S^+I^-	3-D cubic (<i>Ia3d</i>)	1.5-4.6
SBA-1	$C_n(C_2H_5)_3$ N ⁺ Br ⁻ or Cl ⁻ ($12 \leq n \leq 18$)	$S^+X^-I^+$	3-D cubic (<i>Pm3n</i>)	1.5-3.0
SBA-3	$C_n(CH_3)_3$ N ⁺ Br ⁻ or Cl ⁻ ($12 \leq n \leq 18$)	$S^+X^-I^+$	2-D hexagonal (<i>p6mm</i>)	1.5-3.5
SBA-12	Brij 76 C ₁₈ EO ₁₀	S^0I^0	3-D hexagonal (<i>intergrowth</i>)	3.0-5.0
SBA-15	P123 EO ₂₀ PO ₇₀ EO ₂₀	(N ⁰ H ⁺) (X ⁻ I ⁺)	2-D hexagonal (<i>p6mm</i>)	4.0-15
SBA-16	F127 EO ₁₀₆ PO ₇₀ EO ₁₀₆	(N ⁰ H ⁺) (X ⁻ I ⁺)	3-D cage-like cubic (<i>Im3m</i>)	4.7-12
KIT-1	C ₁₆ (CH ₃) ₃ N ⁺ Cl ⁻	S+I ⁻	Disordered	3.4
KIT-6	Blend of P123 and butanol	(N ⁰ H ⁺) (X ⁻ I ⁺)	3-D cubic (<i>Ia3d</i>)	4.0-11.5
FDU-1	B50-6600 EO ₃₉ BO ₄₇ EO ₃₉	(N ⁰ H ⁺) (X ⁻ I ⁺)	3-D cage-like cubic (<i>Fm3m</i>)	8.0-14
FDU-12	F127 and trimethylbenzene (TMB)	(N ⁰ H ⁺) (X ⁻ I ⁺)	3-D cage-like cubic (<i>Fm3m</i>)	6.0-12.5
MCF	Blend of P123 and TMB	(N ⁰ H ⁺) (X ⁻ I ⁺)	Disordered	20-42
MSU-X	Tergitol 15-S- <i>n</i> C ₁₁₋₁₅ EO _{<i>n</i>} $7 \leq n \leq 30$ Triton X-100, X-114 P64 EO ₁₃ PO ₃₀ EO ₁₃	N ⁰ I ⁰	Disordered	2.0-5.8
MSU-H	P123 EO ₂₀ PO ₇₀ EO ₂₀	N ⁰ I ⁰	2-D hexagonal (<i>p6mm</i>)	7.5-12
HMS	Alkylamines (C8-C18)	S ⁰ I ⁰	Disordered	2.3-4.0

material, indicating that SBA-15 type material may have better thermal and hydrothermal stability. Unlike the 2d-hexagonal pore arrangement shown in MCM-41 type material, SBA-15 has numerous micropores interconnecting the mesopores, making this material suitable for serving as templates in nanocasting applications.³⁴ Based on the similar concept of soft-templating method, tremendous efforts have been made to develop other types of mesoporous silica materials by varying factors like reaction condition, types of surfactant, silica precursor, and even additives.³⁴⁻³⁷ Table 1-1 lists the structural diversity of the most common mesoporous silica materials prepared using cationic or non-ionic surfactants as the SDA.

Another class of mesoporous silica materials is AMS-*n* series (Anionic surfactant-templated Mesoporous Silica) developed by Che *et al.* using anionic surfactant in combination with organosilane groups as co-structure-directing agent (CSDA).³⁸⁻⁴¹ As depicted in Figure 1-3, the negatively charged carboxylic head groups of the anionic surfactant interact electrostatically with positively charged amine or ammonium groups of 3-aminopropyltrimethoxysilane (APS) or *N*-trimethoxysilylpropyl-*N,N,N*-trimethylammonium chloride (TMAPS). Subsequently, the organosilane co-condenses with the TEOS to form the silica framework. High-resolution transmission electron microscopy (HRTEM) and powder X-ray diffraction studies of this type of materials have revealed structural diversity as a function of reaction condition and the type of surfactants.⁴¹ One feature of the AMS material is that a great amount of amine groups are accessible inside the pores, which provides an alternative method for functionalizing mesoporous silica materials.⁴² We followed similar approach by using our home-made bio-compatible phosphate monoester (PME) surfactant as the structure direction agent (SDA) along with 3-aminopropyltrimethoxysilane (APS) as the

CSDA to synthesize a series of materials (PME-MSNs).⁴³ By varying the ratio of SDA and CSDA, we can tune the particle morphology from isolated spheres to aggregated tubules, and the meso-structure from wormholes to radially-aligned pores. More details and application of PME-MSNs are included in Chapter 2.

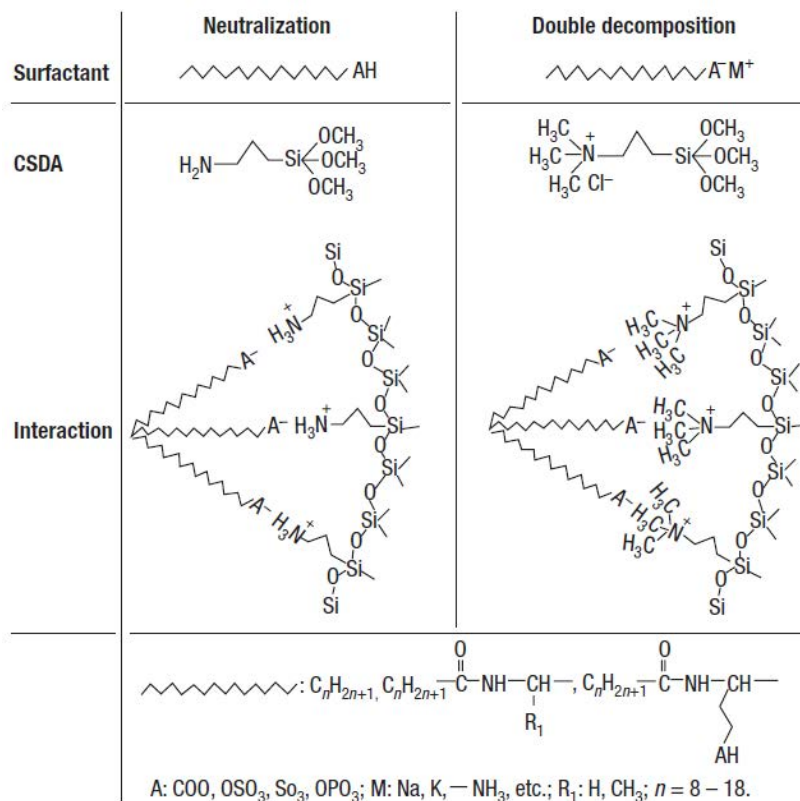


Figure 1-3 Schematic representation of the two types of interactions between amino groups and anionic surfactant head groups.³⁸

In contrast to crystalline zeolite, ordered mesoporous materials are structurally amorphous, suggesting a disordered wall structure.⁴⁴ This implies that well-ordered mesoporous material can be prepared using element combinations found in its analogues like aerogels, xerogels, organic-inorganic hybrid materials and even metals or alloys. Many of these hybrid materials have been well developed including periodic mesoporous organosilica

(PMOs),⁴⁵⁻⁴⁷ mesoporous metal oxide,^{48,49} metal-doped MCM-41²³ and so forth. Although the amorphous wall structure may limit the industrial application of ordered mesoporous material due to relatively low thermal stability,^{1,8} their special physicochemical properties such as much-larger pore size, pore volume, surface area and abundant silanol groups provide more opportunities for other applications. More details about synthesis, characterizations and applications of ordered mesoporous silica materials will be discussed in the following sections.

1.2 Synthesis of mesoporous silica materials

Kresge and co-workers proposed a “liquid-crystal templating (LCT)” mechanism for the formation of mesostructure in their original 1992 paper.²¹ As shown in Figure 1-4, in this hypothesis, the structure of silica-framework was pre-determined by the organization of surfactant molecules, which self-assemble to form a LC phase in aqueous solution (*pathway a*). The silicate species then occupy the void space between the hexagonally aligned lyotropic crystal phases and condense on the top of micellar rods.

Since the micelle solution is very sensitive to the characteristics of the solution, they also suggested that the addition of silicate precursors could possibly assist the ordering of the surfactants into specific mesophases (*pathway b*).^{21,50} Further investigation revealed that MCM-41 can form at concentrations where only spherical micelles are present (1 wt%), which strongly supported the cooperative pathway b. Monnier *et al.* proposed a “charge density matching” model which includes three steps involving in the cooperative pathway.⁵¹

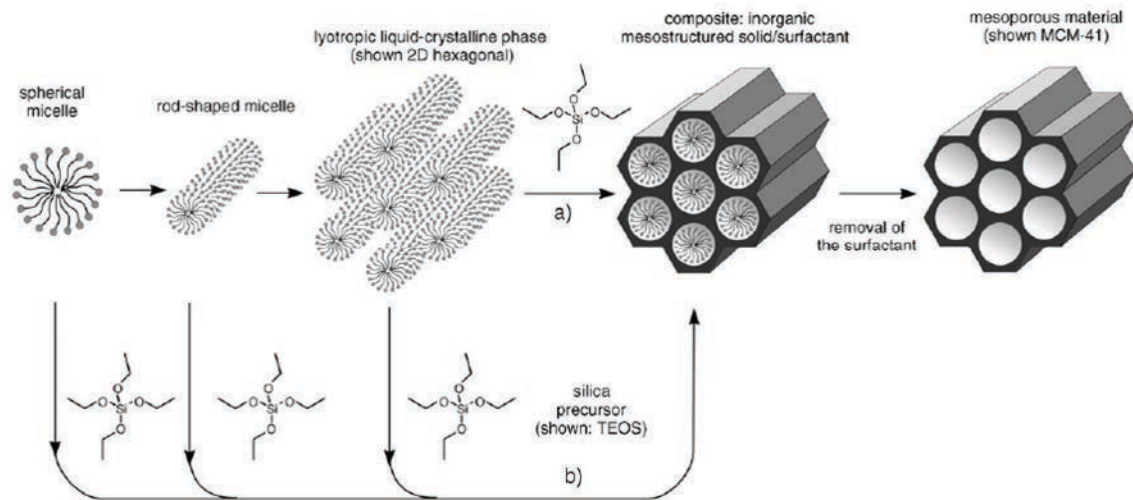


Figure 1-4 Formation of mesoporous materials by structure-directing agent: a). true liquid-crystal template mechanism, b). cooperative liquid-crystal template mechanism.

- a. Multidentate binding of the silicate poly-ions to the cationic head groups through electrostatic interactions leading to a surfactant-silica interface
- b. Preferential silicate polymerization in the interface region
- c. Subsequent charge density matching between the surfactant and the silicate

At the first stage, the surfactant molecules are in dynamic equilibrium between self-assembled micelles and independent molecules. The addition of silicate species would displace the negatively charged counter ions (Br^- or Cl^-) of surfactants to form organic-inorganic composite micelles. The third step is the polymerization of silicate species to yield inorganic framework. This hypothesis can also be rationalized by using the surfactant packing parameter g value:^{52,53}

$$g = \frac{V}{a_0 lc}$$

Where V is the total volume of the hydrophobic chains, a_0 is the effective head group area, and l_c is the critical length of the hydrophobic tail. As shown in Table 1-2, the g value can be used to estimate the structure of micelles, depending on the molecular geometry of surfactant and the size and charge of the polar head group. Additionally, pH, ionic strength and temperature can be included in the parameters of V , a_0 , and l_c . According to this equation, one can expect that spherical aggregates would be favored with surfactant molecules bearing larger head groups. On the other hand, bi-continuous cubic or lamellar structure would be formed if the hydrophobic chains of surfactants are branched. It is noted that the factor a_0 represents the effective head group area of surfactants, which is strongly dependent on the degree of dissociation of the head groups, ionic strength and other factors, which could potentially influence the characteristics of the solution. This implies that during the synthesis of mesoporous silica material the addition of silica species would largely affect a_0 due to the charge matching. In addition, the pH value, concentration, temperature and even stirring rate of the reaction solution are factors of the degree of hydrolysis of silica precursor (different degree of multidentate charge-matching with surfactants), resulting in a structural diversity of mesoporous silica materials despite using the same reactants.

Huo *et al.* summarized a generalized cooperative formation mechanism on the basis of the specific electrostatic interactions between an inorganic species (I) and a surfactant head group (S).^{48,55} As depicted in Figure 1-5, the organic-inorganic interaction are built by electrostatic force in the case of ionic surfactants as SDA (route a-d); on the other hand, hydrogen bonding ties surfactant molecules and silica precursors together while nonionic surfactants are used as templates (route e-f). It is noted that an auxiliary element is essential

Table 1-2 Surfactant packing parameter g and predicted mesophases.⁵⁴

g value	Expected structure	Representative examples
<1/3	Hexagonal (hcp)	SBA-2
1/3	Bicontinuous	SBA-1
1/2	Hexagonal	MCM-41, FSM-16
1/2-2/3	Bicontinuous	MCM-48
1	Lamellar	MCM-50

in some cases. For instance, a metal cation is needed to be added to the synthetic solution when anionic surfactant is the SDA (route c). Our group has used this S⁻M⁺T pathway to develop a mesoporous silica-supported Uranyl (UO₂²⁺) catalyst for photo-oxidation of alcohol,⁵⁶ in which sodium dodecyl sulfate (SDS) was used as the surfactant and uranyl nitrate hexahydrate was added as the metal cation. Despite the fact that this material did not show a high order of mesoporosity, the nitrogen sorption result (588 m² g⁻¹) and XRD pattern proved its mesoporous structure. Also, the earlier-mentioned SDA-CSDA templating method for the synthesis of anionic-templated mesoporous silica (AMS) is designed based on the same concept described here.

Another plausible mechanism called “aggregate-growth” was introduced by Rankin and co-workers in 2004 when they were studying an unique mesoporous silica nanoparticle with

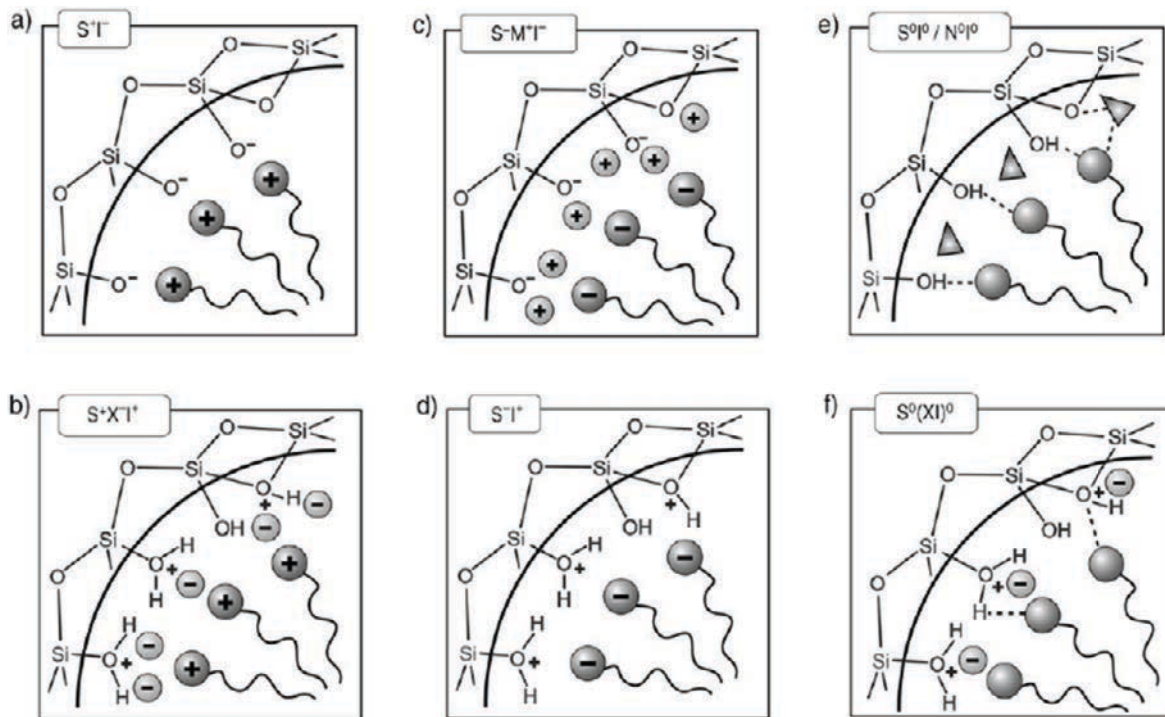


Figure 1-5 Interactions between the inorganic species and the head group of the surfactant with consideration of the possible synthetic pathway.³⁶

radially-aligned porous structure (Figure 1-6a).⁵⁷ In this hypothesis, they suggested that the mesophase is not determined only by the self-assembled structure of surfactants, but thermodynamically controlled by the rearrangement of the “micelle-silica” composite. As shown in Figure 1-6b, when silicon species condense with surfactant micelles, small “micelle-silica” nuclei will form at the initial stage. These nuclei then aggregate into larger composite materials, which are soft and unordered due to the incomplete condensation of silica. Subsequently, a re-alignment process occurs inside the nanoparticles, and the mesostructure is controlled by the thermodynamic stability of the material under the reaction conditions. They examined samples collected from different reaction times through the course of the reaction under TEM, and observed a clear transition from disordered clusters to larger nanoparticles with radially-aligned mesopores. Our PME-MSN (phosphate monoester-

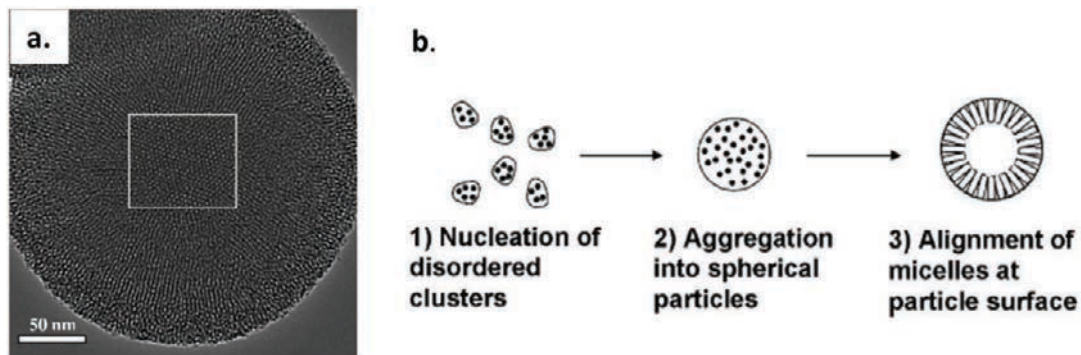


Figure 1-6 a. TEM images of mesoporous silica with radially-aligned mesopores prepared by Rakin *et al.* **b.** Schematic representation of “aggregate-growth” model.⁵⁷

templated mesoporous silica nanoparticle) materials also featured the similar radial-like mesophase.⁴³ We found that the radially-aligned mesostructure exists not only in spherical nanoparticles but also in tubular-shape nanoparticles and other aggregates. Additionally, we also observed a clear phase-transition when studying variations in CSDA to PME ratios. Indeed, our results strongly supported the “aggregate-growth” model. Similar mesostructural transitions have also been reported elsewhere.⁵⁸⁻⁶³ More discussion would be included in Chapter 2.

1.3 Functionalization of mesoporous silica materials

As previously mentioned, there are abundant silanol groups ($\equiv\text{Si-OH}$) on the surface of mesoporous silica materials owing to its amorphous wall structure. With these reactive silanol groups, one can effectively immobilize organic functional groups onto a silica surface through either covalent bonding or hydrogen bonding. In general, functionalization through covalent bonding is favored in most of applications. Hydrogen bonding pathway, although facile, usually results in undesired leaching problems due to weak interaction.⁸

The large surface area of mesoporous materials can be split into two categories: external surface and internal surface. Approximately 90% of all surface silanol groups are on the internal surface of the mesopores. This suggests that by carefully choosing the functionalization approach, ideally, we can effectively and selectively functionalize the mesoporous silica material with different functional groups.⁶⁴⁻⁶⁶ There are two common methods for functionalization of mesoporous silica materials with organosilanes. 1) postsynthetic functionalization of silicas (also refers to grafting method); 2) direct synthesis method. Both methods have advantages and disadvantages and will be discussed as follows:

1). Grafting Method

This process is carried out primarily by reaction of organosilanes such as $(R'O)_3SiR$, $ClSiR_3$ or silanzanes $HN(SiR_3)_3$, with the silanol groups ($\equiv Si-OH$) on the material surface. As shown in Figure 1-7, a variety of functional groups can be easily immobilized onto the silica surface as long as the organosilanes can diffuse into the mesopores. The advantage of this method is that the mesostructure of the starting silica material is usually retained under the synthetic condition, although the pore size might be reduced to a certain degree depending on the size of the R group and the degree of occupation.^{36,65}

However, the major drawback of this modification method is that, the organosilanes would preferentially react at the pore opening and on the external surface during the initial stage of the synthetic process, which impairs the diffusion of further molecules deeply into the center of pores, leading to a nonhomogeneous distribution of the organic functional groups.³⁶ Furthermore, in the cases of bulky R groups used or higher concentration of

organosilanes, mesopores might be occasionally blocked and result in poor accessibility of functional groups.

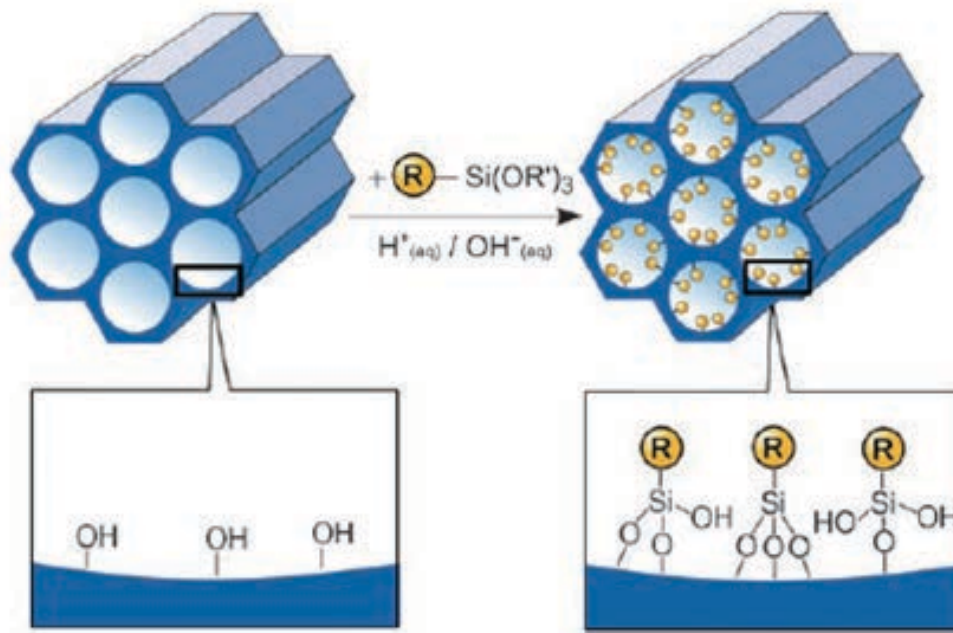


Figure 1-7 Grafting method for organic modification of mesoporous silica material with $(R'O)_3SiR$. R= organic functional group.³⁶

2). Co-condensation method

As depicted in Figure 1-8, the co-condensation method provides an alternative route to synthesize organically functionalized mesoporous silica in a one-pot synthesis.^{36,64-66} When an organosilane $(R'O)_3SiR$ is added along with TEOS into the reaction solution they co-condense to form the silica framework, and the organic residues are covalently anchored to the pore wall. Since the organic functionalities (R) are usually hydrophobic they tend to intercalate into the hydrophobic region of surfactant micelles, causing the incorporated organic functionalities to project into the pores.⁶⁷ In addition, because the organic groups are

direct components of the silica framework pore blocking is not an issue in this method. Moreover, it is believed that this functionalization method provides more homogeneous distribution of organic units over the grafting method.^{36,65} Despite these merits, this direct-synthesis method also has some disadvantages. First, the addition of organosilanes may dramatically change the characteristic of the reaction solution, which might result in a change of mesoscopic order of the resulting product, and often times ending up with disordered or non-porous material. This situation may be worse as

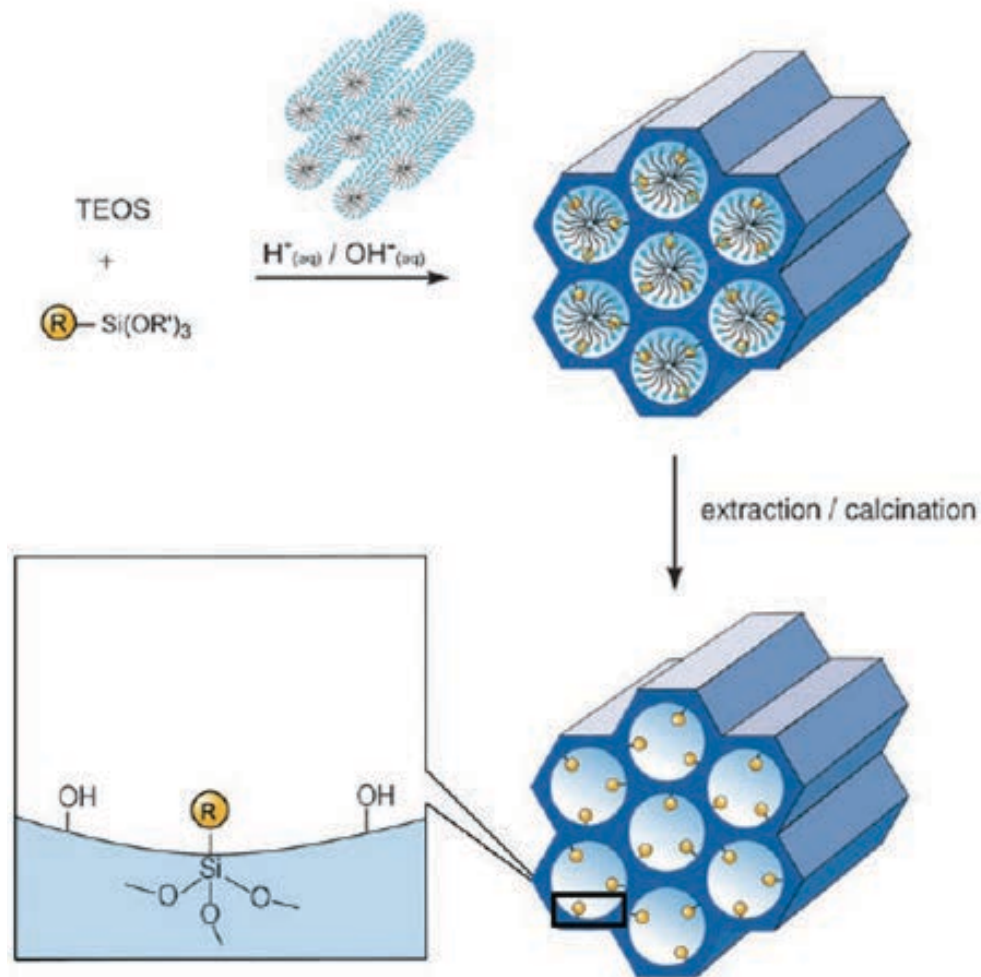


Figure 1-8 Schematic representation of co-condensation (one-pot synthesis) method.³⁶

the concentration of organosilane has increased. Second, a phase separation problem may occur if the organosilane is poorly soluble in the surfactant solution, or if its hydrolysis or condensation rates differ greatly from that of TEOS. Furthermore, it has been reported that some of organic functional groups introduced via the co-condensation method may not be accessible due to the fact that they are embedded inside the silica matrix.⁶⁸ Moreover, the stability of organic functionalities in either acidic or basic aqueous media needs to be carefully considered. This would also limit the options of functionalities which can be applied to mesoporous silica materials.

1.4 Control of particle morphology of mesoporous silica materials (size, shape)

One of major applications of mesoporous silica materials lies in the biological applications such as drug delivery systems, imaging reagents and bio-sensors.^{26,28,29} Particle size and shape are highly related to the biocompatibility and cellular uptake behavior of mesoporous silica materials.⁶⁹⁻⁷² For example, smaller spherical nanoparticles were found to be more biocompatible than larger amorphous bulk materials. Different shapes of nanoparticles have also demonstrated different endocytosis kinetics.⁷¹ In addition, mesoporous silica nanoparticles (MSNs) within the size domain of 100-200 nm tend to accumulate in tumor tissues much more readily than in normal tissues due to the enhanced permeability and retention (EPR) effect of macromolecules.⁷³ Therefore, it is crucial for the application of mesoporous silica materials to control the particle morphology. Different

methods have been developed by our group and others.^{67,69,74-90} For instance, K. Unger and co-workers first reported the synthesis of micrometer- and submicrometer-sized (400-1100 nm) MCM-41 type mesoporous silica nanoparticles (MSNs) by using a modified Stöber process,^{75,76} in which a significant amount of ethanol was added into the reaction mixture as the controlling reagent. Cai *et al.* synthesized a MCM-41 type MSNs with relatively uniform size around 110 nm by simply diluting the reaction concentration.⁸⁶ By changing the base from sodium hydroxide to aqueous ammonia, they also obtained a submicrometer-sized mesoporous silica rod with 0.3-0.6 μm in diameter and 1 μm in length.

Our group has also developed a co-condensation method for controlling the particle morphology of MSNs.⁶⁷ The MSN materials can be obtained with different sizes and shapes ranging from spherical, twisted columns, rods, tubular particles by properly choosing the added organosilanes. We concluded that the change of particle morphology was a result of the difference in the hydrophilicity/hydrophobicity of the organosilane precursors. It is interesting to note that by fine tuning the concentration of added organosilanes or using mixed silanes, particle morphology can also be well controlled. All materials obtained from this method showed high surface areas ($> 600 \text{ m}^2 \text{ g}^{-1}$), narrow pore size distribution (2.0-2.9 nm), and large pore volume (up to $0.78 \text{ cm}^3 \text{ g}^{-1}$), despite the fact that the mesostructure of some of materials were not ordered. Another strategy developed by our group to synthesize MSNs with morphology control was the use of room-temperature ionic liquids (RTILs) as the structure directing agent (SDA).⁷⁴ A series of RTIL-MSN materials with various particle morphologies, such as spheres, ellipsoids, rods, and tubes, was synthesized with different RTILs. One of RTILs-MSN materials bears a rotational Moiré type of helical mesostructure

which is similar to an AMS material reported by Tatsumi *et al* previously,³⁹ but surprisingly, where they used a chiral amino-acid surfactant as the SDA, and in our case was the non-chiral RTILs.

Garcia-Bennett and co-workers developed an interesting approach to synthesize insolated AMS (anionic surfactant-templated mesoporous silica) nanoparticles.⁸⁷ They introduced a small amount of tri-block copolymer surfactant P123 into the synthetic solution, as a function of dispersing reagents. Above its cloud point (80 °C for P123), the tri-block copolymer was not able to form micelles so that its interaction with silicate species is not expected. The dispersed polymer molecules compartment the nucleation sites and therefore limit the diffusion of silicate oligomers through the synthesis gel. In principle, this strategy is similar to the aforementioned dilution method and Stöber process. The particle morphology is kinetically maneuvered by reducing the probability of nuclei aggregation. We have attempted to apply this strategy to tune the particle size of our PME-MSNs but without success. This might be due to the differences in surfactant structure, as well as the formation mechanism.

SBA-15 type materials have much larger pore size and been considered better candidates for enzyme and protein delivery carriers. However, reports on the particle morphology control of this type of materials are limited.^{68,81,88-90} Zhao *et al.* successfully synthesized a well-dispersed rod-like SBA-15 type material with 1-2 μm in length and 300-500 nm in diameter, by adding a considerable amount of inorganic salts as additives.⁸¹ This material showed high capacity for enzyme immobilization; however, there was no cytotoxicity or other biological applications reported in this study. Another example has been published by a Swedish and English research team led by Prof. V. Alfredsson.⁸⁸ They used triblock

copolymer P104 (EO₆₁PO₂₇EO₆₁) instead of regular P123 (EO₂₀PO₇₀EO₂₀) for the synthesis of SBA-15 type material. By fine-tuning the reaction temperature, the tablet-shaped mesoporous nanoparticles were obtained at 55 °C-60 °C. Interestingly, the particle morphology of the resulting products were very sensitive to the reaction temperature, when synthesized below or above the optimal range of 55 °C-60 °C, the obtained product appeared to be fused particles. Following their strategy, our group has also developed a co-condensation method to synthesize functionalized SBA-15 type mesoporous nanoparticles,⁶⁸ in which we have successfully functionalized the material with four different groups (amino-, aldehyde, cyclopentadiene and mercapto-) by fine-tuning the reaction parameters including concentration, aging temperature and pre-hydrolysis time.

1.5 Recent advancements of functionalized mesoporous silica materials

a). Applications of MSN materials in drug delivery system

As outlined in the previous sections, mesoporous silica nanoparticles (MSNs) have been applied to many areas of interest due to their particular physicochemical properties. For biomedicine applications, MSN materials have demonstrated *in vitro* and *in vivo* biocompatibility.^{91,92} With the separate internal and external surface areas, MSNs have demonstrated potential as drug-delivery and bio-imaging vehicles.^{26,27,29} As shown in Figure 1-9, the outer surface of a pristine MSN can be functionalized first with ligand-receptors for the purpose of targeting specific cell types. Subsequently, biogenetic molecules, like anticancer drugs or imaging reagents, can be loaded into the spacious mesoporous channels

by simple diffusion. To prevent the loaded molecules from premature release, a blocking agent, such as an inorganic nanoparticle or organic macromolecule “gate-keeper”, can be utilized to cap the mesopores. Upon reaching the desired location and time, the cap can be manually released via chemical, heat, light, magnetic field, or pH stimuli. On the basis of this concept, many clever designs using MSN materials as an intracellular drug delivery platform have been developed by our group and others in the past decade.^{69,70,92-113} Herein, I will mainly focus on the drug delivery application of MSNs.

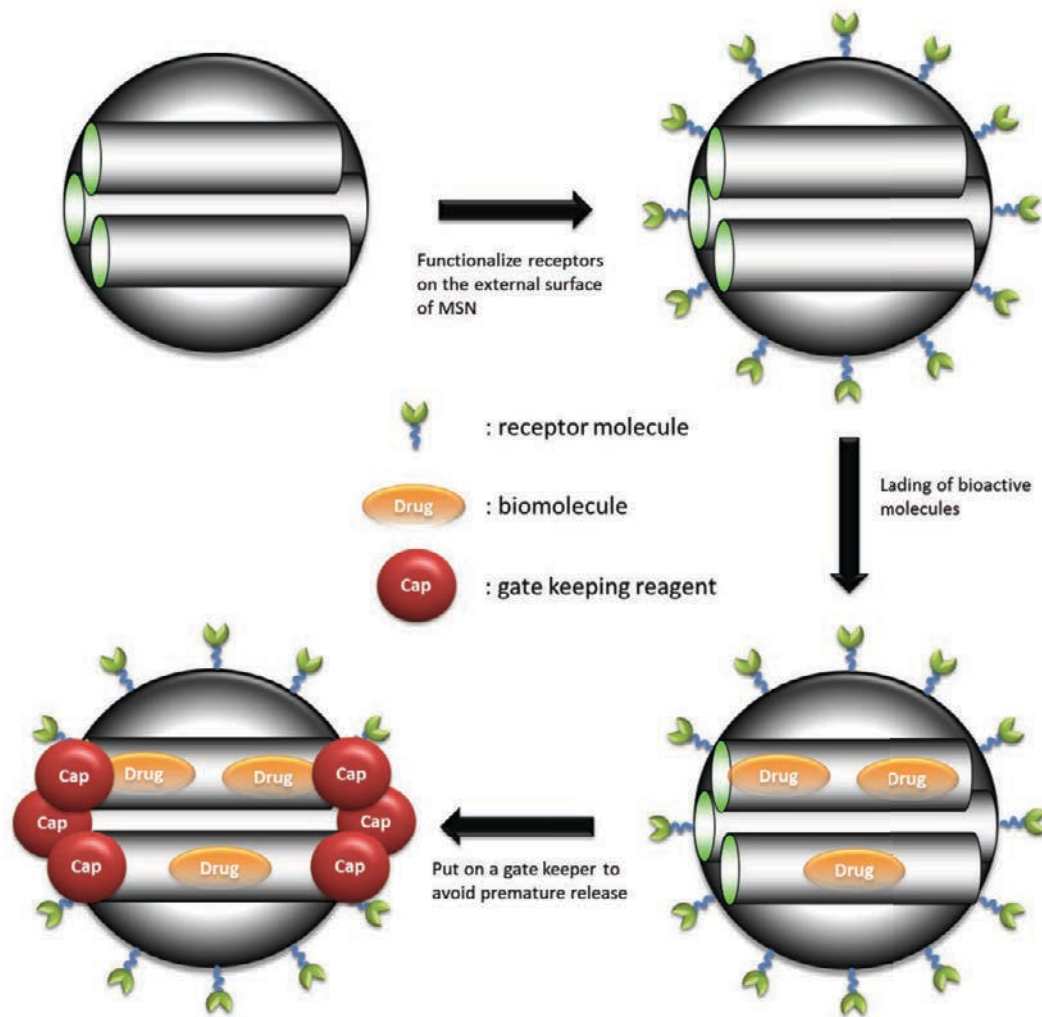


Figure 1-9 Schematic representation of the design of a MSN-based drug delivery vehicle.

For instance, our group first demonstrated the controlled release of neurotransmitters from the mesopores of MSN by using cadmium sulfide (CdS) nanoparticles as caps. In this CdS-NP-MSN system, we utilized a liable disulfide linker to covalently connect the CdS NPs to the MSNs.⁶⁹ This disulfide linker was cleaved upon the addition of dithiothreitol (DTT), which was used as the external stimuli. Biogenic molecules, including adenosine triphosphate (ATP) and vancomycin, were loaded and entrapped in the MSN in this study. We successfully demonstrated that the CdS-NP-MSN system was indeed stimuli-responsive to the DTT concentration in solution. In addition, this controlled-release system showed acceptable biocompatibility *in vitro*. To introduce site-directing capability of the MSN-based delivery system, S. Giri *et al.* developed another hard-cap system using magnetic iron-oxide nanoparticles (IO-NPs) as the gate-keeper.⁷⁰ Again, the IO-NP caps were linked to the MSN via the disulfide bridge; therefore, the same stimuli-responsive release occurred by introducing the reducing agent DTT. The interesting part of this study was that the magnetic nanoparticle-capped MSNs were attracted to specific sites of interest in the presence of a magnetic field. This strategy provided means to target specific areas. Gold nanoparticles (Au-NPs) were also used as another example of hard-cap system. Recently, J. Vivero *et al.* reported a photo-responsive AuNPs-MSNs system using a liable positively-charged nitro-benzene unit as the linker. The AuNPs was capped onto the MSN materials via an electrostatic interaction.²⁹ Upon irradiation with UV-light, the surface charge on the AuNPs would become negative due to the departure of the positively charged nitro-benzene unit, leading to repulsion of negatively charged MSNs and release of the cargo. The authors demonstrated that the photo-induced release of encapsulated fluorescein molecules was successful in solution. For the *in vitro* study, they also observed that the cell proliferation was

inhibited with the paclitaxel-loaded AuNPs-MSN material after irradiation under mild conditions. Besides hard-cap system, soft-cap systems using bulk organic moieties such as dendrimers and polymers as caps have also been developed in our lab. For example, Wei *et al.* coated a layer of poly (L-lysine) on the MSN external surface serving as cap reagents.⁶⁸ The highly positively charged poly (L-lysine)-MSNs showed not only high endocytosis efficiency as well as very low toxicity, but also was resistant to digestion by gastrointestinal enzyme pepsin. To release the loaded cargoes, an enzyme trypsin was applied in this study and the enzymatic degradation of poly(L-lysine) was demonstrated to be very efficient. Although a small degree of leaching occurred with this system due to the porous nature of the poly(L-lysine) layer, it still looks promising that the bio-degradable polymers can serve as a good capping reagent once they were well prepared.

Several unique systems have also been reported by others. The Zink and Stoddart groups developed a series of MSN-based drug delivery system on the basis of their expertise on supramolecules.^{97,106,108-110} They incorporated MSN materials with their synthesized supramolecules such as rotaxane architectures and nano-impellers as the gate keepers to release cargo in a controlled manner. Changes in pH value and photo irradiation are frequently the stimuli for these types of systems. Very recently, they reported a cyclodextrin (CD)-based “nanopiston” system, as shown in Figure 1-10, in which the mesopores are blocked at higher pH, and opened when decreasing pH.¹⁰⁶ The release profile in solution showed that the release rate can be well-controlled by fine tuning the pH value. At pH 7, there was no obvious leaching of loaded molecules, demonstrating no premature release occurred. Once decreasing the pH value of the solution to pH 5, an immediate 40% release

functionalization with hydrophobic organic groups on the MSN materials is necessary to improve the loading efficiency. For example, Zink and co-workers reported an azobenzene impellers functionalized MSN system for the delivery of an anticancer drug camptothecin (CPT),⁹⁸ in which they observed improved loading capacity compared to the unfunctionalized MSNs. This was later concluded as the hydrophobic interactions between azobenzene moieties and CPT molecules. The approach of modifying MSN surface with hydrophobic groups may be able to significantly increase the loading efficiency; however, another issue arises. Once the drugs are loaded inside the hydrophobic mesopores, they are resistant to release in the aqueous, physiological conditions. To overcome this issue, we designed a surfactant-assistant drug delivery system, as depicted in Scheme 1-1, in which the

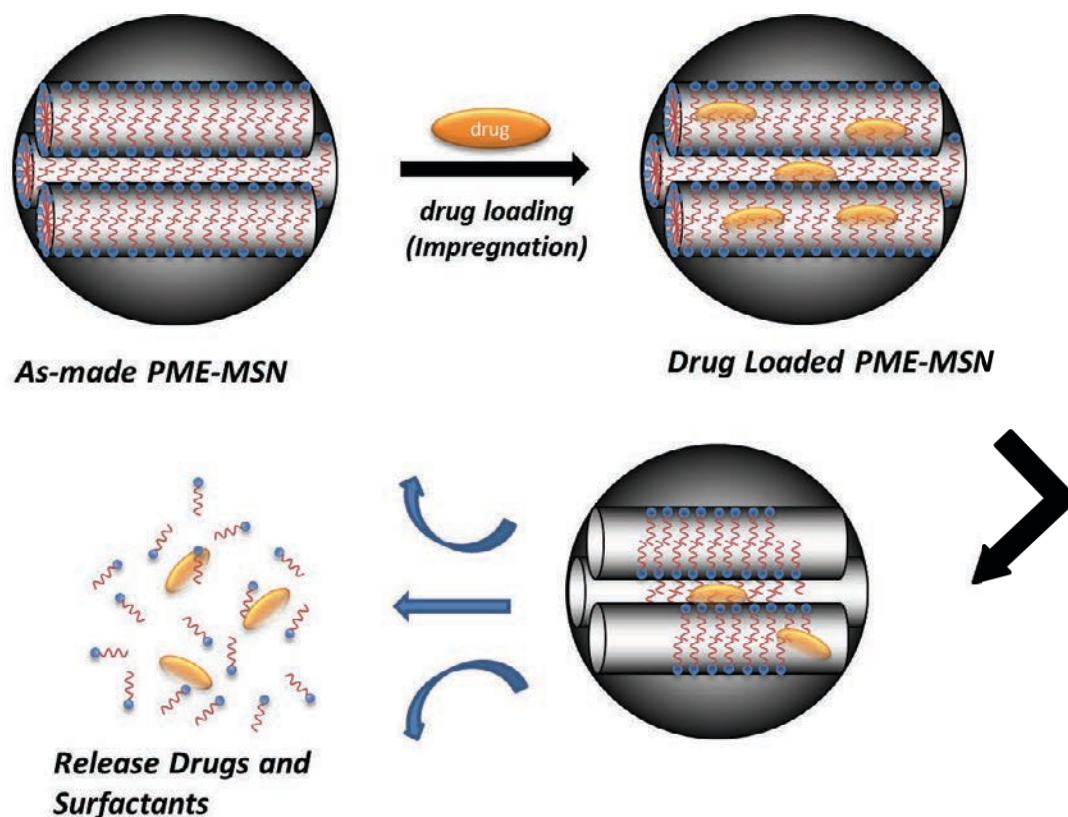


Figure 1-11 Schematic representation of surfactant-assisted drug delivery system.

hydrophobic drugs are loaded inside the surfactant-containing MSN materials.⁴³ During release process, the drug molecules would release along with the biocompatible surfactants into the physiological solution. In Chapter 2, we have proven that this system can not only increase the loading capacity three times higher than that of un-functionalized MSNs, but also more than 90 % of loaded drugs are released through the assistance of the biocompatible surfactants.

b). Applications of MSN materials in heterogeneous catalysis

Heterogeneous catalysts are of great interests in both scientific and industrial areas due to their recyclability, enhanced catalytic reactivity, and selectivity.^{8,10,23,25,114-117} Among many conventional solid supports, mesoporous silica materials for heterogeneous catalysis have attracted attention from scientists since the discovery two decades ago. Three major sub-categories based on mesoporous silica nanoparticles as heterogeneous catalysts have been extensively studied: MSN-based organocatalyst, single-site heterogeneous catalyst (SSHC), and supported metal nanoparticle catalyst. Recent developments of these catalytic systems have achieved great success from both our group and others. Herein, I would like to concentrate on some of important inventions and make connections to my own works in the following chapters.

i). Supported-organocatalyst

The MSN-based organocatalyst can be simply synthesized via either grafting or co-condensation method with the pre-synthesized organocatalyst-silane. By properly designing the functional groups and the pathway of functionalization, many catalytic systems including

acid catalysts,¹¹⁷⁻¹²³ base catalysts,¹²⁴⁻¹²⁹ N-heterocyclic carbenes,¹³⁰⁻¹³⁴ 2,2,6,6-Tetramethylpiperidinyloxy (TEMPO)¹³⁵⁻¹³⁷ and others have been reported for a variety of chemical reactions. For example, Chen *et al.* synthesized a dialkylaminopyridine (DMAP)-functionalized MSN catalysts for Baylis-Hillman, acylation, and silylation reactions.¹²⁴ This MSN-supported base catalyst was very efficient toward these reactions and showed good product selectivity and recyclability. Ngo and co-workers designed a MSN supported diarylammonium acid catalyst for esterification of free fatty acid.¹¹⁹ An interesting acid-base organocatalyst supported on SBA-15 materials for Michael addition of ketones was reported by S. Jain *et al.*¹²³ This organocatalyst was not directly grafted onto the silica surface, but instead, interacted with the pre-grafted azide groups via an azide-alkyne click chemistry method. The post-synthesis method provided an easy alternative route for preparing supported organocatalysts. In addition, this bifunctional acid-base catalyst exhibited superior catalytic reactivities and diastereoselectivities toward the Michael addition reaction of ketones. TEMPO, an organocatalyst for metal-free aerobic oxidation reactions, has also been immobilized on the mesoporous silica materials by Karimi and co-workers.^{135,137} This catalyst was very efficient in converting primary and secondary alcohols to corresponding aldehydes and ketones under oxygen atmosphere. It was also proved to be recyclable for at least 14 times with continued quantitative yields. N-heterocyclic carbenes (NHC) are known for their properties of being electron-rich and sterically restricting, and numerous applications have been reported as strong ligands in organometallics and as organocatalysts in many chemical transformations.^{138,139} The most common method for preparing NHC catalysts is the deprotonation of the corresponding azolium salts. Lu *et al.* reported an NHC-functionalized MCM-41 material as a catalyst for the fixation reaction of carbon dioxide.¹³⁴

This catalyst is efficient at absorbing carbon dioxide molecules, followed by the cycloaddition with epoxides or aziridines to yield the corresponding dioxolanones or oxazolidinones. The catalytic performance of this heterogeneous catalyst has shown to be comparable to its homogeneous counterpart. In addition, results indicate that the catalyst can be recycled multiple times without significant loss in catalytic reactivity, owing to carbon dioxide as a protective group.

Besides mono-functionalized MSN catalysts, bi- or multi-functionalized MSN can also be prepared by incorporating secondary functional groups via previously described methods. With the interactions of supplementary secondary groups, numerous new catalytic systems have been reported.^{118,122,126,140-143} Lin and co-workers synthesized a series of bi-functional MSN catalysts with different molar ratio of 3-[2-(2-aminoethylamino)ethylamino]-propyl (AEP) groups as catalytic sites and ureidopropyl (UDP) groups as supplements, for base-catalyzed aldol, Henry, and cyanosilylation reactions.¹⁴⁰ The working principle, as illustrated in Figure 1-12, is based on a cooperative catalysis system, in which the carbonyl group of the aldehyde substrate was activated by a UDP group through hydrogen bonding, followed by a base-catalyzed nucleophilic addition. Their results showed that all synthesized bi-functional MSN catalysts performed better than any mono-functional catalysts, demonstrating the effect of cooperative catalysis. Another example of cooperative catalysis using bifunctional MSN was demonstrated by M. Davis *et al.*^{122,143} They developed different functionalization methods to tune the distance between two functional groups (thiol and sulfonic acid groups), and found that the catalyst having acid and thiol groups separated by three

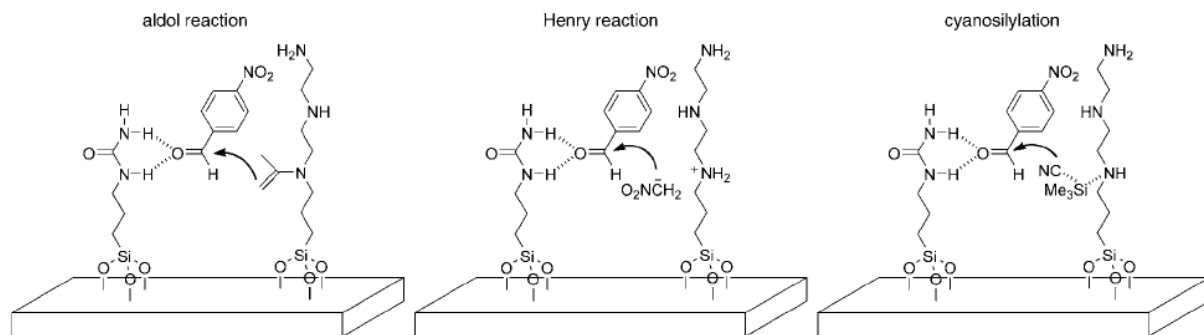


Figure 1-12 AEP and UDP groups may activate the electrophile and nucleophile cooperatively to enhance the reaction rates of the desired catalytic reactions.¹⁴⁰

carbon atoms was approximately three times more active than materials containing both functional groups randomly distributed in the condensation of acetone and phenol to bisphenol.

The secondary functional group may not only serve as a co-catalyst directly interacting with the substrate, but it can also be a surface modifier which alters the silica surface for controlling the mass transportation of substrates or products. Our group has reported that by altering the hydrophobicity/hydrophilicity of the secondary groups, the product ratio of a competitive nitro-aldol reaction can be selectively controlled.¹²⁶ When hydrophilic groups like UDP were used as the surface modifier, in the presence of AEP groups as catalyst, the more hydrophilic benzaldehyde derivative in the reactant mixture would be converted to the corresponding product more efficiently than the hydrophobic substrate. While switching the secondary group to a hydrophobic allyl or thiol group the opposite results were observed. Following this concept, in Chapter 3, we develop another bifunctional catalyst with bulky diarylammonium triflate (DAT) groups as acid catalytic sites and pentafluorophenyl (PFP) groups as surface modifiers for esterification reactions.¹¹⁸ Due to strong interactions between

PFP groups and the silica surface, we proved that the incorporated PFP groups would tend to lie down on the silica surface in the presence solvent, creating an extreme hydrophobic fluorinated surface. The design of principle, as shown in Figure 1-13, is to utilize the hydrophobic local environment to expel the produced water molecules, which are the byproduct of the esterification reaction, out of the mesopores, so as to drive the equilibrium dehydration reaction toward the product end.

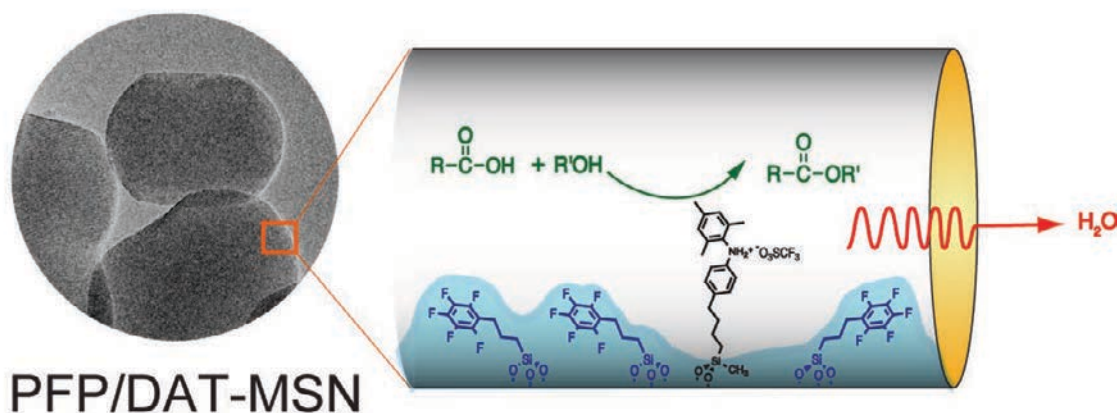


Figure 1-13 Illustration of the working principle of bifunctional PFP/DAT MSN catalyst for esterification reactions.¹¹⁸

ii). Single-site heterogeneous catalyst (SSHC)

The general definition of single-site heterogeneous catalyst is “a catalyst constituted by a metal atom, ion, or small cluster of atoms, held by surface ligands to a rigid framework”.²⁵

These catalytic sites are individually isolated inside the hosting structure and do not interact with each other. Silica materials have long been known to be very good supports for SSHC due to the surface silanol groups which could serve as strong chelating ligands toward transition metals without any further functionalization. For example, Basset *et al.* have

reported several Si surface-bonded metal complex systems more than two decades ago.^{144,145} This study has now been extended to the field of mesoporous silica materials, where the much larger surface area and tunable pore size properties have created a variety of SSHC catalysis systems. A distinct example of directly grafting metal active center onto MSN surface through silanol groups is the Ti^{IV} catalyst developed by Maschmeyer and co-workers.¹⁴⁶ This catalyst has shown to be an exceptionally efficient catalyst for epoxidation of alkenes using alkyl hydroperoxides. In order to produce isolated, tetrahedral Ti^{IV} centers and avoid the tendency to form Ti-O-Ti bond, a great advance was made by the authors when

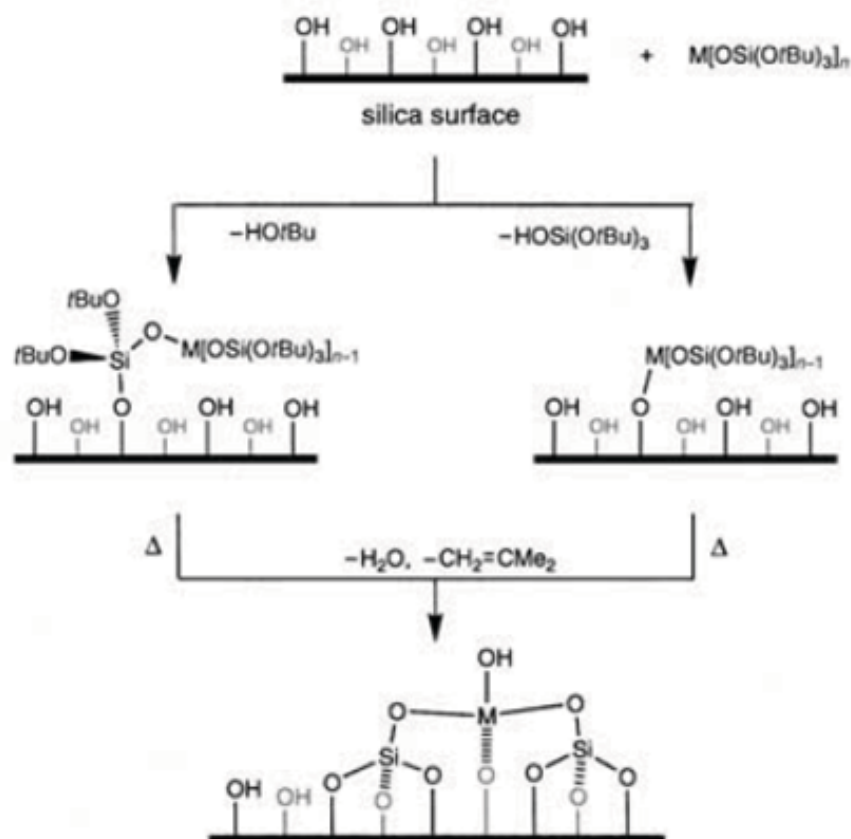


Figure 1-14 The Tilley method of preparing single-site catalysts on mesoporous silica through thermolytic molecular precursors such as $\text{M}[\text{OSi}(\text{OtBu})_3]_n$ (where $\text{M} = \text{Ti}, \text{Fe}, \text{Cr} \dots$).¹⁴⁹

Ti^{IV} active centers were grafted onto the inner walls of mesoporous silica using an organometallic precursor, in particular titanocene dichloride (Ti(Cp)₂Cl₂) (Cp=C₅H₅). By using the similar approach, several supported metal ion catalysts including Mo^{VI}, Cr^{VI}, and VO^{IV} have been reported.^{147,148} Tilley *et al.* developed another strategy to incorporate the metal ion into the silica framework, as depicted in Figure 1-14, in which the thermolytic molecular precursors such as M[OSi(OtBu)₃]_n (where M = Ti, Fe, Cr) were directly grafted onto the silica surface, followed by a hydrolysis process to yield the desired catalyst.^{149,150}

Organometallic complexes can also be anchored on the mesoporous silica, serving as single-site heterogeneous catalysts. In general, the metal complexes can be introduced in two distinct strategies as shown in Figure 1-15. For the sequential approach, an organosilane linker was first put on the silica surface via either the co-condensation or grafting method.¹⁵¹ The organic linker group can be used directly as a ligand to coordinate with the metal center, or can further connect to another specific ligand, which later is used to grab the metal center. On the other hand, the convergent approach is more straightforward, in which the organometallic complex was synthesized prior to incorporating on the mesoporous support. Many SSHC based on MSNs have been recently reported.^{148,151} For instance, Mckittrick and his colleagues prepared an isolated Ti-centered catalyst for polymerization of ethylene demonstrating the efficiency of the sequential approach.¹⁵² Jin *et al.* reported an N-heterocyclic carbene (NHC)-Pd catalyst on porous silica to catalyze the Suzuki-Miyaura coupling reaction.¹⁵³ The catalyst was synthesized via the convergent approach and exhibited excellent catalytic reactivity toward the Suzuki coupling reaction in a number of substrates. In addition to immobilizing single-site molecular catalysts to solid surface by covalent

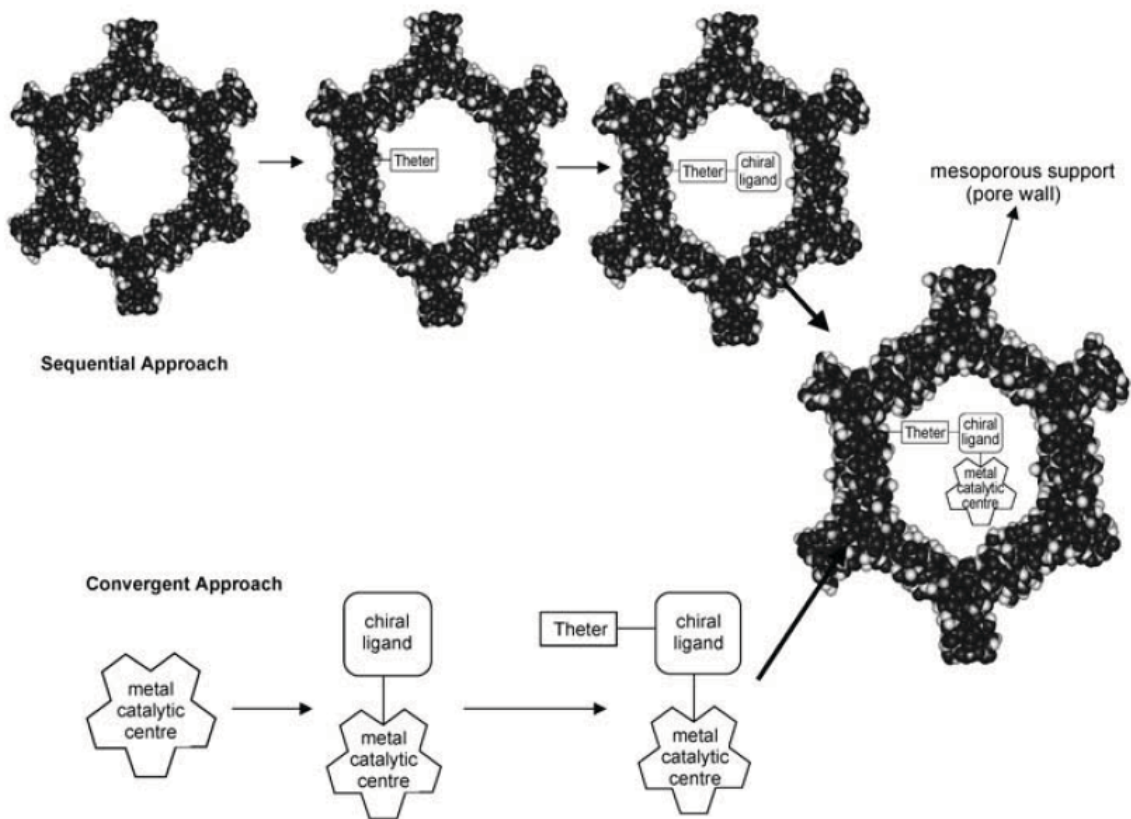


Figure 1-15 Two distinct approaches for the incorporation of organometallic complexes onto mesoporous silica.¹⁵¹

bonding, Bianchini *et al.* and Thomas *et al.* have reported the non-covalent immobilization by taking advantage of the strong hydrogen bonding between the silanol-rich silica surface and the triflate or sulfonate groups.^{154,155} Very recently, we have developed a MSN-supported Pt-complex catalyst for the hydroarylation of unactivated olefins (Figure 1-16).¹⁵⁶ This solid catalyst shows excellent thermal stability and comparable catalytic reactivity to that of homogeneous counterpart. In addition, we have also proven that the product selectivity can be tuned by the changing the tether. Further investigation on the effect of introducing secondary groups is still ongoing.

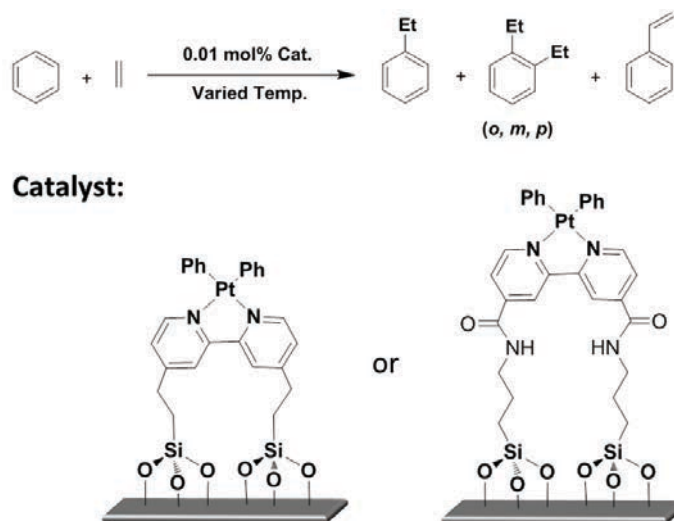


Figure 1-16 Hydroarylation of unactivated olefins catalyzed by MSN-supported Pt complex catalysts.¹⁵⁶

Another merit for mesoporous silica as solid supports for SSHC is the essence of confinement effect. In enantioselective catalysis, it is well known that the product selectivity is highly dependent on the steric hindrance of catalytic centers. Given that the chiral organometallic catalysts were imbedded inside the mesopores, the well-defined pores can help block the entry of substrates from certain directions, so as to significantly enhance the enantioselectivity. A series of systematic studies investigating this confinement effect have been done by J. M. Thomas *et al.*^{148,151,155,157} They first designed a Rh(I) catalyst with a small chiral ligand immobilized on the mesoporous silica materials for the asymmetric hydrogenation of (*E*)- α -phenylcinnamic acid and methyl 2-oxo-2-phenylacetate.¹⁵⁷ They found that the enantioselectivity of products was greatly boosted when the catalyst was grafted inside the meso-channels, as shown in Figure 1-17. A dramatic drop in *ee* value was observed when the catalyst was immobilized on the

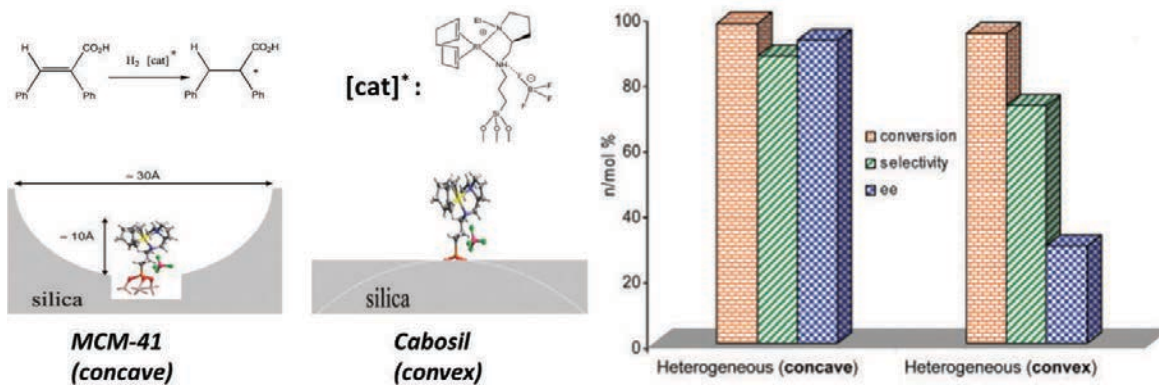


Figure 1-17 Comparison of Rh(I) catalyst immobilized on internal surface and external surface of mesoporous silica material in asymmetric hydrogenation of (E) - α -phenylcinnamic acid.¹⁵⁷

external surface of silica support. It is interesting to note that both catalysts have exhibited similar catalytic reactivity, implying that the reaction kinetics will not be hampered by the confined mesostructure if the pore size of the support is properly chosen. In addition, the concave-type of immobilized Rh (I) catalyst showed superior conversion and enantioselectivity over its homogeneous analogue. The hypothesis of the confinement effect of supported mesoporous silica catalysts was further supported by the results of asymmetric hydrogenation of methyl 2-oxo-2-phenylacetate using different pore size of mesoporous silica as supports (Figure 1-18).¹⁵⁵ It is clear to see that the enantioselectivity of the product is disproportional to the pore size of supports. The smaller pore size would provide stronger confinement effect, leading to greater enhancement in ee value.

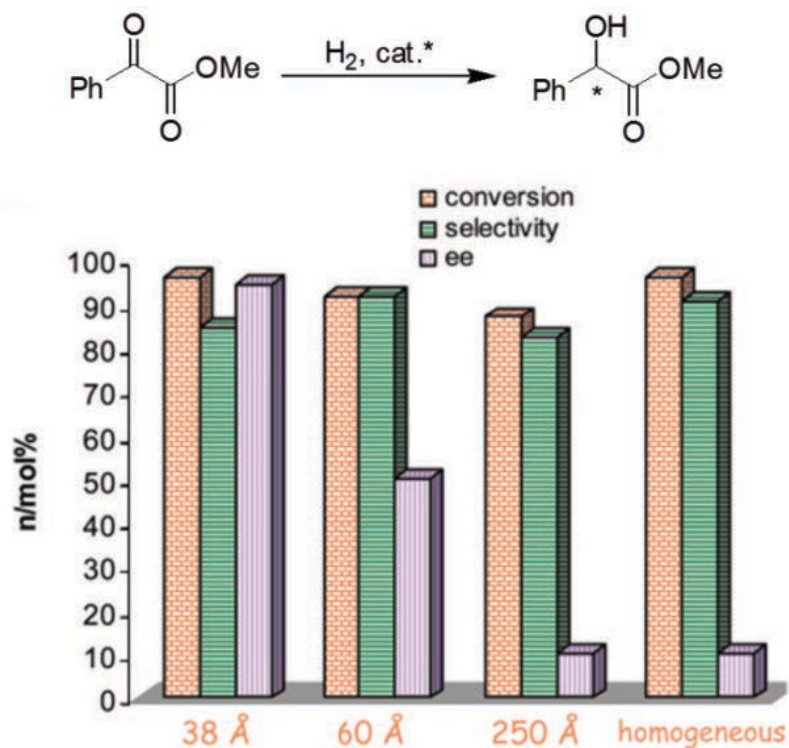


Figure 1-18 Comparison of confinement effect in different pore size of mesoporous silica materials.¹⁵⁵

iii) Supported metal nanoparticle catalyst

As regarded as “*semi-heterogeneous catalysis*”, the field of using metal nanoparticles (NPs) in catalysis is at the frontier between homogeneous and heterogeneous catalysis, and has gained great interest from scientists in the past decade.¹¹⁴ Nord *et al.* pioneered the catalytic applications of NPs on nitrobenzene reduction in the 1940s.^{158,159} Later in the 1970, Parravano reported on the use of AuNPs for hydrogen-atom transfer between CO and CO_2 .¹⁶⁰ An important breakthrough of this field has been unveiled by Haruta’s studies on the AuNPs catalyzed CO oxidation by using molecular oxygen at low temperature.^{161,162} Subsequently, numerous catalytic systems based on a variety of metal NPs including Au, Ag, Pd, Pt, Rh, Co,

Ni, and metal oxides have been developed. Many synthetic strategies for the preparation of metal NPs have been disclosed, among those the most common methods are impregnation, co-precipitation, deposition/precipitation, sol-gel, gas-phase organometallic deposition, and micro-emulsion.¹¹⁴ One of concerns for the use of metal NPs in catalysis is their tendency to agglomerate due to the high surface energy. Therefore, surface stabilizers are usually necessary for metal nanoparticles. Many systems have been developed, such as polymers,¹⁶³ dendrimers,¹⁶⁴ surfactants,¹⁶⁵ micro-emulsions,¹⁶⁶ oxide supports,¹⁶⁷ carbon supports¹⁶⁸ and mesoporous silica supports.²³ In this section, I would like to focus on the development of mesoporous silica supported metal NPs and their application in catalysis.

Mesoporous silica materials with ordered mesopores, tunable pore size, large surface area and pore volume are favorable for the synthesis of mono-dispersed metal NP catalysts by the confinement in their well-defined pore matrix. In addition, the silanol-rich surface, as mentioned in the previous section, can also help stabilize the metal ions, which can be further reduced to form metal NPs. In general, there are three strategies for the synthesis of mesoporous silica supported metal NPs catalyst:²³ First, the incipient wetness method (impregnation), this method is usually initially used since its simplicity for manipulating the metal precursors and solid supports. Its working principle is to utilize the surface silanol groups to grab the impregnated metal ions, followed by a reduction process which is typically carried out by either a hydrogen reduction at elevated temperature or a chemical reduction. The key factor in the formation of mono-dispersed metal NPs within the mesopores lies in the reduction process. It is known that the surface-grafted metal ions possess high mobility through the silanol groups under thermal treatment,^{169,170} suggesting

that there exists a competition between thermodynamics and kinetics during the formation of metal crystals. Thermodynamic control tends to result in the formation of large metal crystals, while kinetic control leads to smaller particles. The relevance of particle size of metal NPs and reduction temperature has been studied by Ryoo *et al.*¹⁷¹ In addition, it has also been reported that a bimodal distribution or a mixture of metal compositions could be obtained if more than one metal source were applied.^{172,173} Therefore, it is critical for the incipient wetness method to control the synthesis parameters to obtain the monodispersed metal NPs within the channels of mesoporous silica materials. In Chapter 4, we have developed a sequential impregnation method in the preparation of MSN supported Pd-Au bimetallic NP catalyst for the catalysis of aerobic oxidative esterification of alcohols.¹⁷⁴ As illustrated in Figure 1-19, we first introduced the Au source into the MSN by utilizing a synthesized positively-charged Au(I) complex instead of the commonly used commercially available negatively-charged HAuCl_4 .¹⁷⁵ Under basic synthetic conditions, the strong electrostatic interaction between the negatively-charged silica surface and the Au(I) complex would significantly enhance the loading efficiency. Subsequently, $\text{Pd}(\text{OAc})_2$ was impregnated into the Au-MSNs in organic solvent, followed by a mild hydrogen reduction to yield the resulting bimetallic NP catalyst. By fine-tuning the ratio of Pd and Au, we determined that the Pd-rich bimetallic Pd-Au MSN catalyst showed the best catalytic reactivity toward the tandem catalysis of aerobic oxidative esterification.

The second method used frequently for the preparation of mesoporous silica supported metal NPs is the “*in situ* encapsulation” method. This method is a type of direct synthesis, in which the pre-synthesized metal NPs or metal precursors were added into the reaction

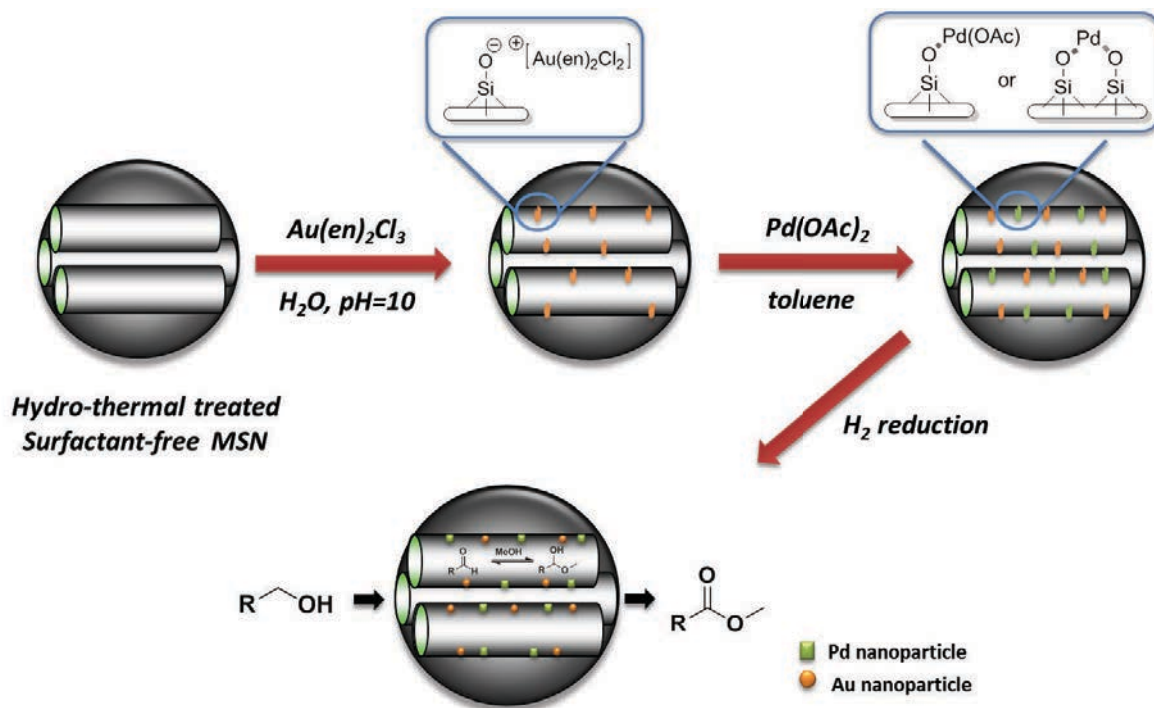


Figure 1-19 Schematic representation of the synthesis of MSN-supported Au-Pd bimetallic NPs catalyst by using sequential impregnation method.¹⁷⁴

solution during the synthesis of mesoporous silica materials, followed by removal of surfactants and subsequent reduction process. By properly choosing the metal precursors and the reaction conditions, mesoporous materials loaded with mono-dispersed metal NPs can be obtained. For example, Somarjai and co-workers have synthesized several SBA-15 type materials with Au, Pt, and Ag metal NPs by using this approach.¹⁷⁶ Materials with different size of encapsulated metal NPs ranging from 2 nm- 20 nm were obtained by changing the concentration of metal precursors. The TEM images also showed that most metal NPs in the size range of 2 nm – 10 nm were well distributed inside the mesopores, while those NPs larger than 10 nm were embedded inside the framework or outside the mesoporous supports. One key factor to this method is that one needs to carefully select the metal precursors and

protecting ligands to match the surfactant assembly and to avoid destroying the ordered structure of the mesoporous materials.^{177,178} As mentioned previously in the co-condensation method section, the formation of mesoporous materials is highly dependent on the characteristics of the synthetic solution. Moreover, it has also been reported that the loading amount of metal by this method is still limited due to the complexity of synthetic condition.

The most popular method used in this field is the “organometallic strategy” (surface functionalization method). As mentioned in the SSHC section, many organic functional groups can be grafted onto the silica surface and serve as ligands to coordinate with metal precursors.²⁵ The obtained metal complexes can then be reduced by hydrogen reduction or chemical reduction to yield metal NPs. Due to the strong interactions between the organic ligands and metal precursors, this method has proven to be more efficient in loading capacity than the incipient wetness method and the encapsulation. In addition, since most organic ligands were located inside the internal surface area of mesoporous silica, the formed metal NPs are mostly encapsulated within the mesopores.²³ Another advantage of this technique is that the particle size of the metal NPs can be controlled owing to the surface functionalized ligands serving as stabilizers for preventing the metal NPs from aggregating.¹⁷⁹ Utilizing this method, remarkable work has been reported in recent years. For example, J. Clark *et al.* synthesized SBA-15 materials grafted with a series of pyridine-type ligands for complexation with Pd precursors, followed by a mild hydrogen reduction process to yield the encapsulated Pd NPs within the SBA-15 meso-channels.¹³⁵ These catalysts then were tested for aerobic oxidation of alcohols to yield corresponding aldehydes and ketones, and proved to be very efficient and robust toward this type of reaction. A variety of alcohol substrates have been

examined and even aliphatic primary alcohols can be converted to aldehydes quantitatively under mild reaction conditions. Yang *et al.* synthesized Au-Pd bimetallic catalysts supported on amine-functionalized SBA-16 mesoporous materials for solvent-free aerobic oxidation of benzyl alcohol.¹⁸⁰ By fine tuning Au and Pd molecular ratio, the best catalytic conversion with 8667 TOF (h^{-1}) can be obtained from the Pd-rich Au-Pd bimetallic catalyst (Au : Pd = 1 : 5). For some metal ions such as Ag^+ , which shows high mobility on the silica surface and tends to diffuse out of the mesopores and form large particles during the thermal treatment, the surface functionalization method has shown to be more suitable for the synthesis of encapsulated metal NPs catalysts.^{23,181} Bao and co-workers developed a facile auto-reduction route to fabricate mono-dispersed Ag NPs on mesoporous silica materials.¹⁸² As represented in Figure 1-20, the amine-functionalized SBA-15 materials was further reacted with formaldehyde to form a new, reusable, fixed, reducing functional group $-\text{NHCH}_2\text{OH}$. Once they introduced the Ag precursor, $\text{Ag}(\text{NH}_3)_2\text{NO}_3$, Ag NPs were readily generated and encapsulated within the SBA-15 channels. The TEM images show that Ag NPs with a narrow particle size distribution were mostly located inside the mesopores. In addition, this material exhibited very high thermal stability, in which there is no obvious agglomeration or sintering observed after a thermal treatment at 573K for 1h. These authors also claimed that other metals such as Pt, Pd, and Au NPs can be obtained with high dispersion and homogeneity within the mesoporous silica materials by using the same synthetic strategy.²³

However, several concerns about the surface functionalization method have been underlined with the undesired interference between the organic ligands and the metal NP catalysts. First, although the surface-bound ligands are used to stabilize the metal NPs they

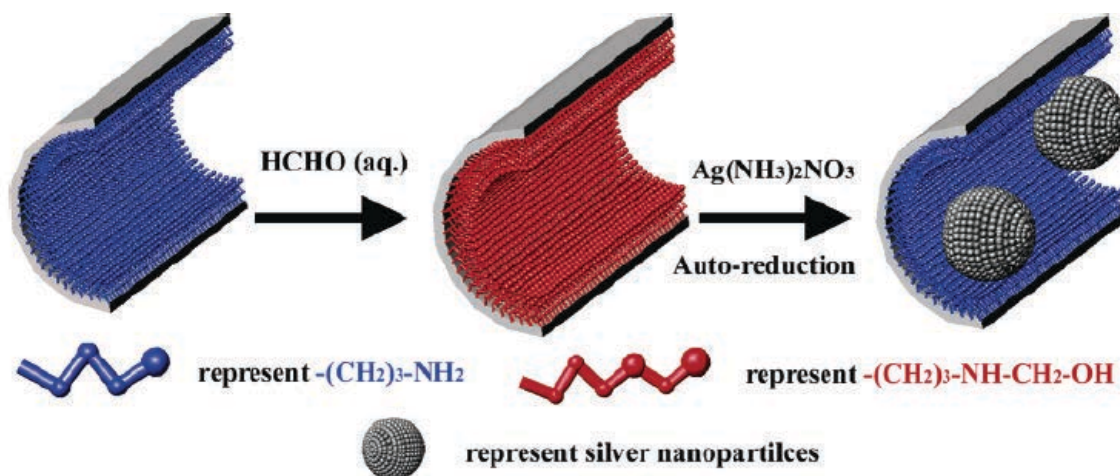


Figure 1-20 Schematic representation of a facile *in situ* auto-reduction route to fabricate highly dispersed Ag NPs within the channels of mesoporous materials.¹⁸²

also occupy many catalytic sites on the metal surface, resulting in a decrease of accessible metal surface. In fact, it has been reported by Mou *et al.* that Au NPs supported on mesoporous silica synthesized via the impregnation method showed higher catalytic reactivity in CO oxidation reaction than the catalyst prepared by using the surface functionalization method.¹⁸³ Furthermore, the organic ligands may unexpectedly participate in the reaction, resulting in occurrences of side-chain reactions, and sometimes causing the deactivation of the catalyst. For instance, Au NPs have been suggested to be capable of oxidizing primary and secondary amines into corresponding imines and enamines under molecular oxygen atmosphere.¹⁸⁴ If someone utilizes amine groups as ligands to synthesize encapsulated Au NPs catalyst for the purpose of aerobic oxidation reaction, we can expect that a competitive oxidation reaction may occur on the surface of Au NPs. There is no doubt that the competition between amine ligands and reaction substrates would moderate the catalytic performance of Au NPs. Therefore, a careful selection of surface functionalities and the types of catalytic reactions needs to be taken beforehand.

Summary

This chapter reviews the recent developments of mesoporous silica materials and their applications in the fields of drug delivery and catalysis. Although the industrial applications of mesoporous silica materials are limited nowadays, they still look promising in the areas of fine-chemical productions and bio-applications, regarding to their special physicochemical properties. Featuring large pore sizes, well-ordered mesostructures, enormous surface area and great biocompatibility, mesoporous silica has demonstrated to be an excellent candidate for intracellular delivery. By properly functionalizing with biogenic molecules, we can even manipulate this smart device in a more complicated manner, such as the design of imaging agents or bio-sensors. On the other hand, in the case of heterogeneous catalysis, numerous delicate catalytic systems have also been developed on the basis of mesoporous silica materials, including organocatalysts, organometallic catalysts, multi-functional catalysts, single-site heterogeneous catalysts, and metal nanoparticle catalysts and so forth. The well-defined mesopores provide confined local environment for catalysis, significantly enhancing both selectivity and reactivity. The concept of “nano-reactor” can be further applied to design more efficient heterogeneous catalysts.

Reference

- (1) Davis, M. E. *Nature (London, United Kingdom)* **2002**, *417*, 813.
- (2) Stein, A. *Advanced Materials (Weinheim, Germany)* **2003**, *15*, 763.
- (3) Cronstedt, A. F. *Proc. Int. Zeolite Conf., 9th* **1993**, *1*, 3.

- (4) Dyer, A. *An introduction to zeolite molecular sieves*; Wiley, John & Sons, Incorporated, 1988.
- (5) Barrer, R. M. *Journal of the Chemical Society* **1948**, 2158.
- (6) Barrer, R. M. *Journal of the Chemical Society* **1948**, 127.
- (7) Barrer, R. M. *Hydrothermal Chemistry of Zeolites*; Academic Press, 1982.
- (8) Ertl, G.; Knozinger, H.; Schuth, F.; Weitkamp, J. *Handbook of Heterogeneous Catalysis*, 2008; Vol. 1.
- (9) Martinez, C.; Corma, A. *Coordination Chemistry Reviews* **2011**, 255, 1558.
- (10) Corma, A. *Chemical Reviews (Washington, D. C.)* **1997**, 97, 2373.
- (11) Venuto, P. B. *Microporous Materials* **1994**, 2, 297.
- (12) Cruciani, G. *Journal of Physics and Chemistry of Solids* **2006**, 67, 1973.
- (13) Davis, M. E.; Saldarriaga, C.; Montes, C.; Garces, J.; Crowder, C. *Nature (London)* **1988**, 331, 698.
- (14) Davis, M. E.; Montes, C.; Hathaway, P. E.; Arhancet, J. P.; Hasha, D. L.; Garces, J. M. *Journal of the American Chemical Society* **1989**, 111, 3919.
- (15) Dessau, R. M.; Schlenker, J. L.; Higgins, J. B. *Zeolites* **1990**, 10, 522.
- (16) Lin, C.-H.; Wang, S.-L.; Lii, K.-H. *Journal of the American Chemical Society* **2001**, 123, 4649.
- (17) Sun, J.; Bonneau, C.; Cantin, A.; Corma, A.; Diaz-Cabanas, M. J.; Moliner, M.; Zhang, D.; Li, M.; Zou, X. *Nature (London, United Kingdom)* **2009**, 458, 1154.
- (18) Chiola, V.; Ritsko, J. E.; Vanderpool, C. D.; (Sylvania Electric Products Inc.).
Application: US, 1971, p 3 pp.

- (19) Di Renzo, F.; Cambon, H.; Dutartre, R. *Microporous Materials* **1997**, *10*, 283.
- (20) Kresge, C. T.; Leonowicz, M. E.; Roth, W. J.; Vartuli, J. C.; Beck, J. S. *Nature (London)* **1992**, *359*, 710.
- (21) Beck, J. S.; Vartuli, J. C.; Roth, W. J.; Leonowicz, M. E.; Kresge, C. T.; Schmitt, K. D.; Chu, C. T. W.; Olson, D. H.; Sheppard, E. W.; et al. *Journal of the American Chemical Society* **1992**, *114*, 10834.
- (22) Wight, A. P.; Davis, M. E. *Chemical Reviews (Washington, DC, United States)* **2002**, *102*, 3589.
- (23) Sun, J.; Bao, X. *Chemistry--A European Journal* **2008**, *14*, 7478.
- (24) Oye, G.; Glomm, W. R.; Vralstad, T.; Volden, S.; Magnusson, H.; Stoecker, M.; Sjoebloom, J. *Advances in Colloid and Interface Science* **2006**, *123-126*, 17.
- (25) Thomas, J. M.; Raja, R.; Lewis, D. W. *Angewandte Chemie, International Edition* **2005**, *44*, 6456.
- (26) Trewyn, B. G.; Giri, S.; Slowing, I. I.; Lin, V. S. Y. *Chemical Communications (Cambridge, United Kingdom)* **2007**, 3236.
- (27) Slowing, I. I.; Vivero-Escoto, J. L.; Trewyn, B. G.; Lin, V. S. Y. *Journal of Materials Chemistry* **2010**, *20*, 7924.
- (28) Slowing, I. I.; Vivero-Escoto, J. L.; Wu, C.-W.; Lin, V. S. Y. *Advanced Drug Delivery Reviews* **2008**, *60*, 1278.
- (29) Vivero-Escoto Juan, L.; Slowing Igor, I.; Trewyn Brian, G.; Lin Victor, S. Y. *Small (Weinheim an der Bergstrasse, Germany)* **2010**, *6*, 1952.
- (30) Hartmann, M. *Chemistry of Materials* **2005**, *17*, 4577.
- (31) Taguchi, A.; Schueth, F. *Microporous and Mesoporous Materials* **2004**, *77*, 1.

- (32) Zhao, D.; Feng, J.; Huo, Q.; Melosh, N.; Frederickson, G. H.; Chmelka, B. F.; Stucky, G. D. *Science (Washington, D. C.)* **1998**, *279*, 548.
- (33) Zhao, D.; Huo, Q.; Feng, J.; Chmelka, B. F.; Stucky, G. D. *Journal of the American Chemical Society* **1998**, *120*, 6024.
- (34) Wan, Y.; Zhao, D. *Chemical Reviews (Washington, DC, United States)* **2007**, *107*, 2821.
- (35) Raman, N. K.; Anderson, M. T.; Brinker, C. J. *Chemistry of Materials* **1996**, *8*, 1682.
- (36) Hoffmann, F.; Cornelius, M.; Morell, J.; Froeba, M. *Angewandte Chemie, International Edition* **2006**, *45*, 3216.
- (37) de Soler-Illia, G. J.; Sanchez, C.; Lebeau, B.; Patarin, J. *Chemical Reviews (Washington, DC, United States)* **2002**, *102*, 4093.
- (38) Che, S.; Garcia-Bennett, A. E.; Yokoi, T.; Sakamoto, K.; Kunieda, H.; Terasaki, O.; Tatsumi, T. *Nature Materials* **2003**, *2*, 801.
- (39) Che, S.; Liu, Z.; Ohsuna, T.; Sakamoto, K.; Terasaki, O.; Tatsumi, T. *Nature (London, United Kingdom)* **2004**, *429*, 281.
- (40) Rodriguez-Abreu, C.; Izawa, T.; Aramaki, K.; Lopez-Quintela, A.; Sakamoto, K.; Kunieda, H. *Journal of Physical Chemistry B* **2004**, *108*, 20083.
- (41) Yokoi, T.; Yoshitake, H.; Tatsumi, T. *Studies in Surface Science and Catalysis* **2004**, *154A*, 519.
- (42) Yokoi, T.; Yoshitake, H.; Yamada, T.; Kubota, Y.; Tatsumi, T. *Journal of Materials Chemistry* **2006**, *16*, 1125.

- (43) Tsai, C.-H.; Vivero-Escoto, J. L.; Slowing, I. I.; Fang, I. J.; Trewyn, B. G.; Lin, V. S. Y. *Biomaterials* **2011**, *32*, 6234.
- (44) Chen, C. Y.; Li, H. X.; Davis, M. E. *Microporous Materials* **1993**, *2*, 17.
- (45) Inagaki, S.; Guan, S.; Fukushima, Y.; Ohsuna, T.; Terasaki, O. *Journal of the American Chemical Society* **1999**, *121*, 9611.
- (46) Melde, B. J.; Holland, B. T.; Blanford, C. F.; Stein, A. *Chemistry of Materials* **1999**, *11*, 3302.
- (47) Asefa, T.; MacLachlan, M. J.; Coombs, N.; Ozin, G. A. *Nature (London)* **1999**, *402*, 867.
- (48) Huo, Q.; Margolese, D. I.; Ciesla, U.; Feng, P.; Gier, T. E.; Sieger, P.; Leon, R.; Petroff, P. M.; Schueth, F.; Stucky, G. D. *Nature (London)* **1994**, *368*, 317.
- (49) Attard, G. S.; Leclerc, S. A. A.; Maniguet, S.; Russell, A. E.; Nandhakumar, I.; Bartlett, P. N. *Chemistry of Materials* **2001**, *13*, 1444.
- (50) Chen, C. Y.; Burkett, S. L.; Li, H. X.; Davis, M. E. *Microporous Materials* **1993**, *2*, 27.
- (51) Monnier, A.; Schuth, F.; Huo, Q.; Kumar, D.; Margolese, D.; Maxwell, R. S.; Stucky, G. D.; Krishnamurty, M.; Petroff, P.; et al. *Science (Washington, DC, United States)* **1993**, *261*, 1299.
- (52) Israelachvilli, J. N.; Mitchell, D. J.; Ninham, B. W. *Journal of the Chemical Society, Faraday Transactions 2: Molecular and Chemical Physics* **1976**, *72*, 1525.
- (53) Israelachvili, J. N.; Mitchell, D. J.; Ninham, B. W. *Biochimica et Biophysica Acta, Biomembranes* **1977**, *470*, 185.
- (54) Huo, Q.; Margolese, D. I.; Stucky, G. D. *Chemistry of Materials* **1996**, *8*, 1147.

- (55) Huo, Q.; Margolese, D. I.; Ciesla, U.; Demuth, D. G.; Feng, P.; Gier, T. E.; Sieger, P.; Firouzi, A.; Chmelka, B. F.; et al. *Chemistry of Materials* **1994**, *6*, 1176.
- (56) Nieweg, J. A.; Lemma, K.; Trewyn, B. G.; Lin, V. S. Y.; Bakac, A. *Inorganic Chemistry* **2005**, *44*, 5641.
- (57) Tan, B.; Rankin, S. E. *Journal of Physical Chemistry B* **2004**, *108*, 20122.
- (58) Yoon, S. B.; Kim, J.-Y.; Kim, J. H.; Park, Y. J.; Yoon, K. R.; Park, S.-K.; Yu, J.-S. *Journal of Materials Chemistry* **2007**, *17*, 1758.
- (59) Ng, J. B. S.; Vasiliev, P. O.; Bergstroem, L. *Microporous and Mesoporous Materials* **2008**, *112*, 589.
- (60) Wang, J.-G.; Li, F.; Zhou, H.-J.; Sun, P.-C.; Ding, D.-T.; Chen, T.-H. *Chemistry of Materials* **2009**, *21*, 612.
- (61) Wang, W.-Q.; Wang, J.-G.; Sun, P.-C.; Ding, D.-T.; Chen, T.-H. *Journal of Colloid and Interface Science* **2009**, *331*, 156.
- (62) Deng, Y.; Cai, Y.; Sun, Z.; Liu, J.; Liu, C.; Wei, J.; Li, W.; Liu, C.; Wang, Y.; Zhao, D. *Journal of the American Chemical Society* **2010**, *132*, 8466.
- (63) Gu, X.; Jiang, T.-L.; Tao, H.-X.; Zhou, S.-T.; Liu, X.-H.; Ren, J.-W.; Wang, Y.-Q.; Lu, G.-Z.; Schmidt, W. *Journal of Materials Chemistry* **2011**, *21*, 880.
- (64) Maschmeyer, T. *Current Opinion in Solid State & Materials Science* **1998**, *3*, 71.
- (65) Sayari, A.; Hamoudi, S. *Chemistry of Materials* **2001**, *13*, 3151.
- (66) Stein, A.; Melde, B. J.; Schrodin, R. C. *Advanced Materials (Weinheim, Germany)* **2000**, *12*, 1403.
- (67) Huh, S.; Wiench, J. W.; Yoo, J.-C.; Pruski, M.; Lin, V. S. Y. *Chemistry of Materials* **2003**, *15*, 4247.

- (68) Huang, W.; Tsai, C.-H.; Kobayashi, T.; Pruski, M.; Chen, H.-T.; Trewyn, B. G.; Lin, V. S.-Y. Manuscript in preparation, 2011.
- (69) Lai, C.-Y.; Trewyn, B. G.; Jeftinija, D. M.; Jeftinija, K.; Xu, S.; Jeftinija, S.; Lin, V. S. Y. *Journal of the American Chemical Society* **2003**, *125*, 4451.
- (70) Giri, S.; Trewyn, B. G.; Stellmaker, M. P.; Lin, V. S. Y. *Angewandte Chemie, International Edition* **2005**, *44*, 5038.
- (71) Trewyn, B. G.; Nieweg, J. A.; Zhao, Y.; Lin, V. S. Y. *Chemical Engineering Journal (Amsterdam, Netherlands)* **2008**, *137*, 23.
- (72) Zhao, Y.; Sun, X.; Zhang, G.; Trewyn, B. G.; Slowing, I. I.; Lin, V. S. Y. *ACS Nano* **2011**, *5*, 1366.
- (73) Matsumura, Y.; Maeda, H. *Cancer Research* **1986**, *46*, 6387.
- (74) Trewyn, B. G.; Whitman, C. M.; Lin, V. S. Y. *Nano Letters* **2004**, *4*, 2139.
- (75) Gruen, M.; Lauer, I.; Unger, K. K. *Advanced Materials (Weinheim, Germany)* **1997**, *9*, 254.
- (76) Unger, K. K.; Kumar, D.; Grun, M.; Buchel, G.; Ludtke, S.; Adam, T.; Schumacher, K.; Renker, S. *Journal of Chromatography, A* **2000**, *892*, 47.
- (77) Huo, Q.; Feng, J.; Schueth, F.; Stucky, G. D. *Chemistry of Materials* **1997**, *9*, 14.
- (78) Qi, L.; Ma, J.; Cheng, H.; Zhao, Z. *Chemistry of Materials* **1998**, *10*, 1623.
- (79) Schulz-Ekloff, G.; Rathousky, J.; Zukal, A. *Microporous and Mesoporous Materials* **1999**, *27*, 273.
- (80) Mou, C.-Y.; Lin, H.-P. *Pure and Applied Chemistry* **2000**, *72*, 137.
- (81) Zhao, D.; Sun, J.; Li, Q.; Stucky, G. D. *Chemistry of Materials* **2000**, *12*, 275.

- (82) Chan, H. B. S.; Budd, P. M.; Naylor, T. d. V. *Journal of Materials Chemistry* **2001**, *11*, 951.
- (83) Lind, A.; du Fresne von Hohenesche, C.; Smatt, J.-H.; Linden, M.; Unger, K. K. *Microporous and Mesoporous Materials* **2003**, *66*, 219.
- (84) Yano, K.; Fukushima, Y. *Journal of Materials Chemistry* **2003**, *13*, 2577.
- (85) Yang, Z.; Lu, Y.; Yang, Z. *Chemical Communications (Cambridge, United Kingdom)* **2009**, 2270.
- (86) Cai, Q.; Luo, Z.-S.; Pang, W.-Q.; Fan, Y.-W.; Chen, X.-H.; Cui, F.-Z. *Chemistry of Materials* **2001**, *13*, 258.
- (87) Garcia-Bennett, A. E.; Lund, K.; Terasaki, O. *Angewandte Chemie, International Edition* **2006**, *45*, 2434.
- (88) Linton, P.; Alfredsson, V. *Chemistry of Materials* **2008**, *20*, 2878.
- (89) Linton, P.; Hernandez-Garrido, J.-C.; Midgley, P. A.; Wennerstroem, H.; Alfredsson, V. *Physical Chemistry Chemical Physics* **2009**, *11*, 10973.
- (90) Linton, P.; Wennerstroem, H.; Alfredsson, V. *Physical Chemistry Chemical Physics* **2010**, *12*, 3852.
- (91) Hudson, S. P.; Padera, R. F.; Langer, R.; Kohane, D. S. *Biomaterials* **2008**, *29*, 4045.
- (92) Zhao, Y.; Trewyn, B. G.; Slowing, I. I.; Lin, V. S. Y. *Journal of the American Chemical Society* **2009**, *131*, 8398.
- (93) Radu, D. R.; Lai, C.-Y.; Jefthinija, K.; Rowe, E. W.; Jefthinija, S.; Lin, V. S. Y. *Journal of the American Chemical Society* **2004**, *126*, 13216.

- (94) Radu, D. R.; Lai, C.-Y.; Wiench, J. W.; Pruski, M.; Lin, V. S. Y. *Journal of the American Chemical Society* **2004**, *126*, 1640.
- (95) Vivero-Escoto, J. L.; Slowing, I. I.; Wu, C.-W.; Lin, V. S. Y. *Journal of the American Chemical Society* **2009**, *131*, 3462.
- (96) Zhu, Y.; Shi, J.; Shen, W.; Dong, X.; Feng, J.; Ruan, M.; Li, Y. *Angewandte Chemie, International Edition* **2005**, *44*, 5083.
- (97) Angelos, S.; Johansson, E.; Stoddart, J. F.; Zink, J. I. *Advanced Functional Materials* **2007**, *17*, 2261.
- (98) Lu, J.; Liong, M.; Zink, J. I.; Tammanoi, F. *Small (Weinheim an der Bergstrasse, Germany)* **2007**, *3*, 1341.
- (99) Vallet-Regi, M.; Balas, F.; Arcos, D. *Angewandte Chemie, International Edition* **2007**, *46*, 7548.
- (100) Lin, Q.; Huang, Q.; Li, C.; Bao, C.; Liu, Z.; Li, F.; Zhu, L. *Journal of the American Chemical Society* **2010**, *132*, 10645.
- (101) Lu, J.; Liong, M.; Li, Z.; Zink, J. I.; Tamano, F. *Small (Weinheim an der Bergstrasse, Germany)* **2010**, *6*, 1794.
- (102) Wang, L.-S.; Wu, L.-C.; Lu, S.-Y.; Chang, L.-L.; Teng, I. T.; Yang, C.-M.; Ho, J.-a. *ACS Nano* **2010**, *4*, 4371.
- (103) Chen, C.; Geng, J.; Pu, F.; Yang, X.; Ren, J.; Qu, X. *Angewandte Chemie, International Edition* **2011**, *50*, 882.
- (104) Vallet-Regi, M.; Colilla, M.; Gonzalez, B. *Chemical Society Reviews* **2011**, *40*, 596.
- (105) Zheng, H.; Gao, C.; Peng, B.; Shu, M.; Che, S. *Journal of Physical Chemistry C* **2011**, *115*, 7230.

- (106) Zhao, Y.-L.; Li, Z.; Kabehie, S.; Botros, Y. Y.; Stoddart, J. F.; Zink, J. I. *Journal of the American Chemical Society* **2010**, *132*, 13016.
- (107) Lu, J.; Choi, E.; Tamanoi, F.; Zink Jeffrey, I. *Small (Weinheim an der Bergstrasse, Germany)* **2008**, *4*, 421.
- (108) Meng, H.; Xue, M.; Xia, T.; Zhao, Y.-L.; Tamanoi, F.; Stoddart, J. F.; Zink, J. I.; Nel, A. E. *Journal of the American Chemical Society* **2010**, *132*, 12690.
- (109) Thomas Courtney, R.; Ferris Daniel, P.; Lee, J.-H.; Choi, E.; Cho Mi, H.; Kim Eun, S.; Stoddart, J. F.; Shin, J.-S.; Cheon, J.; Zink Jeffrey, I. *J Am Chem Soc* **2010**, *132*, 10623.
- (110) Ferris, D. P.; Lu, J.; Gothard, C.; Yanes, R.; Thomas, C. R.; Olsen, J.-C.; Stoddart, J. F.; Tamanoi, F.; Zink, J. I. *Small (Weinheim an der Bergstrasse, Germany)* **2011**, *7*, 1816.
- (111) Balas, F.; Manzano, M.; Horcajada, P.; Vallet-Regi, M. *Journal of the American Chemical Society* **2006**, *128*, 8116.
- (112) Doadrio, J. C.; Sousa, E. M. B.; Izquierdo-Barba, I.; Doadrio, A. L.; Perez-Pariente, J.; Vallet-Regi, M. *Journal of Materials Chemistry* **2006**, *16*, 462.
- (113) Vallet-Regi, M. *Chemistry--A European Journal* **2006**, *12*, 5934.
- (114) Astruc, D.; Lu, F.; Aranzaes, J. R. *Angewandte Chemie, International Edition* **2005**, *44*, 7852.
- (115) White, R. J.; Luque, R.; Budarin, V. L.; Clark, J. H.; MacQuarrie, D. J. *Chemical Society Reviews* **2009**, *38*, 481.
- (116) Hutchings, G. J. *Chemical Communications (Cambridge, United Kingdom)* **2008**, 1148.

- (117) Corma, A.; Garcia, H. *Chemical Reviews (Washington, DC, United States)* **2003**, *103*, 4307.
- (118) Tsai, C.-H.; Chen, H.-T.; Althaus, S. M.; Mao, K.; Kobayashi, T.; Pruski, M.; Lin, V. S. Y. *ACS Catalysis* **2011**, *1*, 729.
- (119) Ngo, H. L.; Zafiroopoulos, N. A.; Foglia, T. A.; Samulski, E. T.; Lin, W. *Energy & Fuels* **2008**, *22*, 626.
- (120) Margolese, D.; Melero, J. A.; Christiansen, S. C.; Chmelka, B. F.; Stucky, G. D. *Chemistry of Materials* **2000**, *12*, 2448.
- (121) Alvaro, M.; Corma, A.; Das, D.; Fornes, V.; Garcia, H. *Chemical Communications (Cambridge, United Kingdom)* **2004**, 956.
- (122) Zeidan, R. K.; Hwang, S.-J.; Davis, M. E. *Angewandte Chemie, International Edition* **2006**, *45*, 6332.
- (123) Jain, S. L.; Modak, A.; Bhaumik, A. *Green Chemistry* **2011**, *13*, 586.
- (124) Chen, H.-T.; Huh, S.; Wiench, J. W.; Pruski, M.; Lin, V. S. Y. *Journal of the American Chemical Society* **2005**, *127*, 13305.
- (125) Wang, Q.; Shantz, D. F. *Journal of Catalysis* **2010**, *271*, 170.
- (126) Huh, S.; Chen, H.-T.; Wiench, J. W.; Pruski, M.; Lin, V. S. Y. *Journal of the American Chemical Society* **2004**, *126*, 1010.
- (127) Anan, A.; Vathyam, R.; Sharma, K. K.; Asefa, T. *Catalysis Letters* **2008**, *126*, 142.
- (128) Cheng, S.; Wang, X.; Chen, S.-Y. *Topics in Catalysis* **2009**, *52*, 681.
- (129) Ribeiro, S. M.; Serra, A. C.; Gonsalves, A. M. d. A. R. *Applied Catalysis, A: General* **2011**, *399*, 126.

- (130) Yang, H.; Han, X.; Li, G.; Ma, Z.; Hao, Y. *Journal of Physical Chemistry C* **2010**, *114*, 22221.
- (131) del Pozo, C.; Corma, A.; Iglesias, M.; Sanchez, F. *Green Chemistry* **2011**, *13*, 2471.
- (132) Liu, G.; Hou, M.; Wu, T.; Jiang, T.; Fan, H.; Yang, G.; Han, B. *Physical Chemistry Chemical Physics* **2011**, *13*, 2062.
- (133) Liu, G.; Hou, M.; Wu, T.; Jiang, T.; Fan, H.; Yang, G.; Han, B. *Physical chemistry chemical physics : PCCP* **2011**, *13*, 2062.
- (134) Zhou, H.; Wang, Y.-M.; Zhang, W.-Z.; Qu, J.-P.; Lu, X.-B. *Green Chemistry* **2011**, *13*, 644.
- (135) Karimi, B.; Abedi, S.; Clark, J. H.; Budarin, V. *Angewandte Chemie, International Edition* **2006**, *45*, 4776.
- (136) Brunel, D.; Fajula, F.; Nagy, J. B.; Deroide, B.; Verhoef, M. J.; Veum, L.; Peters, J. A.; van Bekkum, H. *Applied Catalysis, A: General* **2001**, *213*, 73.
- (137) Karimi, B.; Badreh, E. *Organic & Biomolecular Chemistry* **2011**, *9*, 4194.
- (138) Enders, D.; Niemeier, O.; Henseler, A. *Chemical Reviews (Washington, DC, United States)* **2007**, *107*, 5606.
- (139) Lin, J. C. Y.; Huang, R. T. W.; Lee, C. S.; Bhattacharyya, A.; Hwang, W. S.; Lin, I. J. B. *Chemical Reviews (Washington, DC, United States)* **2009**, *109*, 3561.
- (140) Huh, S.; Chen, H.-T.; Wiench, J. W.; Pruski, M.; Lin, V. S. Y. *Angewandte Chemie, International Edition* **2005**, *44*, 1826.
- (141) Chen, H.-T.; Trewyn, B. G.; Wiench, J. W.; Pruski, M.; Lin, V. S. Y. *Topics in Catalysis* **2010**, *53*, 187.

- (142) Huang, Y.; Xu, S.; Lin, V. S. Y. *Angewandte Chemie, International Edition* **2011**, *50*, 661.
- (143) Margelefsky, E. L.; Zeidan, R. K.; Dufaud, V.; Davis, M. E. *Journal of the American Chemical Society* **2007**, *129*, 13691.
- (144) Basset, J. M.; Choplin, A. *Journal of Molecular Catalysis* **1983**, *21*, 95.
- (145) Coperet, C.; Chabanas, M.; Saint-Arroman, R. P.; Basset, J.-M. *Angewandte Chemie, International Edition* **2003**, *42*, 156.
- (146) Maschmeyer, T.; Rey, F.; Sankar, G.; Thomas, J. M. *Nature (London)* **1995**, *378*, 159.
- (147) Thomas, J. M.; Raja, R. *Studies in Surface Science and Catalysis* **2004**, *148*, 163.
- (148) Sakthivel, A.; Zhao, J.; Kuehn, F. E. *Catalysis Letters* **2005**, *102*, 115.
- (149) Jarupatrakorn, J.; Tilley, T. D. *Journal of the American Chemical Society* **2002**, *124*, 8380.
- (150) Fujdala, K. L.; Tilley, T. D. *Journal of Catalysis* **2003**, *216*, 265.
- (151) Thomas, J. M.; Johnson, B. F. G.; Raja, R.; Sankar, G.; Midgley, P. A. *Accounts of Chemical Research* **2003**, *36*, 20.
- (152) McKittrick, M. W.; Jones, C. W. *Journal of the American Chemical Society* **2004**, *126*, 3052.
- (153) Qiu, H.; Sarkar, S. M.; Lee, D.-H.; Jin, M.-J. *Green Chemistry* **2008**, *10*, 37.
- (154) Bianchini, C.; Burnaby, D. G.; Evans, J.; Frediani, P.; Meli, A.; Oberhauser, W.; Psaro, R.; Sordelli, L.; Vizza, F. *Journal of the American Chemical Society* **1999**, *121*, 5961.

- (155) Raja, R.; Thomas, J. M.; Jones, M. D.; Johnson, B. F. G.; Vaughan, D. E. W. *Journal of the American Chemical Society* **2003**, *125*, 14982.
- (156) Andreatta, J. R.; Chen, H.-T.; Sun, X.; Tsai, C.-H.; Gunnoe, T. B.; Trewyn, B.; Lin, V. S.-Y. Manuscript in preparation, 2011.
- (157) Jones, M. D.; Raja, R.; Thomas, J. M.; Johnson, B. F. G.; Lewis, D. W.; Rouzaud, J.; Harris, K. D. M. *Angewandte Chemie, International Edition* **2003**, *42*, 4326.
- (158) Rampino, L. D.; Nord, F. F. *Journal of the American Chemical Society* **1941**, *63*, 2745.
- (159) Rampino, L. D.; Nord, F. F. *Journal of the American Chemical Society* **1941**, *63*, 3268.
- (160) Parravano, G. *Journal of Catalysis* **1970**, *18*, 320.
- (161) Haruta, M.; Kobayashi, T.; Sano, H.; Yamada, N. *Chemistry Letters* **1987**, 405.
- (162) Haruta, M.; Yamada, N.; Kobayashi, T.; Iijima, S. *Journal of Catalysis* **1989**, *115*, 301.
- (163) Kidambi, S.; Dai, J.; Li, J.; Bruening, M. L. *Journal of the American Chemical Society* **2004**, *126*, 2658.
- (164) Chung, Y.-M.; Rhee, H.-K. *Journal of Molecular Catalysis A: Chemical* **2003**, *206*, 291.
- (165) Yoon, B.; Kim, H.; Wai, C. M. *Chemical Communications (Cambridge, United Kingdom)* **2003**, 1040.
- (166) Ohde, H.; Wai, C. M.; Kim, H.; Kim, J.; Ohde, M. *Journal of the American Chemical Society* **2002**, *124*, 4540.

- (167) Schauer mann, S.; Hoffmann, J.; Johane k, V.; Hartmann, J.; Libuda, J.; Freund, H.-J. *Angewandte Chemie, International Edition* **2002**, *41*, 2532.
- (168) Reetz, M. T.; Helbig, W. *Journal of the American Chemical Society* **1994**, *116*, 7401.
- (169) Besson, S.; Gacoin, T.; Ricolleau, C.; Boilot, J.-P. *Chemical Communications (Cambridge, United Kingdom)* **2003**, 360.
- (170) Gabaldon, J. P.; Bore, M.; Datye, A. K. *Topics in Catalysis* **2007**, *44*, 253.
- (171) Shin, H. J.; Ryoo, R.; Liu, Z.; Terasaki, O. *Journal of the American Chemical Society* **2001**, *123*, 1246.
- (172) Huang, M. H.; Choudrey, A.; Yang, P. *Chemical Communications (Cambridge)* **2000**, 1063.
- (173) Junges, U.; Jacobs, W.; Voigt-Martin, I.; Krutzsch, B.; Schueth, F. *Journal of the Chemical Society, Chemical Communications* **1995**, 2283.
- (174) Tsai, C.-H.; Huang, W.; Chen, H.-T.; Trewyn, B. Manuscript in Preparation, 2011.
- (175) Zhu, H.; Liang, C.; Yan, W.; Overbury, S. H.; Dai, S. *Journal of Physical Chemistry B* **2006**, *110*, 10842.
- (176) Zhu, J.; Konya, Z.; Punte s, V. F.; Kiricsi, I.; Miao, C. X.; Ager, J. W.; Alivisatos, A. P.; Somorjai, G. A. *Langmuir* **2003**, *19*, 4396.
- (177) Liu, H.; Ma, D.; Blackley, R. A.; Zhou, W.; Bao, X. *Chemical Communications (Cambridge, United Kingdom)* **2008**, 2677.
- (178) Prashar, A. K.; Hodgkins, R. P.; Kumar, R.; Devi, R. N. *Journal of Materials Chemistry* **2008**, *18*, 1765.

- (179) Yang, C.-m.; Liu, P.-h.; Ho, Y.-f.; Chiu, C.-y.; Chao, K.-j. *Chemistry of Materials* **2003**, *15*, 275.
- (180) Chen, Y.; Lim, H.; Tang, Q.; Gao, Y.; Sun, T.; Yan, Q.; Yang, Y. *Applied Catalysis, A: General* **2010**, *380*, 55.
- (181) Zhang, W.-H.; Shi, J.-L.; Wang, L.-Z.; Yan, D.-S. *Chemistry of Materials* **2000**, *12*, 1408.
- (182) Sun, J.; Ma, D.; Zhang, H.; Liu, X.; Han, X.; Bao, X.; Weinberg, G.; Pfaender, N.; Su, D. *Journal of the American Chemical Society* **2006**, *128*, 15756.
- (183) Chi, Y.-S.; Lin, H.-P.; Mou, C.-Y. *Applied Catalysis, A: General* **2005**, *284*, 199.
- (184) Zhu, B.; Lazar, M.; Trewyn, B. G.; Angelici, R. J. *Journal of Catalysis* **2008**, *260*, 1.

CHAPTER 2. SURFACTANT-ASSISTED CONTROLLED RELEASE OF HYDROPHOBIC DRUGS USING ANIONIC SURFACTANT TEMPLATED MESOPOROUS SILICA NANOPARTICLES

Modified from a paper published in *Biomaterials* **2011**, *32*, 6234

Chih-Hsiang Tsai, Juan L. Vivero-Escoto, Igor I. Slowing, I-Ju Fang, Brian G. Trewyn, and
Victor S.-Y. Lin

Abstract

A series of mesoporous silica nanoparticles (MSNs) were synthesized using the co-structure directing method. A non-toxic anionic surfactant, undec-1-en-11-yltetra(ethylene glycol) phosphate monoester (PMES), was used as a structure directing agent (SDA) together with aminopropyltrimethoxysilane that functioned as a co-structure directing agent (CSDA). The morphology and mesoporous structure of these materials were tuned by changing the molar ratio of CSDA and SDA. The formation mechanism of these PMES-MSN materials was discussed, and in agreement with the “aggregate-growth” mechanism proposed by Rankin *et al.* We also found that the PMES-MSNs with radially-aligned mesostructure were suitable for nanocasting applications.

For biological applications, these PMES-MSN materials containing PMES inside the pores showed excellent biocompatibility *in vitro*. The cellular internalization and endosome escape of PMES-MSNs in cervical cancer cells (HeLa) was demonstrated by flow cytometry and confocal fluorescence microscopy, respectively. The PMES-MSNs were used as drug

delivery carriers for resveratrol, a low water-solubility drug, by taking advantage of the hydrophobic environment created by the PMES micelle inside the pores. This surfactant-assisted delivery strategy was tested under physiological conditions showing an increase of the drug loading compared to the material without surfactant and steady release of resveratrol. In addition, the resveratrol-loaded PMES-MSN proved to be stimuli-responsive to the concentration of Ca^{2+} . A cascade pattern of release profile was obtained by a stepwise addition of Ca^{2+} into the mixture. Finally, the therapeutic properties of resveratrol-loaded PMES-MSNs were evaluated *in vitro* using HeLa and Chinese ovarian cells. We envision that this surfactant-assisted drug delivery method using MSNs as nanovehicles would lead to a new generation of carrier materials for intracellular delivery of a variety of hydrophobic therapeutic agents.

1. Introduction

Every year hundreds of new therapeutic drugs emerge from drug discovery programs; however, the majority of these innovative drugs display very poor aqueous solubility, resulting in poor bioavailability and low pharmacokinetics *in vivo*.¹⁻³ To overcome this hurdle different strategies based on nanomaterials have been developed such as liposomes, polymers, dendrimers and inorganic nanoparticles.⁴⁻¹² Mesoporous silica nanoparticles (MSNs) have attracted a great deal of attention due to their growing applications in nanomedicine and biotechnology.¹³⁻¹⁶ Recently, MSN materials with large surface area and pore volumes have been investigated for their potential use as drug delivery system.¹⁷⁻²¹ In

addition, the MSN platform possesses other advantageous properties important to therapeutic nanocarriers such as facile multi-functionalization, excellent biocompatibility *in vivo* and *in vitro*, easy endocytosis by a wide variety of cell types and biodegradability.²²⁻³⁰ Different strategies have been used to encapsulate therapeutic agents; typically, the drug molecules are loaded into the channels of MSNs after removal of the surfactant template. In addition, drug-loaded MSNs can be further capped with organic nanodevices and/or inorganic nanoparticles to develop “zero premature release” intracellular delivery systems.³¹⁻³⁹ However due to the hydrophilic surface properties of MSNs the entrapment of hydrophobic drugs is usually very low. To overcome this issue, different research groups have functionalized the interior surface of MSNs with hydrophobic groups to increase the loading and improve the release kinetics of low-water solubility drugs.^{18,40,41} One interesting approach is to take advantage of the surfactant template as an adjuvant to increase the amount of drug loaded and to improve the release kinetics of therapeutic agents under physiological conditions. Nevertheless, few reports were found in the literature that applied this methodology.^{42,43} One probable reason is that the surfactant template typically used for synthesizing MSNs is cetyltrimethylammonium bromide (CTAB). CTAB is a highly toxic surfactant not suitable as a drug delivery adjuvant for neither *in vitro* nor *in vivo* applications.⁴⁴ Indeed, Shi and co-workers recently reported on the application of MSNs as anticancer drug delivery vehicles where the surfactant, CTAB, was used as the toxic agent. Interestingly, in this paper they also demonstrated the surfactant-assisted drug delivery approach using camptothecin.⁴⁵ This therapeutic agent was loaded into the channels of MSNs still containing CTAB to increase the toxicity of this material. However, the further development of MSN-based surfactant-assisted drug delivery systems will require non-toxic surfactant templates with adjuvant properties. Herein, we report the

synthesis and therapeutic applications *in vitro* of a series of novel radial MSNs via the co-structure directing route.⁴⁶⁻⁴⁸ We first synthesized a phosphate monoester anionic surfactant (PMES) that was used as structure-directing agent (SDA) and aminopropyltrimethoxysilane as co-structure directing agent (CSDA). These nanomaterials present unique morphology and mesopore structure that can be tuned by changing the molar ratio of CSDA and SDA. A clear trend of phase transition was observed as the increase of the amount of CSDA. In addition, by scrutinizing TEM images, we suggested that the formation mechanism of these PMES-MSN materials with unique radially-aligned mesopores follows the aggregate-growth mechanism. To further understand the core structure of PMES-MSNs, we replicated the PMES-MSNs to yield mesoporous carbon using furfuryl alcohol as the carbon source. The reproduced mesoporous carbon material exhibited similar pattern of mesopores as the PMES-MSNs with surface area up to $1400 \text{ m}^2 \text{ g}^{-1}$.

We demonstrated that MSNs containing the PMES inside of the nanochannels (PMES-MSNs) are non-cytotoxic. The endosome escape and cellular internalization of PMES-MSN nanovehicles were observed on cervical cancer (HeLa) cells by confocal microscopy and flow cytometry, respectively. As depicted in Figure 1, we took advantage of the hydrophobic environment of the PMES-MSNs channels to load a poorly water-soluble drug, resveratrol. This is a biogenic agent with novel therapeutic activity and preventative properties toward a wide variety of illnesses such as cancer, heart disease, myocardial infarction, stroke and brain damage.^{49,50} The loading and controlled release of resveratrol was successfully evaluated under simulated physiological conditions. An increased loading amount of resveratrol and sustained controlled release was obtained from the PMES-MSN material. Furthermore, we

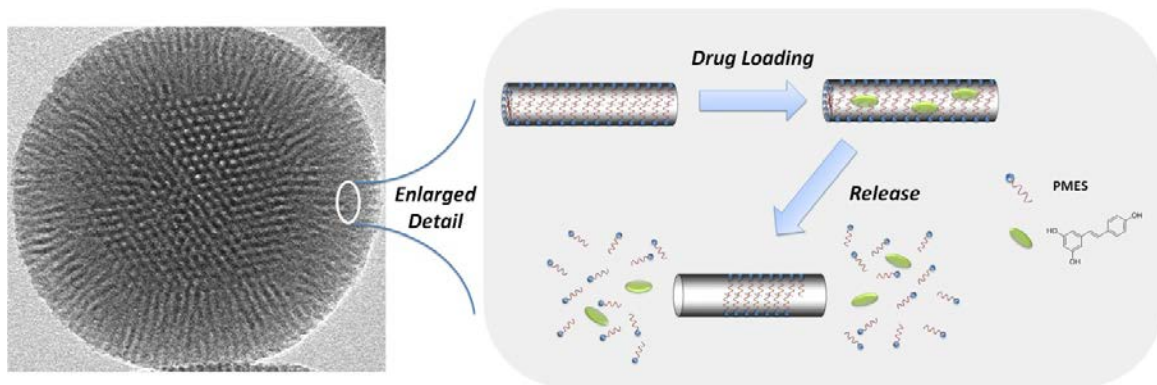


Figure 2-1 Schematic illustration of the surfactant-assisted drug delivery system. Surfactant containing PMES-MSN was soaked into a concentrated resveratrol solution. The hydrophobic tails of surfactant help to adsorb hydrophobic drugs. During the course of release, the surfactant molecules come out together with drugs in a dilute solution.

found that the release of this surfactant-assisted system can be triggered by adding Ca^{2+} ions. Due to strong interaction between Ca^{2+} ions and phosphate groups,⁵¹ the positively charged amine groups (CSDA) would be exchanged to Ca^{2+} , leading to a faster release of Ca-PMES. It is known that calcium ions are a vital element in the process of neurotransmitter release; when Ca^{2+} channels are blocked, neurotransmitter release is inhibited.⁵² Therefore, this particular release system may have great potential for the development of calcium sensors. Finally, the therapeutic effect of this resveratrol-loaded PMES-MSNs system was also tested *in vitro* using Chinese hamster ovarian (CHO) and HeLa cells.

2. Materials and Methods

2.1 Reagents and materials

Aminopropyltrimethoxysilane (APTMS) and tetraethylorthosilicate (TEOS) were purchased from Gelest Inc. Cetyltrimethylammonium bromide, 11-bromoundec-1-ene,

tetraethylene glycol, phosphorus oxychloride, triethylamine, sodium hydroxide, fluorescein isothiocyanate (FITC), aluminum chloride, furfuryl alcohol, resveratrol, and Hoechst 33258 were purchased from Aldrich. Endosome marker (FM 4-64) was purchased from Invitrogen, Inc. Donor equine serum was purchased from HyClone. L-alanyl-L-glutamine, gentamicin sulfate, and penicillin-streptomycin solution were purchased from Mediatech, Inc. All chemicals were used as received.

2.2 Synthesis of undec-1-en-11-yltetra(ethylene glycol) (1)

Compound **(1)** (Scheme 1) was synthesized according to the procedure reported in the literature.⁵³ Briefly, a mixture of 7 mL of NaOH_(aq.) (50%, 88.6 mmol) and 150 mL of tetraethylene glycol (87 mmol) was stirred for 30 min in an oil bath at 100 °C under argon atmosphere. Then 18.6 mL of 11-bromoundec-1-ene (85 mmol) was added dropwise. After 24 h, the reaction mixture was cooled and extracted three times with hexanes. The combined hexanes were dried with magnesium sulfate and concentrated at reduced pressure to afford a yellowish oil. The crude oil was purified by column chromatography on silica gel using ethyl acetate/hexanes (1:1, v/v) to give the pure product (17.83 g, 60.5% yield). Proton NMR of **(1)** matches that has been reported in literatures.

2.3 Synthesis of phosphate monoester surfactant (PMES) (2)

The synthesis of compound **(2)** was carried out according to the following procedure: 50 mL of phosphorus oxychloride (546.2 mmol) and 50 mL of dry benzene were added to a two-neck round-bottom flask, and stirred in an ice bath under argon for 30 min. Then, a solution of 10 g of reagent **(1)** (29 mmol) and 4.1 mL of triethylamine in 50 mL dry benzene

was added dropwise over a period of 3 h. After addition the reaction mixture was stirred for 20 h at room temperature, the resulting salts were filtered and the filtrate was concentrated to give a dark brown oil. To obtain the hydrolyzed product; the crude oil was added dropwise into 100 mL ice-cold water over a period of 1 h under vigorous stirring, and then stirred for additional 5 h at room temperature. The reaction mixture was extracted with copious ethyl acetate. After that, the combined organic portions were washed twice with an aqueous solution of HCl (1.0 M) and brine solution, and finally dried by magnesium sulfate. After the organic solution was concentrated by rotary evaporation, the afforded product was a viscous, yellow oil (8.5 g, 85% yield). ^1H NMR (400MHz, CDCl_3): δ 1.27-1.35 (s, 12H); 1.58 (m, 2H, $J=7\text{Hz}$); 2.04 (dd, 2H, $J=7\text{Hz}$); 3.46 (t, 2H, $J=7\text{Hz}$); 3.59-3.73 (m, 14H); 4.20 (m, 2H); 4.91-5.05 (m, 2H); 5.75-5.87 (m, 1H); ^{31}P NMR (168MHz, CDCl_3): δ 2.67. MS (ESI, m/z): $[\text{M}+\text{H}]^+$ calcd for $\text{C}_{19}\text{H}_{39}\text{O}_8\text{P}$, 427.5; found, 427.

2.4 Synthesis of PMES-templated mesoporous silica nanoparticles (PMES-MSNs)

The synthesis of PMES-MSN materials were carried out following a procedure previously published in the literature with some modifications.⁴⁶ Briefly, the structure-directing agent, PMES, (0.213 g, 0.5 mmol) was dissolved in 100 mL of nanopure water and stirred vigorously at 80 °C for 1 h. Then, APTMS was added dropwise into the solution, followed by the addition of TEOS (1 mL, 4.5 mmol) at the rate of 20 mL h⁻¹. Different molar ratios of APTMS and PMES were used to modify the structural properties of PMES-MSNs (the amount of PMES was kept constant in 0.5 mmol for all the samples), see Table 2-1. The reaction mixture was stirred vigorously at 80 °C for 10 min and then aged at the same temperature for additional 24 h. The resulting as-made PMES-MSNs were isolated by

filtration, washed with 300 mL of nanopure water and 100 mL of methanol, and then dried under vacuum at room temperature overnight. To remove the SDA, two methods were used: calcination at 600 °C for 6 h or acid-extraction. In the case of the acid-extraction the following conditions were used; 100 mg of as-made PMES-MSN material was dispersed in an acid solution of concentrated HCl (2 mL) and acetonitrile (50 mL). This mixture was stirred for 4 h at room temperature, and followed by filtration. Finally, the dispersion was washed with copious amount of water and dried under high vacuum overnight.

2.5 Fluorescein isothiocyanate (FITC) labeled PMES-MSNs (FITC-PMES-MSN)

A solution of FITC (7.8 mg, 0.02 mmol) and APTMS (4.5 μ L, 0.024 mmol) in 2 mL of dry methanol was stirred at room temperature for 2 h under argon. After the reaction was complete, 1.0 mL of this solution was injected into a previously prepared dispersion of 0.1 g of PMES-MSN material in 10 mL of dry toluene. The reaction mixture was refluxed for 6 h under argon. The resulting orange solid was filtered, washed thoroughly with methanol and dried under vacuum for 24 h.

2.6 Carbon replication of PMES-MSN

Typically, the carbon replication of PMES-MSN followed similar strategy developed by Ryoo et al.⁵⁴ First, 85 mg $AlCl_3$ was added into a dry ethanol solution containing 0.7625 g surfactant-free PMES-MSN. The mixture was stirred for 1 hour at room temperature. A great amount of hydrogen chloride gas was generated during the reaction. After reaction, the white powder product Al-PMES-MSN was collected under reduced pressure to remove the ethanol. Second, furfuryl alcohol as the carbon source was impregnated to the Al-PMES-MSN.

Furfuryl alcohol (0.458 mL) was hard pressed portion by portion into the mesopores of Al-PMES-MSN (0.6893 g). The mixture was vortexed for 30 min in between each portion of furfuryl alcohol added. After mixing, the mixture was transferred to a schlenk flask, followed by three cycles of freeze-pump-thaw to remove air and oxygen. The flask was placed in a convection oven at 35 °C for 1 h, then at 90 °C for 8 h. The third step is the pyrolysis process. The afforded polymer-Al-PMES-MSN was placed in a tube furnace for pyrolysis. The temperature ramp was set at 5.4 °C min⁻¹ to 350 °C for 3 h under vacuum. A deep brownish product was obtained after pyrolysis. The resulting product was then analyzed by nitrogen sorption technique to determine if all mesopores were filled with carbon. The impregnation-polymerize-pyrolysis process was repeated three times to obtain the carbon-silica composite material. At final run, the pyrolysis temperature was raised to 900 °C for 2 h. The silica template then was digested by concentrated HF/ethanol (49%) solution to yield the replicated mesoporous carbon.

2.7 Characterization of materials

Surface analysis of the PMES-MSN materials was performed by nitrogen sorption isotherms at 77K with a Micromeritics Tristar surface area and porosity analyzer. The surface area and median pore diameter were evaluated by the Brunauer-Emmett-Teller (BET) and the Barret-Joyner-Halenda (BJH) methods, respectively. The powder diffraction patterns of PMES-MSNs were measured by Scintag XDS-2000 powder diffractometer using a Cu K α radiation source. Low angle diffraction with a 2 θ range of 1 to 7 degrees was used to investigate the long-range order of the materials. Particle morphology was determined by scanning electron microscopy (SEM) using a Hitachi S4700 FE-SEM system with 10 kV

accelerating voltage and 0.005 nA of beam current for imaging. Tecnai G² F20 transmission electron microscopy (TEM) operated at 200 kV was used to examine the mesostructure of materials. Thermogravimetric analysis (TGA) was recorded using TA instruments TGA 2950 thermogravimetric analyzer with a temperature ramp of 2 °C min⁻¹ from 25 °C to 800 °C under air.

2.8 Biocompatibility of PMES-MSNs in vitro

To examine the biocompatibility of the PMES-MSNs, we selected the sample with a molar ratio of CSDA/SDA $x = 2.0$. For clarification, all the *in vitro* and drug delivery experiments were carried out with this material; so, hereafter the term PMES-MSNs will refer to the PMES-MSN-2 sample. HeLa cells were seeded in six-well plates with a density of 1×10^5 cells mL⁻¹ in 3 mL of D-10 medium (Dubelcco Modified Eagle's Medium with horse serum, L-alanyl-L-glutamine, gentamicin sulfate and penicillin-streptomycin solution), and incubated at 37 °C with a 5% CO₂ atmosphere for 24 h. Then, the cells were seeded with different concentrations of PMES-MSN material (10, 20, 50, 100 µg mL⁻¹) in D-10 serum for other 48 h. After the incubation each well was washed with PBS and the cells were trypsinized, centrifuged, and re-suspended in D-10 medium. Viability was determined by the Guava ViaCount cytometry assay (Millipore Corporation).

2.9 Measurement of the internalization of PMES-MSNs in HeLa cells by flow cytometry

HeLa cells were seeded at the density of 1×10^5 cells per well in six-well plates in 3 mL D-10 medium. After incubation for 24 h, the D-10 medium was replaced by 3 mL of FITC labeled PMES-MSN material suspensions at different concentrations (1, 10, 25, 50, and 100

$\mu\text{g mL}^{-1}$) in the serum-free DMEM medium for 10 h. All the tests were run in triplicate. The cells were washed with medium, harvested by trypsinization and, after centrifugation, re-suspended in 0.4% trypan blue PBS solution to quench any fluorescence from material physisorbed to the cell membrane. The samples were analyzed by flow cytometry with a Becton-Dickinson FACSCanto cytometer using a DB-FACS Diva⁵⁵ software. To distinguish the true fluorescence generated by the endocytosed FITC-labeled material from the natural autofluorescence of cells, a threshold of fluorescence intensity was established by performing the flow cytometry analysis on the cells incubated without FITC-labeled material. The threshold was set at an intensity of fluorescence slightly above the highest value observed for control samples (HeLa cells only). The number of cells with endocytosed FITC-labeled material was determined by counting those that showed fluorescence intensity higher than the threshold.

2.10 Intracellular localization of PMES-MSNs in the presence of an endosome marker

HeLa cells were seeded in six-well plates with a density of 5×10^4 cells mL^{-1} in 3 mL of D-10 medium containing coverslips at the bottom of the well. After incubation for 36 h at 37 °C with a 5% CO_2 atmosphere, the D-10 medium was replaced by 3 mL of FITC-labeled PMES-MSN material ($15 \mu\text{g mL}^{-1}$) and endosome marker FM 4-64 ($5 \mu\text{g mL}^{-1}$) in D-10 medium and incubated for another 10 h. The cells were washed with PBS twice and replaced by 3 mL nuclei-staining dye Hoechst 33258 ($8.3 \mu\text{g mL}^{-1}$) in D-10 medium. After incubation for 30 min, the coverslips were placed in microscope slides and visualized under a Leica TCS NT confocal fluorescence microscope system using a 100x oil immersion objective.

2.11 Loading of resveratrol in PMES-MSNs

PMES-MSNs were loaded with resveratrol using the following procedure: resveratrol (11.4 mg, 0.05 mmol) was dissolved in 100 mL of water/ethanol (9:1 v/v). Then, PMES-MSNs (300 mg) were added to 40 mL of this solution and stirred for 24 h at room temperature. All the experiments were protected from light with aluminum foil to avoid the photo-isomerization of resveratrol under UV light (365 nm). After that, the material was centrifuged, washed twice with a solution of water/ethanol (9:1 v/v) to remove any physisorbed resveratrol, and dried under vacuum for 24 h. To quantify the amount of resveratrol loaded in PMES-MSNs, the supernatant and all washing solutions were collected and analyzed by HPLC (Varian, model ProStar 210 coupled with a diode array detector ProStar 335) under the following conditions: Pursuit-C₁₈ column (250 × 4.6 mm, 5 μm particle size) at room temperature, the mobile phase was composed of methanol and water (50/50, v/v) and the flow rate was set at 1 mL min⁻¹. Detection was performed at 286 and 306 nm, which are the characteristic wavelengths of cis- and trans-resveratrol, respectively.

2.12 Release of resveratrol from PMES-MSNs in phosphate buffer solution (pH=7.4)

Resveratrol-loaded PMES-MSN material (10 mg) was re-dispersed in 40 ml of PBS solution (10 mM, pH=7.4) and stirred at room temperature. Aliquots were periodically removed (1 mL) and PMES-MSN material was isolated by centrifuge. The supernatant was analyzed following the HPLC method previously described.

2.13 Calcium stimuli-responsive release of resveratrol from PMES-MSNs in phosphate buffer solution (pH=7.4)

Resveratrol-loaded PMES-MSN material (20 mg) was re-dispersed in 20 ml of PBS solution (10 mM, pH=7.4) and stirred at room temperature. Various amount of calcium nitrate or sodium nitrate were added into the mixture. Aliquots were periodically removed (1 mL) and PMES-MSN material was isolated by centrifuge. The supernatant was analyzed following the HPLC method previously described. For cascade release experiment, 325 mg of $\text{Ca}(\text{NO}_3)_2$ was added for each shot, which was corresponding to 25 mM of $[\text{Ca}^{2+}]$, and aliquots were periodically analyzed following the HPLC method.

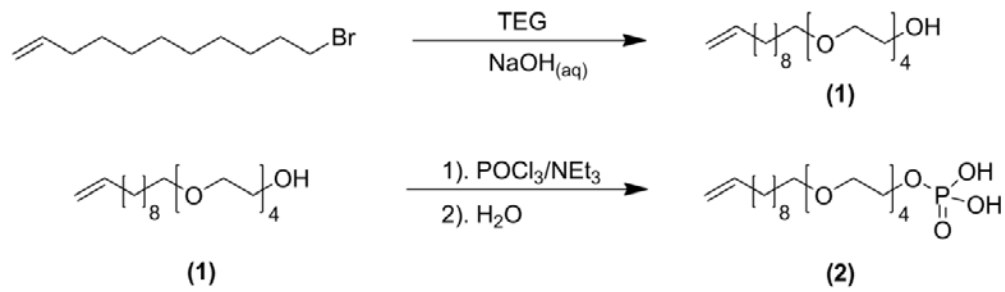
2.14 Intracellular toxicity of resveratrol-loaded PMES-MSNs in vitro

Either HeLa or Chinese ovarian (CHO) cells were seeded in six-well plates with a density of 1×10^5 cells mL^{-1} in 3 mL of D-10 medium (Dubelcco Modified Eagle's Medium with horse serum, L-alanyl-L-glutamine, gentamicin sulfate and penicillin-streptomycin solution), and incubated at 37 °C with a 5% CO_2 atmosphere for 24 h. Then, the cells were seeded with different materials, PMES-MSNs, resveratrol-loaded calcined PMES-MSNs, and resveratrol-loaded PMES-MSNs, at a concentration of $100 \mu\text{g mL}^{-1}$ in D-10 serum for other 48 h. After the incubation each well was washed with PBS and the cells were trypsinized, centrifuged, and re-suspended in D-10 medium. Viability was determined by the Guava ViaCount cytometry assay (Millipore Corporation).

3. Results and Discussion

3.1. Preparation and characterization of PMES-MSNs

To construct the PMES-MSN materials, we first synthesized the surfactant PMES. The synthetic pathway is detailed on the experimental section and outlined in Scheme 2-1. This surfactant contains an anionic, phosphate head group; ethylene glycol units to improve its biocompatibility and solubility in aqueous solutions; a hydrophobic moiety for the formation of micelles and loading of hydrophobic molecules; finally, a functional group at the end of the hydrophobic chain for further modification. The capability of self-assembly of PMES molecules was measured by dynamic light scattering (DLS) technique. It is noted that at neutral aqueous solution, self-assembled aggregates of PMES can be detected at concentration around 1 mM. (Figure 2-S1) In basic solution (pH =11), PMES tended to self-assemble at concentration as low as 0.6 mM. This can be attributed to deprotonation of phosphoric acid group to phosphate group in higher pH conditions, which results in larger effective head group area favoring the formation of spherical micelle. These results demonstrated that PMES are capable of serving as structure directing agent for the synthesis of mesoporous materials. The synthesis of the nanostructured materials was carried out by following a co-structure directing method previously reported in the literature with slight modifications.⁴⁶ By fine-tuning the reaction conditions and the molar ratio of CSDA/SDA, we have successfully synthesized a series of mesoporous silica nanoparticles with different particle size, morphology, and mesopore structure (PMES-MSN-x; where x denoted as the APTMS/PMES molar ratio; x = 1.0, 1.5, 2.0, 2.5, 3.0, and 4.0). It is noteworthy to point out that we did not observe the formation of mesoporous material in the absence of CSDA (x = 0).



Scheme 2-1 Synthetic pathway of phosphate monoester surfactant (PMES).

The particle size and morphology of the PMES-MSN-*x* materials were characterized by SEM (Figure 2-2). The micrographs showed that the particle size increased with higher values of *x*. For instance, when the molar ratio is equal to 1.0, the material obtained is spherical-shaped nanoparticles with a size distribution around 150 nm (Figure 2-2a). When the molar ratio was increased to 2.0, the materials continued to be monodisperse nanoparticles with spherical morphology but having a larger particle size around 300 nm (Figure 2-2c). Further increase of the molar ratio resulted in micron-sized aggregated materials (Figure 2-2e to 2f).

The mesopore structure of these materials was determined by TEM, powder X-ray diffraction (PXRD), and nitrogen sorption isotherms. Figure 2-3 shows the TEM images of calcined PMES-MSN-*x* materials. As was observed with the particle size of the PMES-MSN-*x* materials, CSDA/SDA molar ratio also affects the pore structure of the MSNs. For example, at small *x* value the resulting product shows urchin-like mesopore arrangement (Figure 2-3a). Once the ratio is increased, the pore structure starts to transform from urchin-like to a radially-aligned pore pattern, as can be seen in Figures 2-3b-3f. It is interesting to

note that even the rod-like particle shows radial orientation of the mesopores (Figure 2-3f). In addition to the pore structure becomes more ordered, the

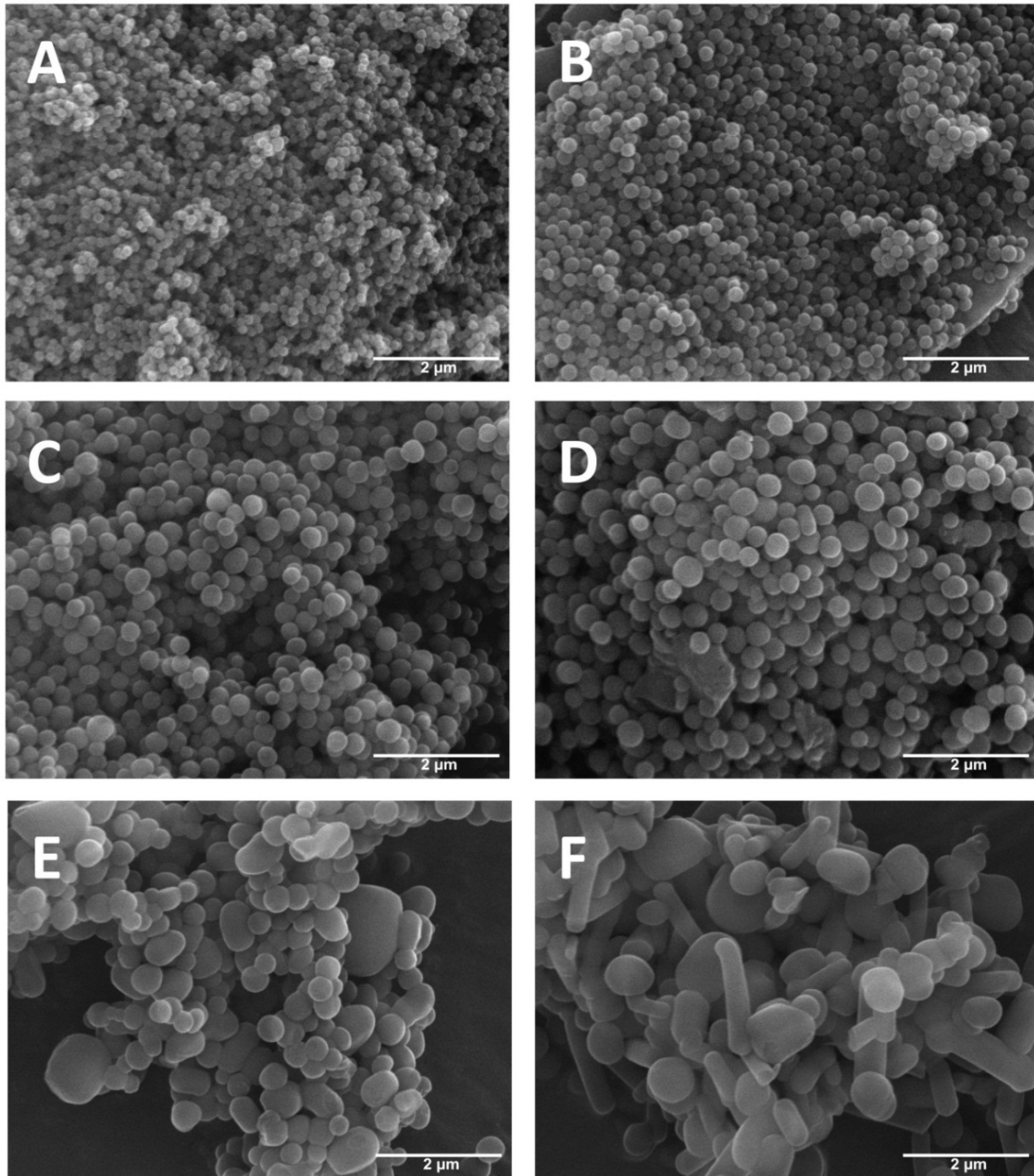


Figure 2 SEM images of samples synthesized with different molar ratios of APTMS to PMES. PMES concentration was 5 mM in all cases. (a) PMES-MSN-1; (b) PMES-MSN-1.5; (c) PMES-MSN-2; (d) PMES-MSN-2.5; (e) PMES-MSN-3; (f) PMES-MSN-4.

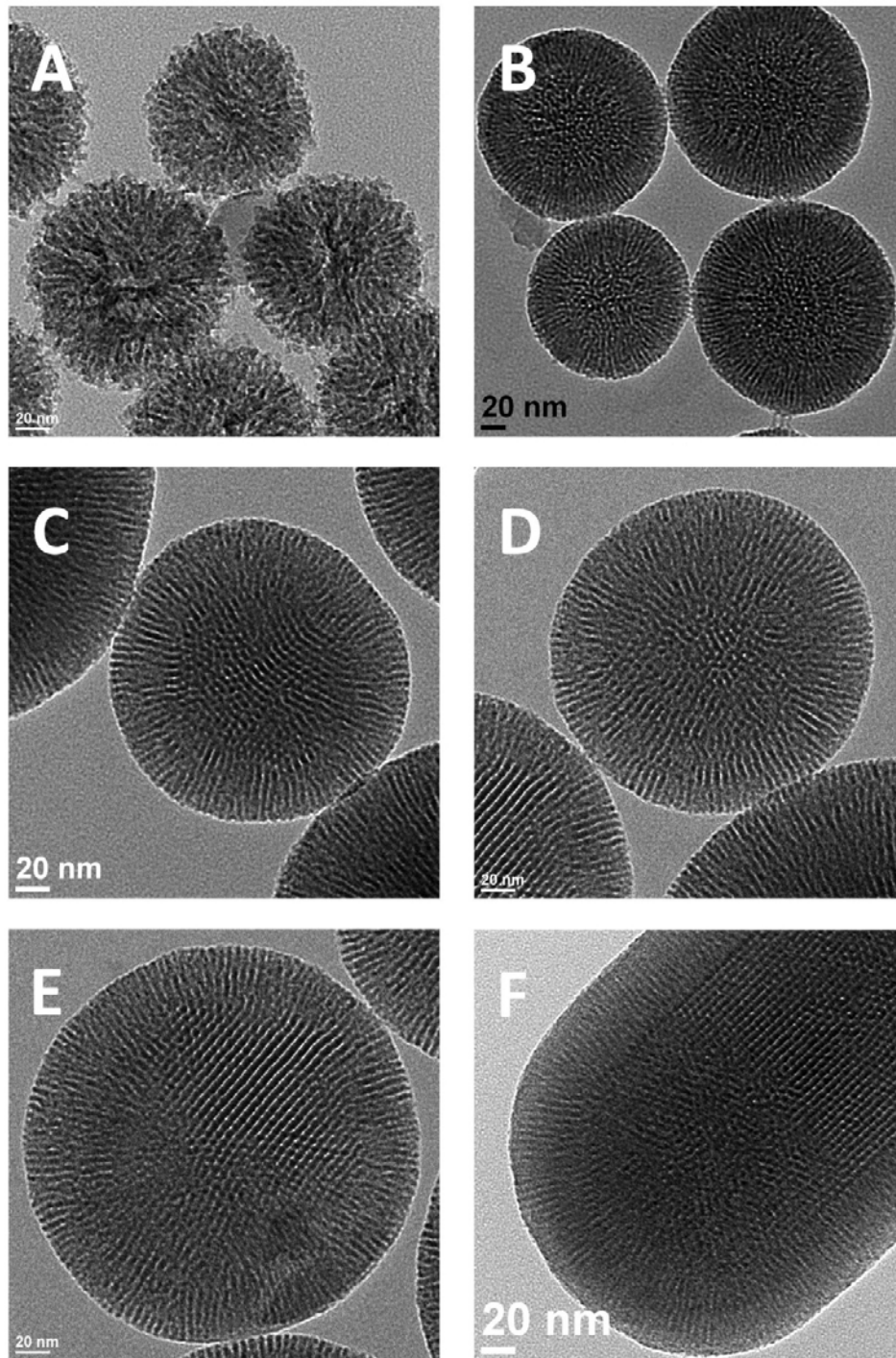


Figure 2-3 TEM images of surfactant-free samples synthesized with different molar ratios of APTMS to PMES. PMES concentration was 5mM in all cases. (a) PMES-MSN-1; (b) PMES-MSN-1.5; (c) PMES-MSN-2; (d) PMES-MSN-2.5; (e) PMES-MSN-3; (f) PMES-MSN-4.

particle surface also becomes smoother with the increase of the x value, which could be indicative of more complete condensation of materials.⁵⁶ Powder XRD patterns of calcined PMES-MSN-x materials confirmed these observations (Figure 2-4 and Table 2-1). As was depicted in TEM images, PXRD data confirmed that the PMES-MSN-x materials improve their pore structure ordering along with the increase in the ratio of x. The PXRD patterns of PMES-MSN-1 and PMES-MSN-1.5 displayed a broad peak around $2\theta=1.5^\circ$, characteristic of materials with disordered mesochannels. In addition, nitrogen sorption isotherms of PMES-MSN-1 material exhibit the type IV pattern with large hysteresis loop starting at $P/P_0=0.45$ (Figure 2-5a), as a possible indication of slit-shaped mesostructure. This feature was also

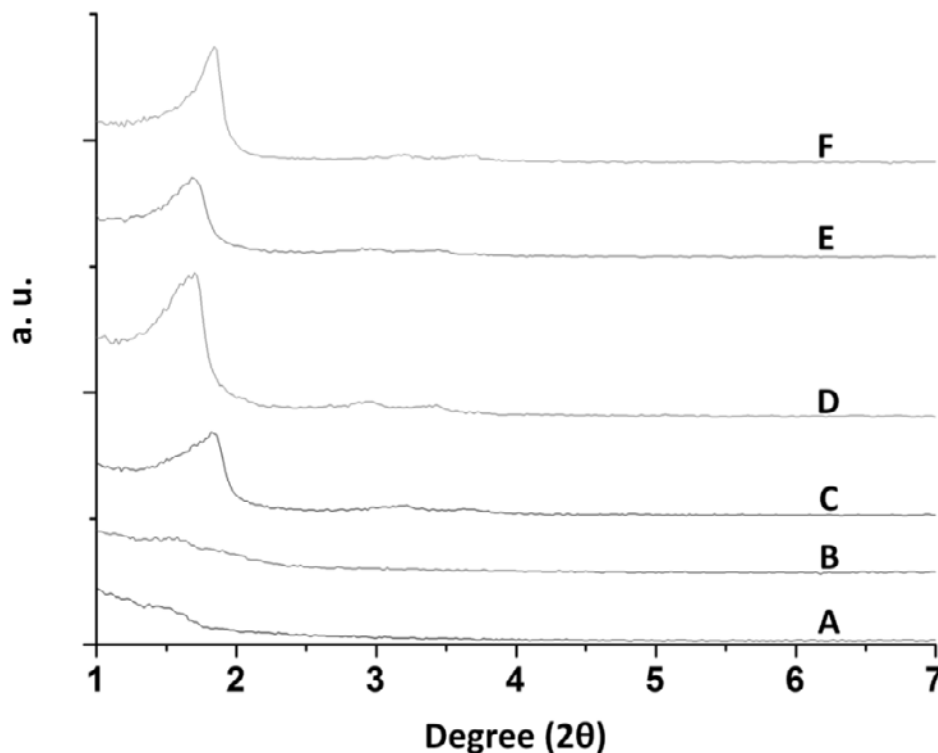


Figure 2-4 Powder X-ray diffraction pattern of calcined PMES-MSNs: (a) PMES-MSN-1; (b) PMES-MSN-1.5; (c) PMES-MSN-2; (d) PMES-MSN-2.5; (e) PMES-MSN-3; (f) PMES-MSN-4.

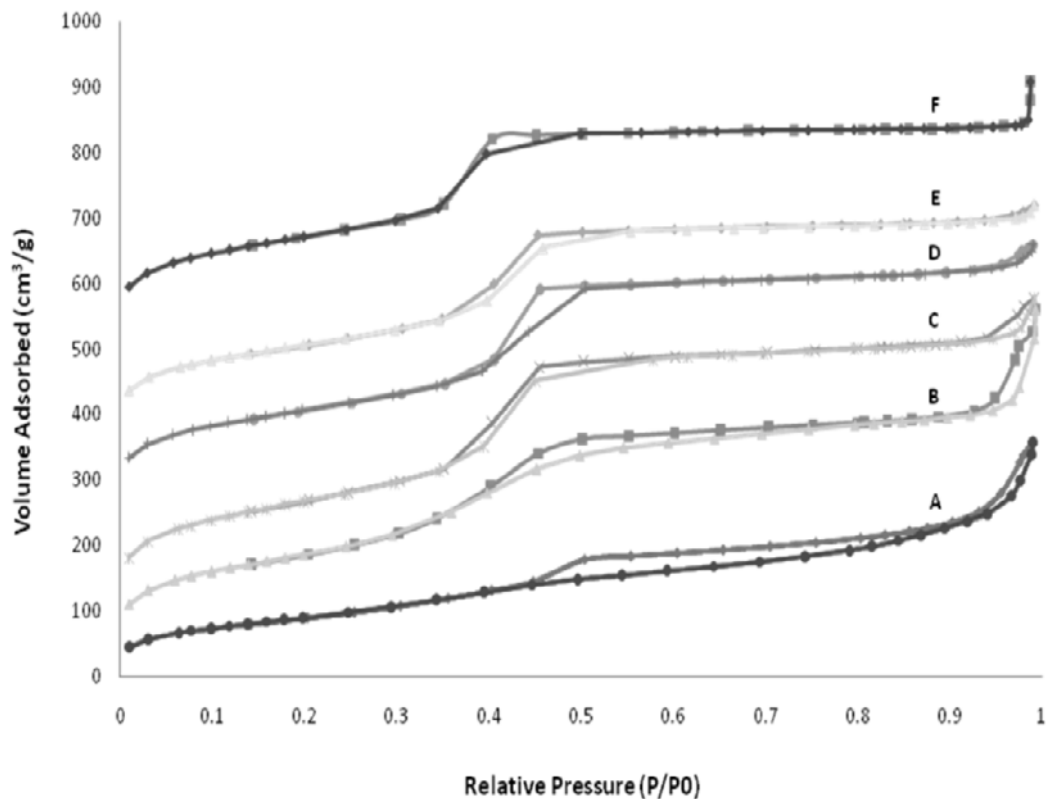


Figure 2-5 Nitrogen sorption isotherms of calcined PMES-MSNs: (a) PMES-MSN-1; (b) PMES-MSN-1.5; (c) PMES-MSN-2; (d) PMES-MSN-2.5; (e) PMES-MSN-3; (f) PMES-MSN-4.

observed in the TEM images (Figure 2-3a). As the ratio x increases, PMES-MSN- x materials with well-ordered radially aligned mesopores are observed, as it is demonstrated by the three peaks of the typical XRD pattern of the mesoporous silica with the 2D hexagonal symmetry (Figure 2-4c to 4f). Moreover, nitrogen sorption plots showed type IV isotherms confirming the mesoporosity of these materials (Figure 2-5c to 5f). It is interesting to note that the nitrogen isotherms of PMES-MSN-1.5 material are in transition from slit-like mesochannels to cylindrical mesopores (Figure 2-5b), which is in agreement with the transformation observed by TEM images. The structural parameters of PMES-MSN- x materials are summarized in Table 2-1. All the samples, with exception of PMES-MSN-1, have BET

surface area and pore volume larger than $550 \text{ m}^2 \text{ g}^{-1}$ and $0.5 \text{ cm}^3 \text{ g}^{-1}$, respectively. The pore size of these PMES-MSN-x samples is around 3-4 nm, as calculated from BJH method.

Table 2-1 The physicochemical structural data of PMES-MSNs.

Sample (PMES-MSN-x)*	d_{100}^9 [a]	a_0^9 [b]	S_{BET} [m^2/g] [c]	D_{BJH}^9 [d]	V_p [cm^3/g] [e]
PMES-MSN-1	-----	-----	313.58	Broad range	0.43
PMES-MSN-1.5	-----	-----	574.46	2.7-3.3	0.61
PMES-MSN-2	4.85	5.6	684.19	3.4	0.71
PMES-MSN-2.5	5.30	6.12	568.87	3.7	0.59
PMES-MSN-3	5.19	5.99	566.16	3.4	0.54
PMES-MSN-4	4.79	5.53	599.52	3.1	0.53

* x denoted as the APTMS/PMES molar ratio. [a] Calculated from XRD data. [b] The lattice parameter calculated by $a=2d_{100}/\sqrt{3}$. [c] S_{BET} represents the surface area calculated by BET method. [d] D_{BJH} represents the pore diameter evaluated from BJH method. [e] Pore volume, calculated at $P/P_0 = 0.97$.

Two mechanisms have been proposed for the synthesis of MSNs with radially oriented mesopores; the “nucleation and growth” mechanism reported by Van Tendeloo and co-workers,^{22,57} and the “aggregate and growth” mechanism described by Rankin and co-workers.⁵⁸ The first mechanism is based on the formation of 3D-cubic nuclei at the initial stage of the reaction (nucleation), followed by the epitaxial growth of the cylindrical channels from the nuclei. On the contrary, the “aggregate and growth” mechanism explains the formation of radially oriented pores by the formation of micelle- silica composites that initially nucleate to afford disordered clusters. These clusters then aggregate into spherical particles, followed by re-alignment of micelles at the particle surface. Interestingly, the authors also observed the formation of peanut shape nanoparticles that seemed to be formed

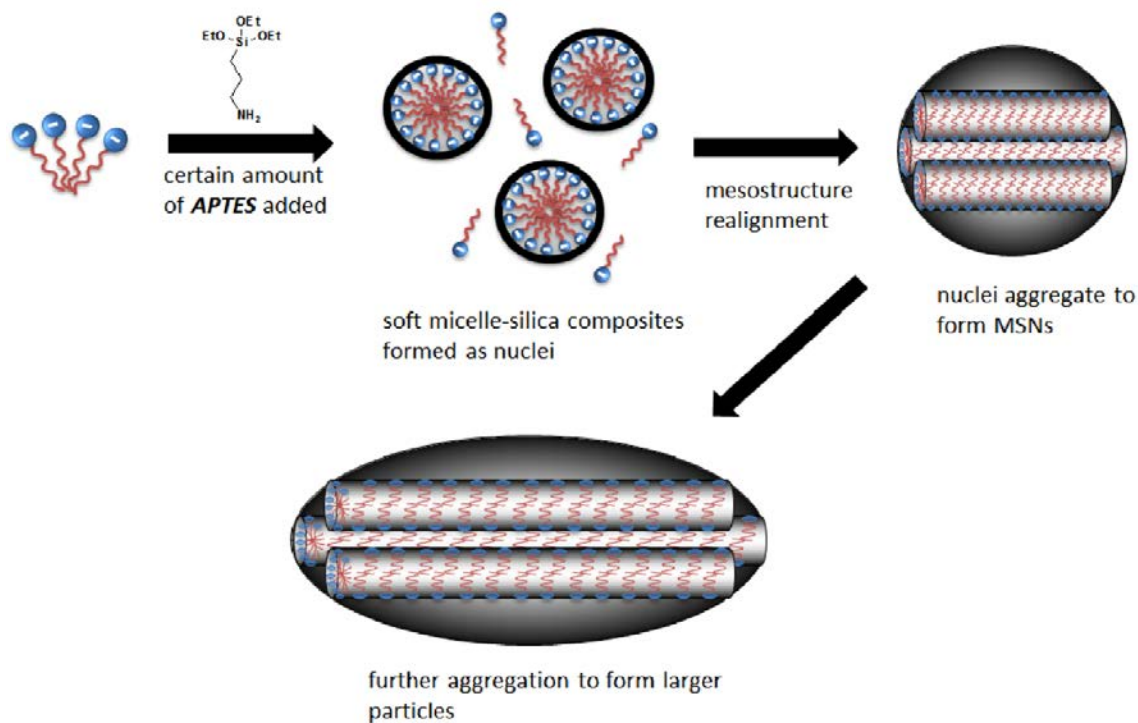


Figure 2-6 Schematic representation of formation mechanism of PMES-MSNs.

by aggregation of two or more spherical particles. The formation of the radial orientation of mesopores is postulated to be driven by, “the interface between the silica/surfactant phase and the mixed ethanol/water solvent being equally attractive toward polar and nonpolar species”.⁵⁸ Recently, Wang and co-workers also suggested this mechanism to account for the formation of anionic surfactant-templated MSNs with radially oriented mesopores.⁵⁹ In our case, some evidences indicate that the formation of PMES-MSNs could be following the steps described by the aggregate and growth mechanism as shown in Figure 2-6. First, we observed many dumbbell-shaped particles in the case of higher x of PMES-MSNs (Figure 2-2d to 2f), that appear to be formed by fusion of two or more individual spherical particles. If the mechanism was nucleation and growth by monomer addition, then all particles would be expected to be spherical since the rate of growth should be the same in all directions. In

addition, the orientation of the mesopores in the particle shell is always radial to its surface, even in dumbbell-shaped nanoparticles (Figure 2-3f). This implies that the alignment of the mesopores in the shell could form independently of the mesopores in the core. This observation supports the interfacial orientation mechanism proposed by Rankin and co-workers.⁵⁸ Finally, as was rationalized by Wang and co-workers, the electrostatic interaction sites between the SDA (PMES) and CSDA (APTMS) plays an important role to control the mesostructure of the silica nanoparticles.⁵⁹ We described above that for the synthesis of PMES-MSNs the increase of the ratio CSDA to SDA improved the pore structure ordering, a value of $x \geq 2.0$ afforded radially aligned pore patterns. This performance can be explained by the amount of interaction sites between PMES and APTMS. When x is below 2.0, the charge density matching between head-groups of surfactant molecules and amino groups of the APTMS is not favorable for the formation of stable micelle-silica composites, due to the fact that the phosphate head-groups bear two negative charges under this reaction conditions.⁶⁰ At $x \geq 2.0$, a larger amount of interaction sites of PMES and APTMS are formed, giving rise to well-ordered mesostructure.

3.2 Carbon replication of PMES-MSNs

The technique of nanocasting for manufacturing ordered mesoporous carbon (OMC) materials has been widely reported elsewhere.⁵⁴ In principle, mesoporous silica with a specific structure is impregnated with carbon precursors. Subsequent polymerization and pyrolysis of the carbon sources lead to a carbon-silica composite material, where the mesopores of mesoporous silica are filled with carbon. The silica template later is removed by HF or NaOH to give the mesoporous carbon. It is important to note that the mesostructure of

silica template is critical to the nanocasting application. That is, a 3-D mesostructure of silica template, in which mesopores are interconnected with each other, is necessary for the carbon replication. If the mesoporous silica has a 2-D hexagonal structure and no micropores connecting the mesopores, its replica would result in nanorods instead of mesoporous materials. Therefore, the carbon replication of PMES-MSN can help us understand the core structure of the unique radially-aligned mesostructure, or at least, know if the mesopores are interconnected.

Herein, we took PMES-MSN-2.5 as the template, furfuryl alcohol as the carbon precursor, to perform the carbon replication. The silica surface of PMES-MSN-2.5 was first coated with aluminum chloride to improve the adsorption of furfuryl alcohol. After coating, the BET surface area of Al-PMES-MSN dropped a bit to $502 \text{ m}^2 \text{ g}^{-1}$, indicating that a thin layer of aluminum was successfully coated. As detailed in experimental section, furfuryl alcohol was then hard pressed into the mesopores of PMES-MSN-2.5, followed by polymerization and pyrolysis. After the first run of impregnation-polymerization-pyrolysis process, the BET surface area of the composite material was measured to be around $300 \text{ m}^2 \text{ g}^{-1}$, suggesting a partial filling of mesopores. To completely fill the pores, two additional cycles of impregnation-polymerization-pyrolysis were carried out. After the final run, the measured BET surface area of the composite materials has dropped to around $100 \text{ m}^2 \text{ g}^{-1}$ which can be mostly attributed to the external surface of PMES-MSN-2.5. Silica framework of the carbon-silica composite material was removed by washing with HF to obtain the replicated mesoporous carbon. Figure 2-7 represents the SEM and TEM images of carbon replica of PMES-MSN-2.5. SEM images show the carbon replica is still in the form of nanoparticle

with little mesopore arrangement, the mesostructure of PMES-OMC remains radially-aligned, in which the mesopores are mostly perpendicular to the shell of the particle. Unfortunately, the core structure of this material is unresolved. We also applied EDX technique to examine

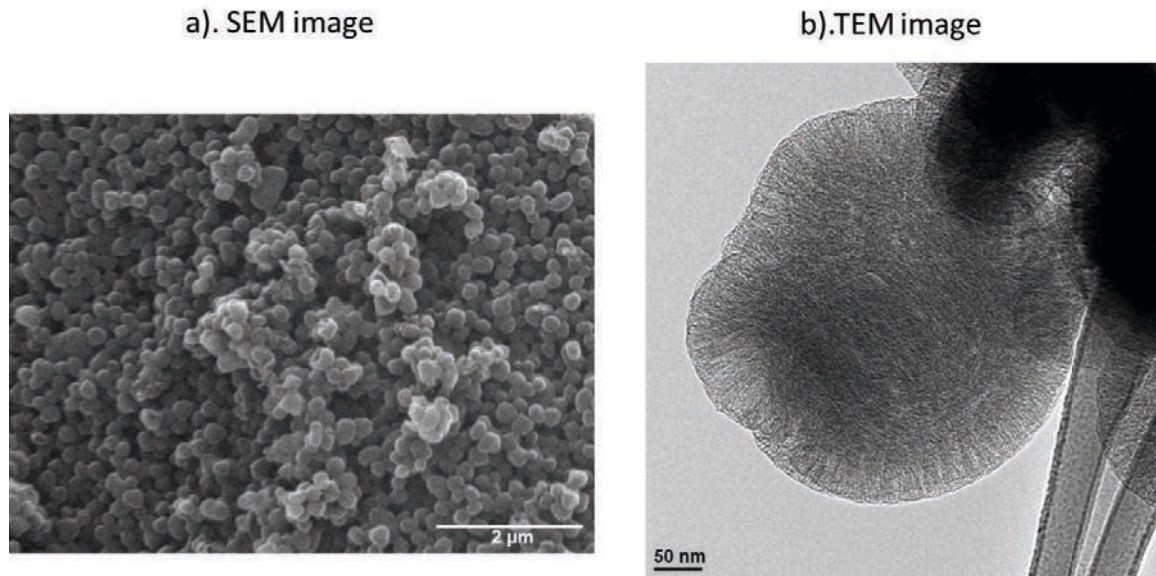
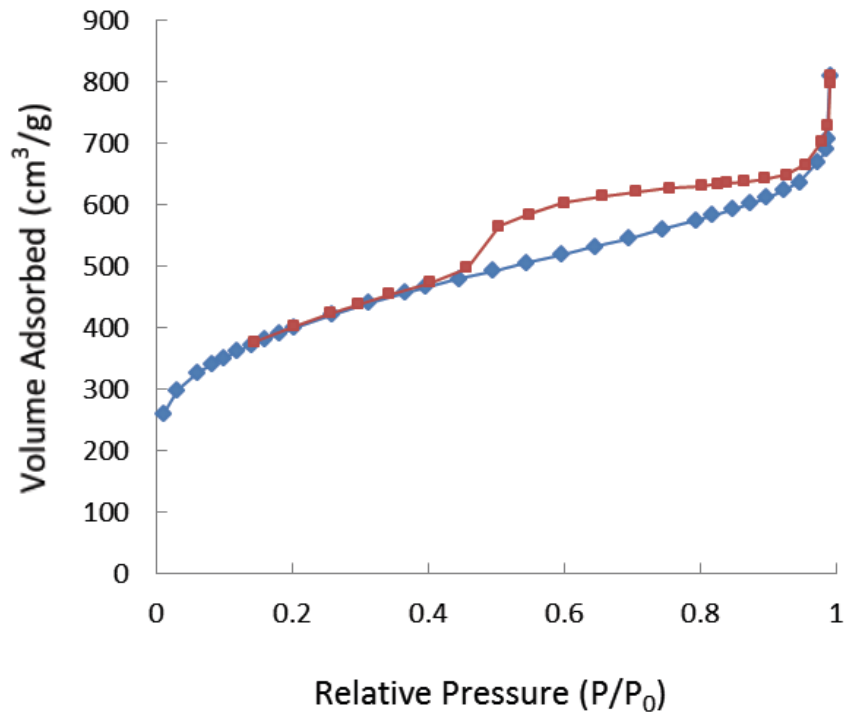


Figure 2-7 a). SEM images of carbon replica of PMES-MSN-2.5; b). TEM images of carbon replica of PMES-MSN-2.5.

PMES-OMC, showing no sign of silica element, indicating the PMES-OMC is a pure carbon material. Nitrogen sorption technique was performed to measure the surface property of PMES-OMC material. This material shows a typical type IV isotherm with a huge hysteresis at around 0.4 P/P_0 , which is characteristic of mesoporous materials (Figure 2-8). The hysteresis pattern of PMES-OMC is similar to that of PMES-MSN-1.0, suggesting a slit-like or urchin-like mesostructure. The calculated BET surface area, as summarized in Table 2-2, is around $1400 \text{ m}^2 \text{ g}^{-1}$ along with the pore volume over $1.00 \text{ cm}^3 \text{ g}^{-1}$. These results suggest our PMES-MSN materials are capable of being templates for nanocasting applications.

Table 2-2 Summary of surface properties of PMES-OMC.

BET Surface Area	BJH Pore Size	BJH Pore Volume	Ave. Size (SEM)
1411.1 m ² g ⁻¹	---- nm	1.03 cm ³ g ⁻¹	150-250 nm

**Figure 2-8** Nitrogen sorption isotherm of PMES-OMC.

3.3 Biocompatibility of PMES-MSNs

We and others have demonstrated that MSNs are non-cytotoxic toward a wide variety of cell lines and red blood cells.^{23,24,26,61,62} However, CTAB containing MSNs are highly toxic due to nature of the surfactant. In contrast to CTAB, anionic surfactants have been shown to have both biocompatibility and biodegradability features.⁴⁴ To demonstrate the biocompatibility of PMES and PMES-MSNs *in vitro*, human cervical cancer (HeLa) cells were used. The *in vitro*

LD₅₀ of PMES in HeLa cells is 50 $\mu\text{g mL}^{-1}$ (data not shown), which is at least 30 times higher than CTAB (1.6 $\mu\text{g mL}^{-1}$).⁴⁴ To examine the biocompatibility of the PMES-MSNs, we selected the sample with molar ratio of CSDA to SDA $x = 2.0$; hereafter PMES-MSNs will refer to PMES-MSN-2. The total amount of organic content of this sample was determined to be 39.2 wt% by TGA. The viability of PMES-MSNs, calcined PMES-MSNs and regular CTAB-MSNs was determined using a Guava ViaCount cytometry assay. Calcined PMES-MSNs and regular CTAB-MSNs were used as control experiments to determine the toxic effect of the presence and type of surfactant, respectively. The surfactant containing and calcined PMES-MSN samples are non-toxic toward HeLa cells under our experimental conditions (LD₅₀ > 100 $\mu\text{g mL}^{-1}$) (Figure 2-9). These data are similar to the one reported on

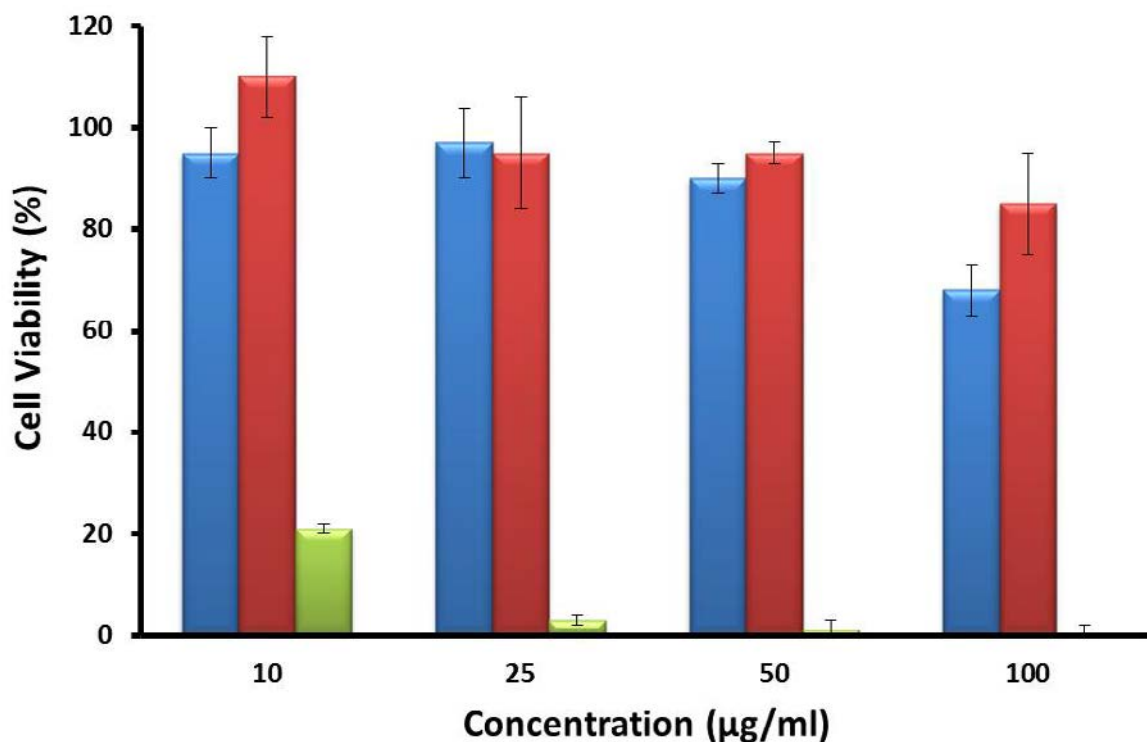


Figure 2-9 Cell viability studies of MSN materials with human cervical cancer (HeLa) cells. All samples were incubated in cell media for 48h.

the literature for typical MSNs.²³ On the contrary, the control sample containing CTAB shows a high toxicity (LD_{50} lower than $10 \mu\text{g mL}^{-1}$) as was expected. Shi and co-workers have recently reported that CTAB containing MSNs are highly toxic even at concentrations as low as $2\text{-}5 \mu\text{g mL}^{-1}$ when incubated with breast cancer MCF-7 cells.⁴⁵

3.4 Intracellular uptake and localization of PMES-MSNs

To investigate the efficiency of endocytosis of PMES-MSNs, the material was labeled with fluorescein (see experimental section). Different concentrations of FITC-labeled PMES-MSNs were then introduced into HeLa cell cultures. The effective concentration (ED_{50}) for the endocytosis of PMES-MSN and the calcined material were 3.0 and $14.9 \mu\text{g mL}^{-1}$, respectively; as calculated from the data obtained by flow cytometry (Figure 2-10). The EC_{50} for calcined PMES-MSNs was close to the EC_{50} of regular MSNs previously reported on the

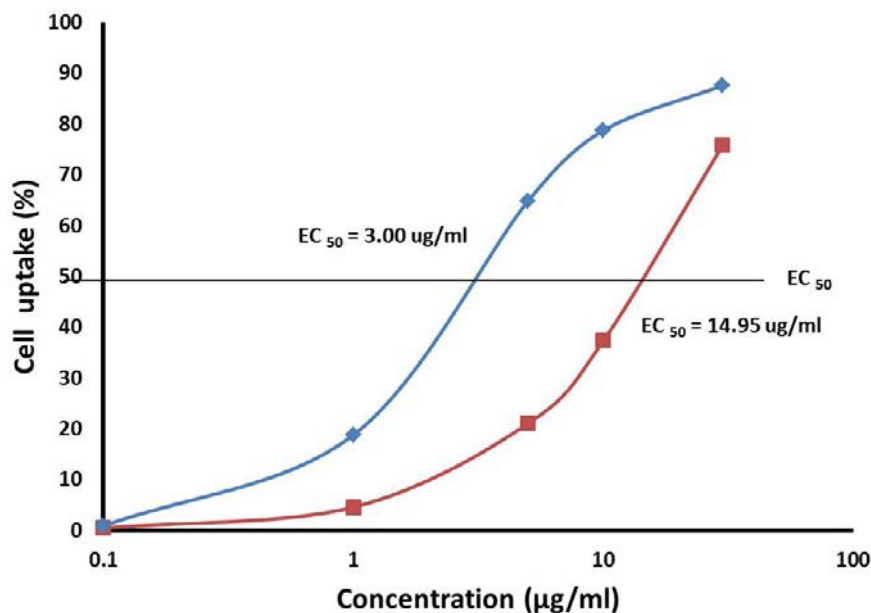


Figure 2-10 Cellular uptake of the synthesized PMES-MSN materials in HeLa cells as a function of the concentration. (■) FITC-PMES-MSN; (◆) FITC-Calcined-PMES-MSN.

literature (Table 2-3). Interestingly, the uptake of PMES-MSN is almost 5-fold higher than the calcined PMES-MSN sample, despite the consistent size and morphology of both materials. We and others have reported that in addition to the structural properties of MSNs, the chemical composition on the surface of this material can be a major factor for the efficiency of internalization.^{23,61} The surface charge of these materials (ζ -potential) was determined by measuring their electrophoretic mobilities. We found a considerable difference in terms of surface charge; the ζ -potential value for PMES-MSNs and the calcined sample were +11.4 and -29.8 mV, respectively (Table 2-3).

Table 2-3 ζ -potential and ED₅₀ of MSN materials.

Sample [a]	ζ -potential [c]	ED ₅₀ ($\mu\text{g ml}^{-1}$)
PMES-MSN-2	11.38 \pm 2.30	3.00
Calcined PMES-MSN-2	-29.85 \pm 4.50	14.95
MSN [b]	-34.73 \pm 3.50	12.98
FAP-MSN [b]	12.81 \pm 1.60	2.73

[a] all samples are FITC-labeled. [b] data referred to ref. 23. [c] measured in 100 mM PBS (pH=7.4) solution.

This variance can be explained by the surface chemistry of each nanomaterial. PMES-MSNs are synthesized using APTMS as the CSDA, these amino groups under physiological conditions will afford abundant positive charges on the surface of PMES-MSNs.⁶³ On the other hand, after calcination we removed all the organic material contained in PMES-MSNs affording a material that contains silanol groups on the surface under physiological conditions. These groups are the origin of the highly negative charge of the calcined PMES-MSN material. We can conclude that the difference observed in the efficiency of intracellular

internalization of PMES-MSNs and calcined PMES-MSNs is in part due to their variation in ζ -potential, which is inherent of the surface chemistry of each material.

To locate PMES-MSNs intracellularly, we analyzed the green fluorescence emitting from the fluorescein groups of FITC-labeled nanoparticles by confocal laser scanning microscopy (CLSM). A series of fluorescence images of different cross-sections of PMES-MSN-containing HeLa cells were obtained by changing the focal depth every 1.2 μm . As depicted in Figure 2-11a, green fluorescence was observed within the cell bodies of these HeLa cells upon excitation at 490 nm, which strongly indicates that PMES-MSN materials were indeed endocytosed by HeLa cells. Red fluorescence was clearly observed from the FM 4-64 stained endosomes upon excitation at 570 nm (Figure 2-11b). By overlapping the green (PMES-MSN) and the red (FM 4-64) fluorescence images, we found that not all the PMES-MSN materials are co-localized with endosomes (Figure 2-11c). This result suggests that some of the PMES-MSN have indeed escaped from endosomes. It has been previously demonstrated that MSNs can escape from endosomes due to a proton-sponge effect.^{23,61} In addition to this mechanism, the PMES that is intracellularly released from the material could interact with the endosome membranes, disrupting the organelle and breaking the endosome. To corroborate this hypothesis, the surfactant was extracted from PMES-MSNs (see section 2.4) to afford the corresponding amino functionalized PMES-MSN derivative. Fluorescence images of this material were obtained by CLSM using HeLa cells (Figure 2-12a to 2-12c). In this case, all the material was co-localized inside the endosomes (yellow spots), which is consistent with our previous observation, i.e., the more positively charged MSN particles

remained trapped within endosomes.²³ These data suggest that the surfactant may indeed enhance the release of material from endosomes.

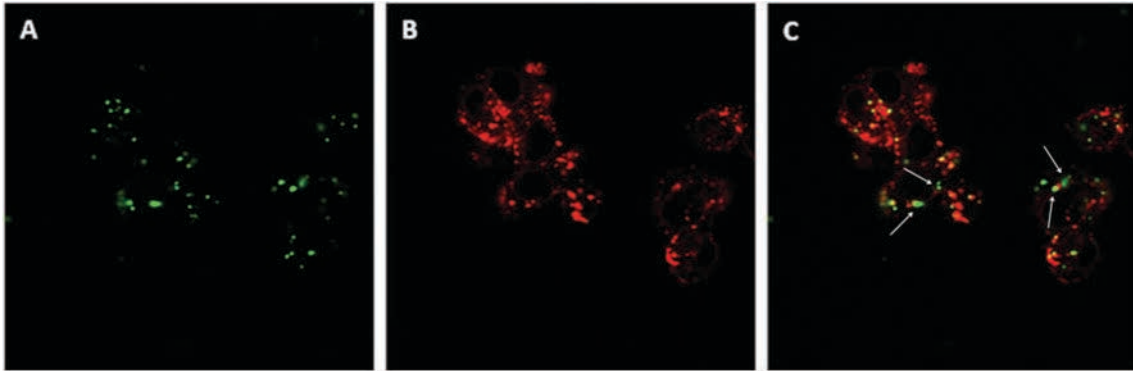


Figure 2-11 Confocal fluorescence images of HeLa cells stained with FM 4-64 and $15 \mu\text{g ml}^{-1}$ suspensions of FITC-PMES-MSN after 10 h incubation. (a) FITC-PMES-MSN (green); (b) FM 4-64 labeled endosomes (red); (c) Fluorescence overlaid image.

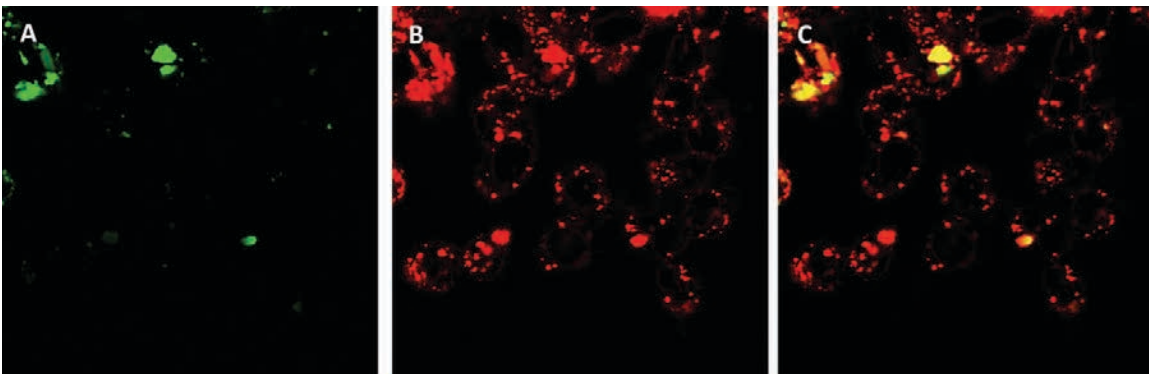


Figure 2-12 Confocal fluorescence images of HeLa cells stained with FM 4-64 and $15 \mu\text{g ml}^{-1}$ suspensions of FITC-PMES-MSN without surfactant after 10 h incubation. (a) FITC-PMES-MSN (green); (b) FM 4-64 labeled endosomes (red); (c) Fluorescence overlaid image.

3.5 In solution and in vitro release of resveratrol-loaded PMES-MSNs

One of the attractive features of MSNs is their outstanding performance as intracellular drug delivery system.²⁰ However, due to the hydrophilic character of their surface, the loading of hydrophobic therapeutic agents is challenging and frequently results in low drug loading efficiencies. To overcome this issue we propose to use the hydrophobic pore of the

PMES-MSNs as an efficient system for transporting and releasing hydrophobic anti-cancer drugs. Recently, a similar approach was published using nanoparticles of magnesium-aluminum layered double hydroxides as delivery vehicle of micelles loaded with camptothecin.⁴² In this work; as a proof of principle, the therapeutic agent trans-resveratrol was used. The therapeutic properties of trans-resveratrol as an anti-cancer, anti-inflammatory and cardiovascular drug in mice and rats have already been reported.^{49,50} Due to its low aqueous solubility and low bioavailability,

Table 2-4 Resveratrol loading efficiency of PMES-MSN materials.

Sample	Amount loaded ($\mu\text{mol g}^{-1}$) [a]	Loading efficiency (%) [b]
PMES-MSN	58.73 \pm 2.13	90
Cal-PMES-MSN	15.15 \pm 0.57	23

[a] all experiments are in triplicate. [b] calculated from original loading solution.

resveratrol administration still remains a big challenge.⁶⁴⁻⁶⁶ Resveratrol was loaded into PMES-MSNs as is described in the experimental section, and calcined PMES-MSNs was used as a control sample. As is shown in Table 2-4, more than 90% of the resveratrol in solution ($58 \mu\text{mol g}^{-1}$) was loaded into PMES-MSN, an amount four times greater than loaded on calcined PMES-MSNs. The release of resveratrol-loaded PMES-MSNs (res-PMES-MSNs) and the control experiment were measured in phosphate buffer solution. Figure 2-13a illustrates the release profiles of the res-PMES-MSNs and control sample. Res-PMES-MSN exhibited a sustained release during the first 4 h before reaching the maximum release, which was about 90% of the original amount of resveratrol loaded. On the contrary, the calcined sample exhibited a burst release in the first 5-10 min where almost 80% of the

drug was released (Figure 2-13b). This fast release was a clear indication that resveratrol was physisorbed on the surface of the calcined PMES-MSN material.

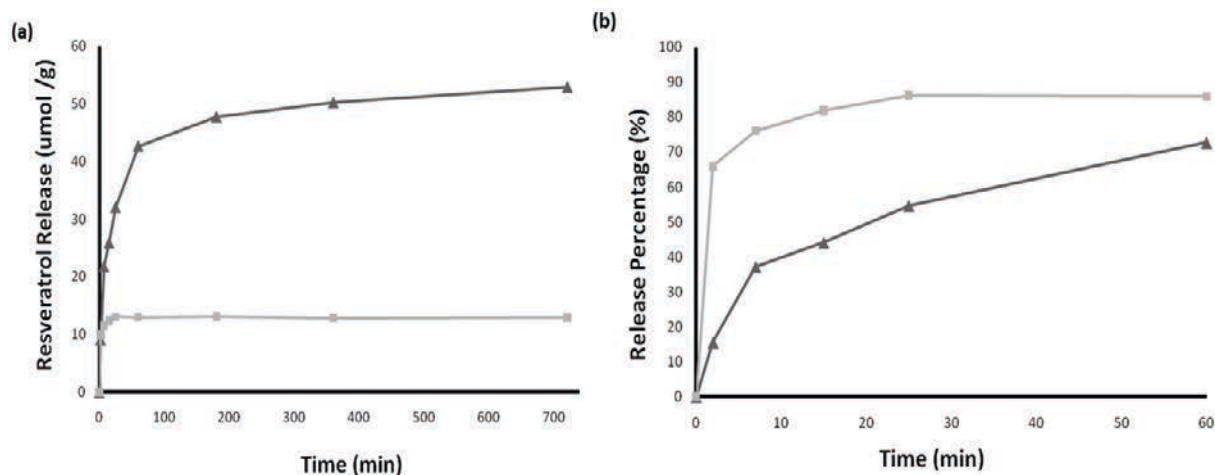


Figure 2-13 (a) Release profiles of resveratrol loaded (▲) PMES-MSN; (■) Cal-PMES-MSN. (b) Comparison of release kinetics of resveratrol loaded (▲) PMES-MSN; (■) Cal-PMES-MSN.

To test *in vitro* the capability of the PMES-MSNs for transporting and releasing resveratrol, the viability of CHO and HeLa cells in the presence of res-PMES-MSN material was measured. As control experiments the viability of both HeLa and CHO cells without material, in presence of resveratrol, PMES-MSNs and calcined PMES-MSNs were also evaluated. After 48 h of incubation, the viability of HeLa and CHO cells were measured via Guava ViaCount cytometry assay. The control experiments for CHO cells did not show considerable cytotoxicity; however, there is a decrease in cell proliferation in the case of PMES-MSNs with HeLa cells (Figure 2-14). The inhibition of cell proliferation of HeLa cells in the presence of res-PMES-MSN material showed an increase in 25%. In addition, the res-PMES-MSN material reduced the viability of CHO cells by almost 30%. Reiter and co-workers reported on the antiproliferative properties of resveratrol with CHO cells; however,

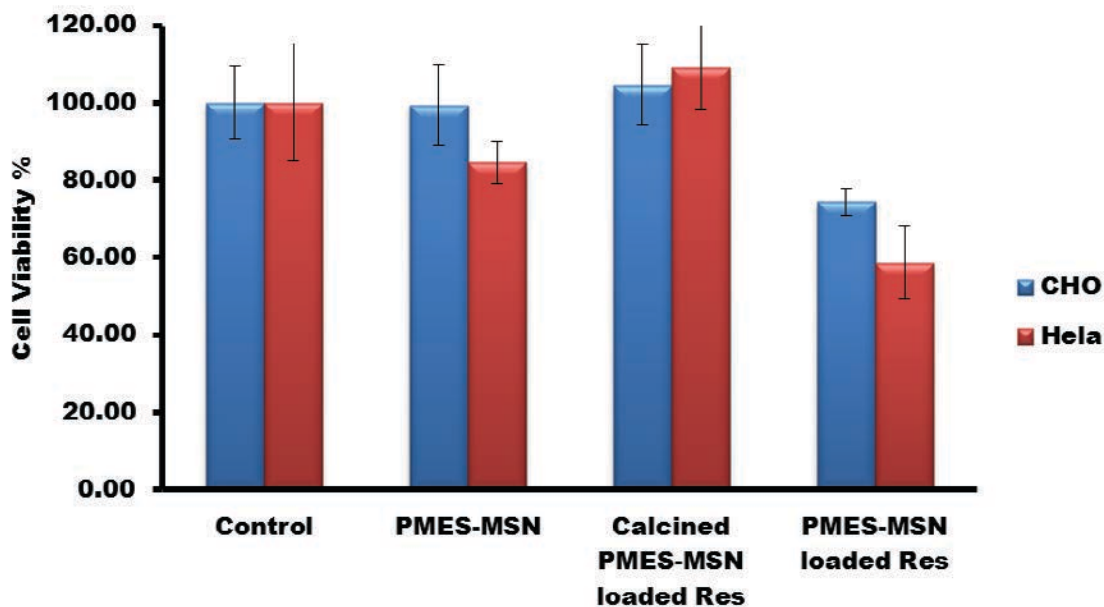


Figure 2-14 Cell viability of HeLa and CHO cells after inoculation with PMES-MSNs, calcined PMES-MSNs and resveratrol-loaded PMES-MSNs.

the cell proliferation inhibition mechanism for this cell type is not known. They determined that at least a concentration of 25 μM of resveratrol is necessary to reduce the amount of CHO cells to 50%.⁶⁷ Our own experiments showed that a concentration of 75 μM of resveratrol in cell media is necessary to inhibit the cell proliferation of CHO cells by approx. 30% (Figure 2-S2). Based on these results we determined that PMES-MSNs increased the efficiency of resveratrol by almost 13 times (see supplementary data for details of the calculations). To rule out the possibility that the inhibition of cell proliferation observed in presence of res-PMES-MSNs was due to just the interaction between PMES and resveratrol, the viability of CHO cells was evaluated using mixed solutions of surfactant and resveratrol. As can be seen from Figure 2-S2, the presence of PMES did not change the cytotoxicity of resveratrol; on the contrary, it slightly enhanced the proliferation of CHO cells. These results

demonstrated that as-made PMES-MSNs are not only able to load higher amounts of resveratrol, but also transporting the drug and efficiently releasing it inside the cells.

3.6 In solution Ca^{2+} stimuli-responsive release of resveratrol-loaded PMES-MSNs

To investigate the stimuli-responsive release of resveratrol-loaded PMES-MSNs, we added various amount of Ca^{2+} or Na^+ into the release solution. The result was illustrated in Figure 2-15. At higher concentration of res-PMES-MSNs in release solution (20 mg MSN/20 ml water), only 23% of resveratrol can be released from the mesopores due to the dynamic equilibrium of PMES molecules in and out of mesopores. The addition of sodium ions did not increase the amount of release, suggesting a weaker interaction between Na^+ and PMES, compared to that between amine groups and PMES. A slight enhancement of release efficiency can be observed when 50 mM of Ca^{2+} was added, in which 32% of resveratrol were released. The Ca^{2+} -responsive behavior becomes prominent when Ca^{2+} concentration is over 100 mM. At $[\text{Ca}^{2+}] = 200 \text{ mM}$, almost 100% of resveratrol were released within 1 h. It is interesting to note that the release kinetics of the Ca^{2+} -responsive profile is very fast, which can be attributed to the strong interaction of Ca-PMES.

A cascade release profile can be obtained when Ca^{2+} were stepwise added, as shown in Figure 2-16. This is evident that this system is highly dependent on the Ca^{2+} concentration. As mentioned earlier, Ca^{2+} is a fundamental element in central nervous system, which triggers the release of neurotransmitters.⁵² Although the amount of calcium added in this study was too high to have real application, it is still promising that a delicate calcium sensor can be designed on the basis of this concept.

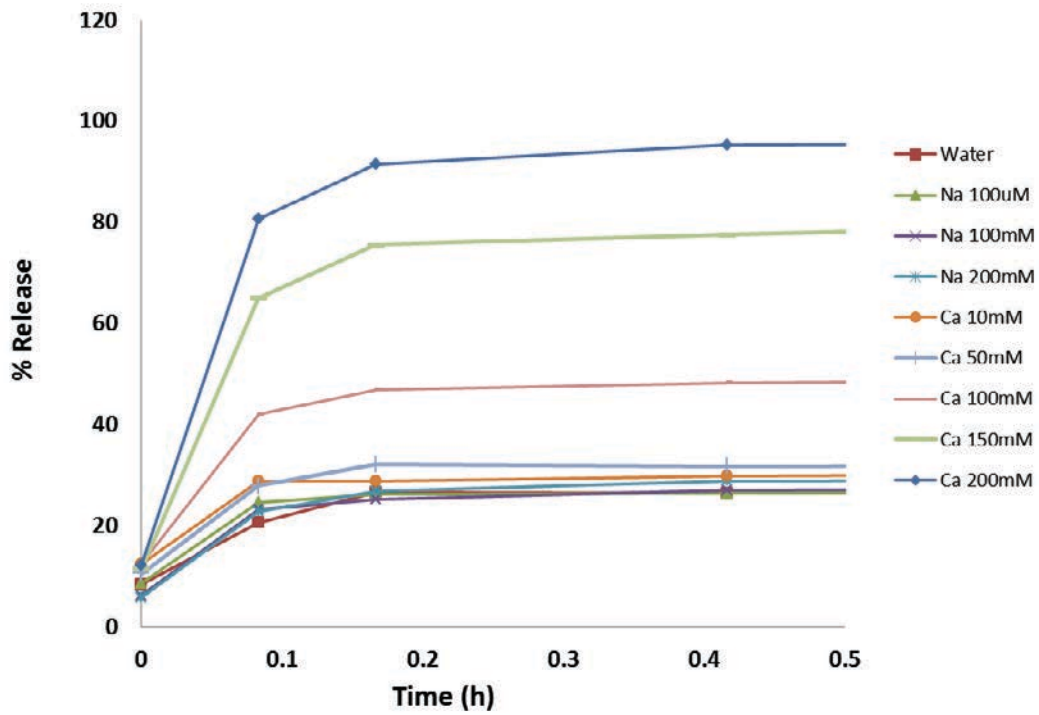


Figure 2-15 Stimuli-responsive release of resveratrol-loaded PMES-MSNs.

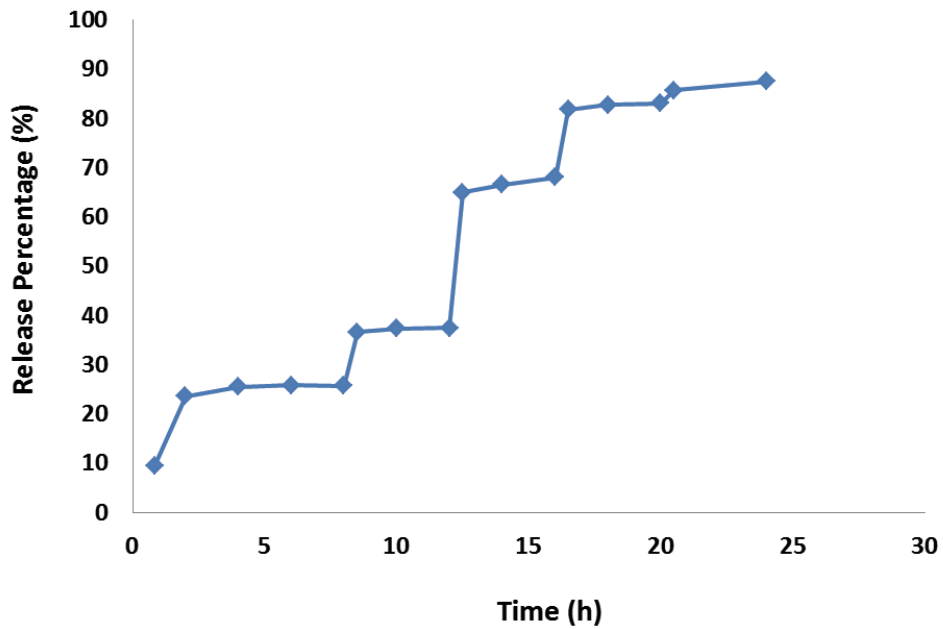


Figure 2-16 A cascade release of resveratrol-loaded PMES-MSN triggered by stepwise addition of Ca²⁺.

4. Conclusions

We have synthesized an anionic surfactant based on undec-1-en-11-yltetra(ethylene glycol) phosphate monoester. This PMES was successfully used as surfactant-directing agent for the synthesis of mesoporous silica nanoparticles. Interestingly, the particle morphology and pore mesostructure of the PMES-MSNs can be tuned by the ratio of co-structure directing agent and structure directing agent. The toxicological properties of the as-made PMES-MSNs were evaluated *in vitro*; we demonstrated that this material is non-cytotoxic toward HeLa and CHO cells. In addition, the cell trafficking features of the nanocarrier were determined by flow cytometry and confocal microscopy. PMES-MSNs are efficiently internalized by HeLa cells ($ED_{50} = 3.0 \mu\text{g mL}^{-1}$) and are able to escape from endosomes. Finally, the properties of PMES-MSNs as drug delivery carriers were evaluated under physiological conditions and *in vitro*. The presence of PMES inside the channels of MSNs increased the amount of resveratrol loaded by almost 4 fold in comparison to calcined PMES-MSNs. Moreover, it modified the release profile, resulting in a sustained release of resveratrol that reached its plateau around 4 h. In addition, we demonstrated the efficient intracellular release of resveratrol using PMES-MSN material as nanocarrier. For instance, we determined that in CHO cells the therapeutic efficiency of resveratrol was increased by a factor of almost 13 times. We envision that this PMES-MSN-based drug delivery system would serve as a new therapeutic method for intracellular delivery of a variety of hydrophobic therapeutic agents.

Acknowledgments

This research was supported by U.S. National Science Foundation (CHE-0809521) and the Biopharmaceuticals & Bioindustrials Initiative of the Plant Science Institute of Iowa State University.

Reference

- (1) Shi, Y.; Porter, W.; Merdan, T.; Li, L.-C. *Expert Opinion on Drug Delivery* **2009**, *6*, 1261.
- (2) Shi, J.; Votruba, A. R.; Farokhzad, O. C.; Langer, R. *Nano Letters* **2010**, *10*, 3223.
- (3) Lipinski, C. *Am Pharm Rev* **2002**, 82.
- (4) Boas, U.; Heegaard, P. M. H. *Chemical Society Reviews* **2004**, *33*, 43.
- (5) Torchilin, V. P. *Nature Reviews Drug Discovery* **2005**, *4*, 145.
- (6) Haag, R.; Kratz, F. *Angewandte Chemie, International Edition* **2006**, *45*, 1198.
- (7) Anglin, E. J.; Cheng, L.; Freeman, W. R.; Sailor, M. J. *Advanced Drug Delivery Reviews* **2008**, *60*, 1266.
- (8) Davis, M. E.; Chen, Z.; Shin, D. M. *Nature Reviews Drug Discovery* **2008**, *7*, 771.
- (9) Ghosh, P.; Han, G.; De, M.; Kim, C. K.; Rotello, V. M. *Advanced Drug Delivery Reviews* **2008**, *60*, 1307.
- (10) Piao, Y.; Burns, A.; Kim, J.; Wiesner, U.; Hyeon, T. *Advanced Functional Materials* **2008**, *18*, 3745.
- (11) Sun, C.; Lee, J. S. H.; Zhang, M. *Advanced Drug Delivery Reviews* **2008**, *60*, 1252.

- (12) Petros, R. A.; De Simone, J. M. *Nature Reviews Drug Discovery* **2010**, *9*, 615.
- (13) Hom, C.; Lu, J.; Tamanoi, F. *Journal of Materials Chemistry* **2009**, *19*, 6308.
- (14) Liong, M.; Angelos, S.; Choi, E.; Patel, K.; Stoddart, J. F.; Zink, J. I. *Journal of Materials Chemistry* **2009**, *19*, 6251.
- (15) Vallet-Regi, M. *Journal of Internal Medicine* **2009**, *267*, 22.
- (16) Vivero-Escoto, J. L.; Trewyn, B. G.; Lin, V. S. Y. *Annual Review of Nano Research* **2010**, *3*, 191.
- (17) Coti, K. K.; Belowich, M. E.; Liong, M.; Ambrogio, M. W.; Lau, Y. A.; Khatib, H. A.; Zink, J. I.; Khashab, N. M.; Stoddart, J. F. *Nanoscale* **2009**, *1*, 16.
- (18) Manzano, M.; Vallet-Regi, M. *Journal of Materials Chemistry* **2010**, *20*, 5593.
- (19) Slowing, I. I.; Vivero-Escoto, J. L.; Trewyn, B. G.; Lin, V. S. Y. *Journal of Materials Chemistry* **2010**, *20*, 7924.
- (20) Vivero-Escoto, J. L.; Slowing, I. I.; Trewyn, B. G.; Lin, V. S. Y. *Small* **2010**, *6*, 1952.
- (21) Zhao, Y.; Vivero-Escoto, J. L.; Slowing, I. I.; Trewyn, B. G.; Lin, V. S. Y. *Expert Opinion on Drug Delivery* **2010**, *7*, 1013.
- (22) Lebedev, O. I.; Van Tendeloo, G.; Collart, O.; Cool, P.; Vansant, E. F. *Solid State Sciences* **2004**, *6*, 489.
- (23) Slowing, I.; Trewyn, B. G.; Lin, V. S. Y. *Journal of the American Chemical Society* **2006**, *128*, 14792.
- (24) Hudson, S. P.; Padera, R. F.; Langer, R.; Kohane, D. S. *Biomaterials* **2008**, *29*, 4045.
- (25) Trewyn, B. G.; Nieweg, J. A.; Zhao, Y.; Lin, V. S. Y. *Chemical Engineering Journal (Amsterdam, Netherlands)* **2008**, *137*, 23.
- (26) Slowing, I. I.; Wu, C.-W.; Vivero-Escoto, J. L.; Lin, V. S. Y. *Small* **2009**, *5*, 57.

- (27) Tsai, C.-P.; Chen, C.-Y.; Hung, Y.; Chang, F.-H.; Mou, C.-Y. *Journal of Materials Chemistry* **2009**, *19*, 5737.
- (28) He, Q.; Zhang, J.; Shi, J.; Zhu, Z.; Zhang, L.; Bu, W.; Guo, L.; Chen, Y. *Biomaterials* **2010**, *31*, 1085.
- (29) Lin, Y.-S.; Haynes, C. L. *Journal of the American Chemical Society* **2010**, *132*, 4834.
- (30) Vivero-Escoto, J. L.; Slowing, I. I.; Lin, V. S. Y. *Biomaterials* **2010**, *31*, 1325.
- (31) Giri, S.; Trewyn, B. G.; Stellmaker, M. P.; Lin, V. S. Y. *Angewandte Chemie, International Edition* **2005**, *44*, 5038.
- (32) Vivero-Escoto, J. L.; Slowing, I. I.; Wu, C.-W.; Lin, V. S. Y. *Journal of the American Chemical Society* **2009**, *131*, 3462.
- (33) Zhao, Y.; Trewyn, B. G.; Slowing, I. I.; Lin, V. S. Y. *Journal of the American Chemical Society* **2009**, *131*, 8398.
- (34) Cauda, V.; Argyo, C.; Schlossbauer, A.; Bein, T. *Journal of Materials Chemistry* **2010**, *20*, 4305.
- (35) Cheng, S.-H.; Lee, C.-H.; Chen, M.-C.; Souris, J. S.; Tseng, F.-G.; Yang, C.-S.; Mou, C.-Y.; Chen, C.-T.; Lo, L.-W. *Journal of Materials Chemistry* **2010**, *20*, 6149.
- (36) Lee, J. E.; Lee, N.; Kim, H.; Kim, J.; Choi, S. H.; Kim, J. H.; Kim, T.; Song, I. C.; Park, S. P.; Moon, W. K.; Hyeon, T. *Journal of the American Chemical Society* **2010**, *132*, 552.
- (37) Schlossbauer, A.; Warncke, S.; Gramlich, P. M. E.; Kecht, J.; Manetto, A.; Carell, T.; Bein, T. *Angewandte Chemie, International Edition* **2010**, *49*, 4734.

- (38) Thomas, C. R.; Ferris, D. P.; Lee, J.-H.; Choi, E.; Cho, M. H.; Kim, E. S.; Stoddart, J. F.; Shin, J.-S.; Cheon, J.; Zink, J. I. *Journal of the American Chemical Society* **2010**, *132*, 10623.
- (39) Wang, L.-S.; Wu, L.-C.; Lu, S.-Y.; Chang, L.-L.; Teng, I. T.; Yang, C.-M.; Ho, J.-a. A. *ACS Nano* **2010**, *4*, 4371.
- (40) Vallet-Regi, M.; Balas, F.; Arcos, D. *Angewandte Chemie, International Edition* **2007**, *46*, 7548.
- (41) Lu, J.; Choi, E.; Tamanoi, F.; Zink, J. I. *Small* **2008**, *4*, 421.
- (42) Tyner, K. M.; Schiffman, S. R.; Giannelis, E. P. *Journal of Controlled Release* **2004**, *95*, 501.
- (43) Clifford, N. W.; Iyer, K. S.; Raston, C. L. *Journal of Materials Chemistry* **2008**, *18*, 162.
- (44) Vlachy, N.; Touraud, D.; Heilmann, J.; Kunz, W. *Colloids and surfaces. B, Biointerfaces* **2009**, *70*, 278.
- (45) He, Q.; Shi, J.; Chen, F.; Zhu, M.; Zhang, L. *Biomaterials* **2010**, *31*, 3335.
- (46) Che, S.; Garcia-Bennett, A. E.; Yokoi, T.; Sakamoto, K.; Kunieda, H.; Terasaki, O.; Tatsumi, T. *Nature Materials* **2003**, *2*, 801.
- (47) Yokoi, T.; Tatsumi, T. *Journal of the Japan Petroleum Institute* **2007**, *50*, 299.
- (48) Gao, C.; Che, S. *Advanced Functional Materials* **2010**, *20*, 2750.
- (49) Baur, J. A.; Sinclair, D. A. *Nature Reviews Drug Discovery* **2006**, *5*, 493.
- (50) Shukla, Y.; Singh, R. *Annals of the New York Academy of Sciences* **2011**, *1215*, 1.
- (51) Emmett, M. *Kidney International, Supplement* **2004**, *90*, S25.
- (52) Llinas, R.; Steinberg, I. Z.; Walton, K. *Biophysical journal* **1981**, *33*, 323.

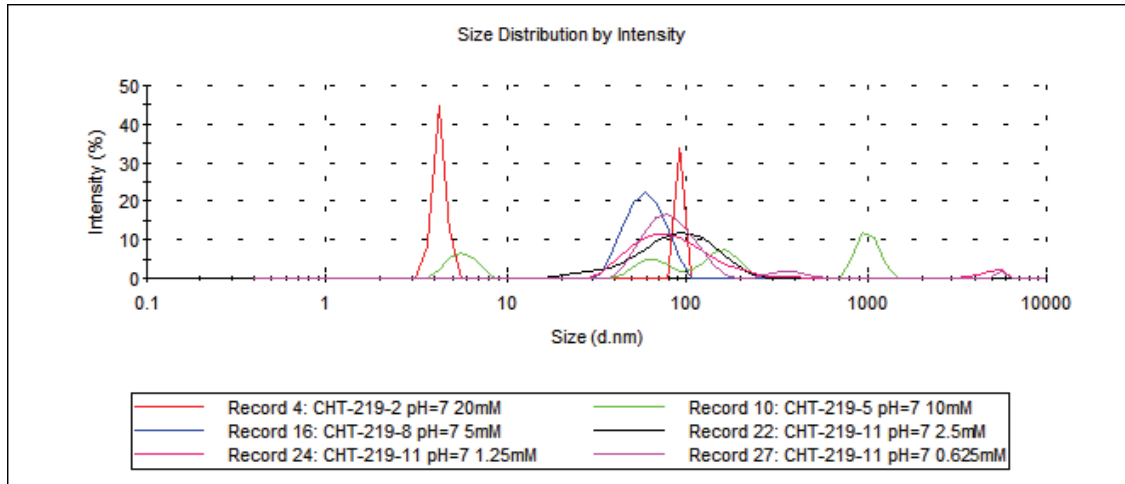
- (53) Pale-Grosdemange, C.; Simon, E. S.; Prime, K. L.; Whitesides, G. M. *Journal of the American Chemical Society* **1991**, *113*, 12.
- (54) Ryoo, R.; Joo, S. H.; Jun, S. *Journal of Physical Chemistry B* **1999**, *103*, 7743.
- (55) Hed, J.; Hallden, G.; Johansson, S. G.; Larsson, P. *Journal of immunological methods* **1987**, *101*, 119.
- (56) Bailey, J. K.; Mecartney, M. L. *Colloids and Surfaces* **1992**, *63*, 151.
- (57) Van Tendeloo, G.; Lebedev, O. I.; Collart, O.; Cool, P.; Vansant, E. F. *Journal of Physics: Condensed Matter* **2003**, *15*, S3037.
- (58) Tan, B.; Rankin, S. E. *Journal of Physical Chemistry B* **2004**, *108*, 20122.
- (59) Wang, J.-G.; Xiao, Q.; Zhou, H.-J.; Sun, P.-C.; Ding, D.-T.; Chen, T.-H. *Journal of Colloid and Interface Science* **2008**, *323*, 332.
- (60) Gao, C.; Qiu, H.; Zeng, W.; Sakamoto, Y.; Terasaki, O.; Sakamoto, K.; Chen, Q.; Che, S. *Chemistry of Materials* **2006**, *18*, 3904.
- (61) Chung, T.-H.; Wu, S.-H.; Yao, M.; Lu, C.-W.; Lin, Y.-S.; Hung, Y.; Mou, C.-Y.; Chen, Y.-C.; Huang, D.-M. *Biomaterials* **2007**, *28*, 2959.
- (62) Zhao, Y.; Sun, X.; Zhang, G.; Trewyn, B. G.; Slowing, I. I.; Lin, V. S. Y. *ACS Nano* **2011**, *5*, 1366.
- (63) Yokoi, T.; Yoshitake, H.; Yamada, T.; Kubota, Y.; Tatsumi, T. *Journal of Materials Chemistry* **2006**, *16*, 1125.
- (64) Walle, T.; Hsieh, F.; DeLegge, M. H.; Oatis, J. E., Jr.; Walle, U. K. *Drug Metabolism and Disposition* **2004**, *32*, 1377.
- (65) Delmas, D.; Aires, V.; Limagne, E.; Dutartre, P.; Mazue, F.; Ghiringhelli, F.; Latruffe, N. *Annals of the New York Academy of Sciences* **2011**, *1215*, 48.

- (66) Walle, T. *Annals of the New York Academy of Sciences* **2011**, 1215, 9.
- (67) Sainz, R. M.; Mayo, J. C.; Tan, D.-X.; Lopez-Burillo, S.; Natarajan, M.; Reiter, R. J. *Biochemical and Biophysical Research Communications* **2003**, 302, 625.

Supporting Information

1. Dynamic light scattering measurement (DLS) of phosphate monoester surfactant (PMES) in PBS solution:

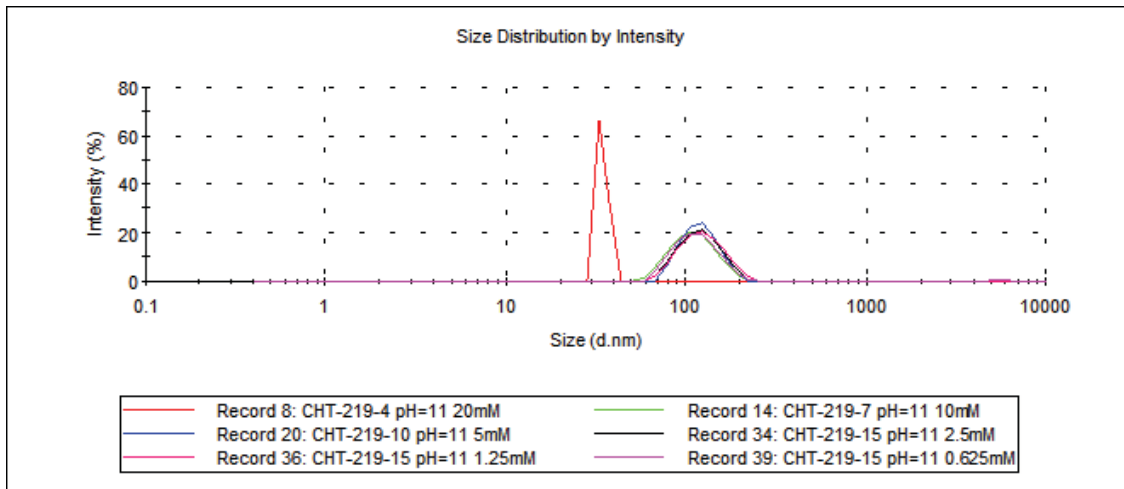
At pH = 7.07,



Concentration	Peak 1 (d, nm) / %	Peak 2 (d, nm) / %	Peak 3 (d, nm) / %	Quality report
20 mM	4.24 / 66.1	91.3 / 33.9	None	Not meet
10 mM	1020 / 31.3	153 / 28.7	5.74 / 21.4	Not meet
5 mM	60 / 100.0	None	None	Not meet
2.5 mM	94.7 / 100.0	None	None	meet
1.25 mM	94.1 / 94.9	4810 / 5.1	None	meet
0.625 mM	82.9 / 91.3	369 / 6.8	5500 / 1.9	Not meet

Figure 2-S1a Summarized results of DLS measurement of PMES in neutral PBS solution.

At pH = 10.99,



Concentration	Peak 1 (d, nm) / %	Peak 2 (d, nm) / %	Peak 3 (d, nm) / %	Quality report
20 mM	34.4 / 100.0	None	None	Not meet
10 mM	112 / 100.0	None	None	Meet
5 mM	122 / 100.0	None	None	Meet
2.5 mM	122 / 100.0	None	None	Meet
1.25 mM	126 / 100.0	None	None	Meet
0.625 mM	116 / 98.7	5390 / 1.3	None	Meet

Figure 2-S1b Summarized results of DLS measurement of PMES in basic PBS solution.

2. Cell viability of resveratrol and PMES/resveratrol:

CHO cells were seeded in six-well plates with a density of 1×10^5 cells mL^{-1} in 3 mL of D-10 medium (Dubelcco Modified Eagle's Medium with horse serum, L-alanyl-L-glutamine, gentamicin sulfate and penicillin-streptomycin solution), and incubated at 37 °C with a 5% CO_2 atmosphere for 24 h. Then, the cells were inoculated with different concentration of resveratrol (10, 25, 50, 75 100 μM) or resveratrol/PMES (36.5 μM) in D-10 serum for other 48 h. After the incubation each well was washed with PBS and the cells were trypsinized, centrifuged, and re-suspended in D-10 medium. Viability was determined by the Guava ViaCount cytometry assay (Guava Technologies, Inc.).

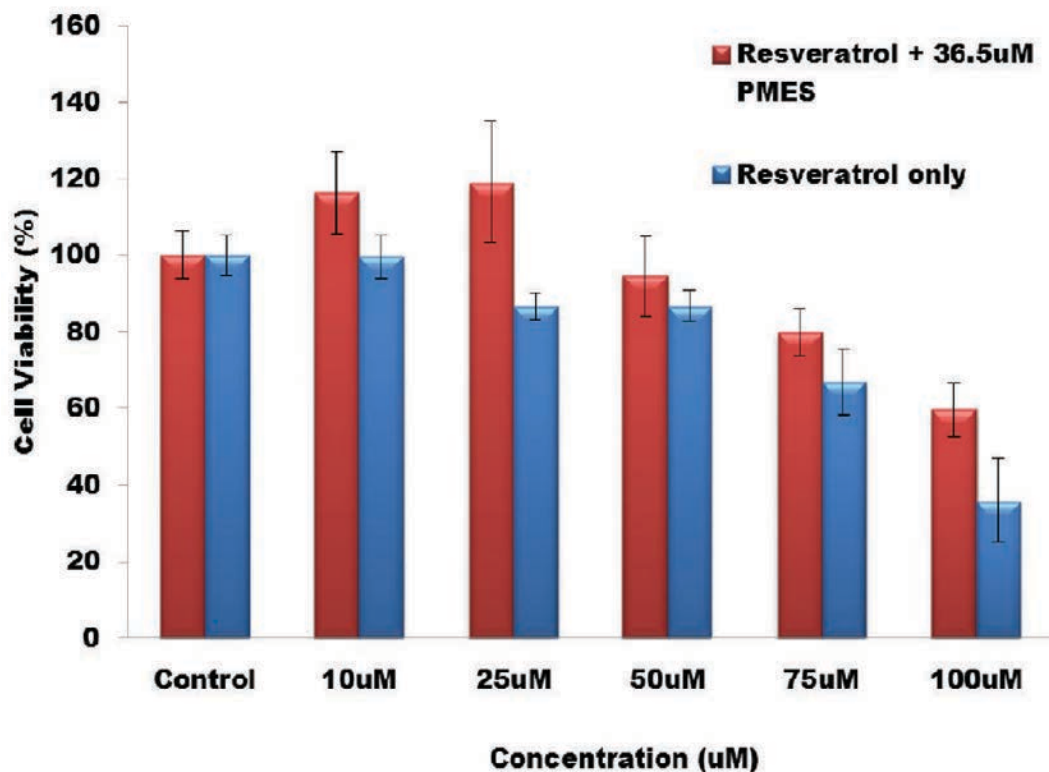


Figure 2-S2 Cell viability of CHO cells in presence of resveratrol or resveratrol/PMES.

3. Calculation of the therapeutic efficiency of res-PMES-MSNs versus resveratrol for inhibition of CHO cells proliferation:

Taking as a base for the calculations an inhibition of CHO cells proliferation of 30%:

Amount of resveratrol used = $75 \mu\text{M} \times 3 \text{ mL} = 225 \text{ nmol}$

Amount of resveratrol used in res-PMES-MSNs = $100 \mu\text{g/mL} \times 58.73 \mu\text{mol/g} \times 3 \text{ mL} = 17.6 \text{ nmol}$

Ratio resveratrol/res-PMES-MSNs = $225/17.6 = 12.8$

CHAPTER 3. RATIONAL CATALYST DESIGN: A MULTIFUNCTIONAL MESOPOROUS SILICA CATALYST FOR SHIFTING THE EQUILIBRIUM REACTION BY REMOVAL OF BYPRODUCT

Modified from a paper published in *ACS Catalysis* **2011**, *1*, 729

Chih-Hsiang Tsai, Hung-Ting Chen, Stacey M. Althaus, Kanmi Mao, Takeshi Kobayashi,
Marek Pruski, and Victor S.-Y. Lin

Abstract

A series of bifunctionalized mesoporous silica nanoparticle (MSN) catalysts, containing a Brønsted acid active site of diarylammonium triflate (DAT) and a pentafluorophenyl propyl (PFP) group, were synthesized via the co-condensation method. These catalysts were well characterized by various techniques. We found that PFP groups behave two structural conformations inside the mesopores through our cutting-edge solid-state NMR techniques. When PFP-MSNs are exposed to dry conditions (under vacuum) PFP groups were present in an upright position; while when the PFP-MSNs were soaked in solvents the PFP groups tended to be in a prone position. We envisioned the PFP-decorated silica surface would be beneficial for catalytic dehydration reactions. In addition, we demonstrated that the activity of bifunctional MSN catalysts is proportional to the loading of immobilized PFP groups in esterification reactions. This could be attributed to the extremely hydrophobic surface created by the PFP groups, which expel water molecules from the confined mesochannels that drives the chemical equilibrium of a dehydration reaction to completion. These bifunctionalized MSN catalysts also exhibited reactivity far superior than two industrially important solid

acids, Amberlyst-15 and Nafion NR-50[®], and were recyclable at least five times with identical yields.

1. Introduction

Recent advancements in the design of mesoporous silica nanoparticle (MSN) materials with surface-anchored functional groups have shown promising potential for applications in heterogeneous catalysis.¹⁻⁶ Not only can such catalysts be easily separated from the products and recycled, but their large surface area ($> 700 \text{ m}^2 \text{ g}^{-1}$), tunable pore diameter (2-10 nm) and well-ordered pore structure allow for precise regulation of mass-transport properties that are crucial for many chemical transformations. Several classes of single-site catalytic systems have been developed using the MSN materials as supports, including organometallic catalysts,⁶⁻⁹ acid catalysts,^{4,10,11} base catalysts¹² and immobilized enzymatic catalysts.¹³ In addition, by introducing multiple functional groups onto the 3D controlled mesoporous surface our group,^{14,15} as well as others,^{5,16-19} have demonstrated that the selectivity and reactivity of MSN-supported catalysts can be effectively enhanced.

In our recent report,²⁰ we detailed the conformations of 3-(pentafluorophenyl)propyl (PFP) groups covalently anchored to the 'dry' MSN support (i.e., in the absence of any solvent molecules inside the pores). We demonstrated that the silica-bound PFP groups exist in two different conformations: (1) the molecules located in the proper vicinity of accessible siloxane groups assume the prone orientation with the aromatic rings centered near the siloxane oxygens, and (2) the remaining PFP functionalities are oriented roughly upright with respect to the silica surface and are more mobile. Both structures were determined by a

number of 2D solid-state NMR experiments and further substantiated by theoretical calculations.²⁰ In particular, the fingerprints of both conformations were obtained in terms of ¹⁹F chemical shifts.

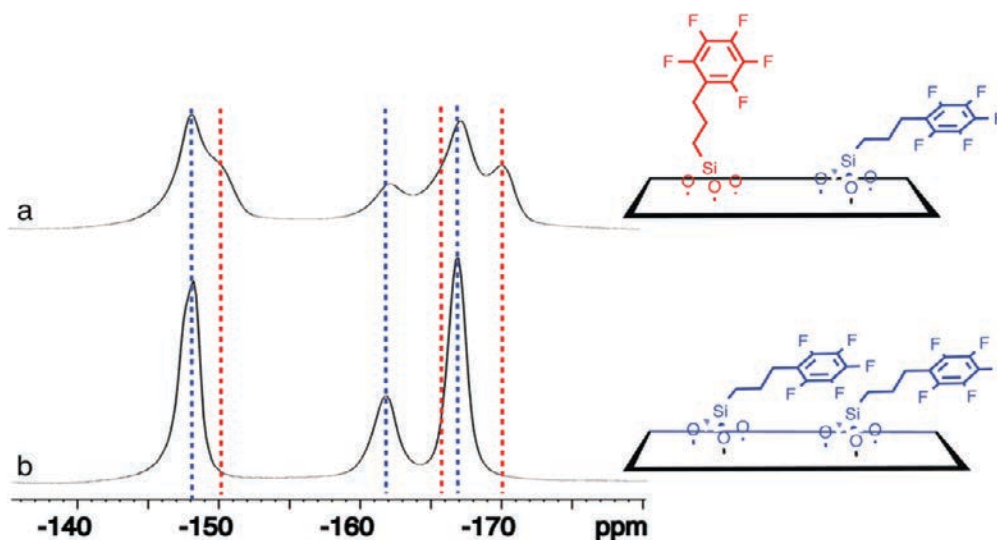


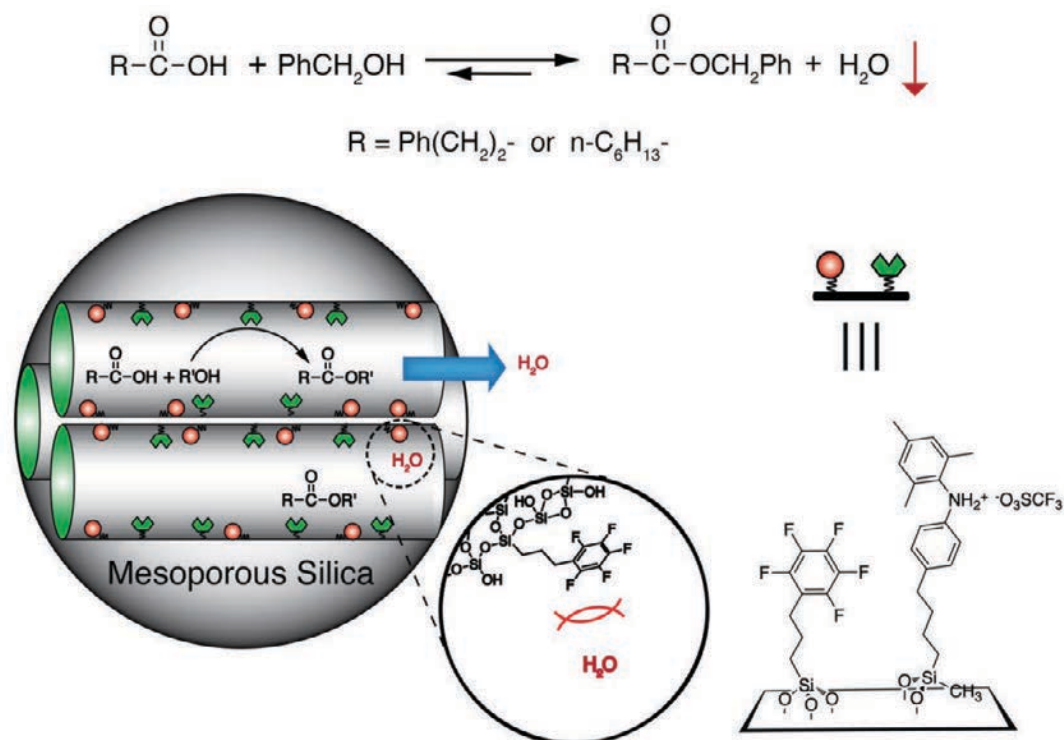
Figure 3-1 ¹⁹F solid-state MAS NMR spectra of PFP-MSN measured in dried conditions (a) and with the mesopores filled with heptane (b). Blue and red lines indicate resonances representing fluorines in ‘prone’ and ‘upright’ PFP functionalities, which are depicted on the right side of the figure. In the presence of solvent, all molecules remain close to the silica surface.

We have since discovered that the conformations of PFP groups change when the pores are filled with solvents. For example, in the presence of heptane, only the resonances representing molecules in prone positions can be detected (Figure 3-1). Secondly, it has been demonstrated by others, both experimentally and theoretically, that fluorine bound to aromatic carbon is a poor hydrogen-bond acceptor, and thus poorly interacts with water.^{21,22}

These findings inspired us to design a new perfluorinated MSN catalyst for esterification reactions, containing a Brønsted acidic diarylammonium triflate (DAT) group serving as a catalyst^{11,23-26} and PFP as a secondary functionality (Scheme 3-1). Rather than controlling the

diffusional penetration of the reactants to the catalytic sites inside the mesopores,¹⁴ we incorporated the PFP groups to suppress the interactions between the reaction byproduct (water) and the silica surface. The benefits of using other secondary functional groups to increase the hydrophobicity of mesoporous catalysts have been already reported for several reactions involving dehydration.²⁷⁻²⁹ Here, we demonstrate that the PFP functionality significantly enhances the catalytic activity in the esterification reaction, and performs better in this capacity than the commonly used trimethylsilyl group (TMS). Furthermore, we compare the catalytic performance of this bifunctionalized MSN-system with commercially available heterogeneous acid catalysts, such as Amberlyst-15 and Nafion NR-50[®], in the esterification of carboxylic acids with benzyl alcohol under our reaction conditions.

Scheme 3-1 Schematic representation of a bifunctional PFP/DAT-MSN.

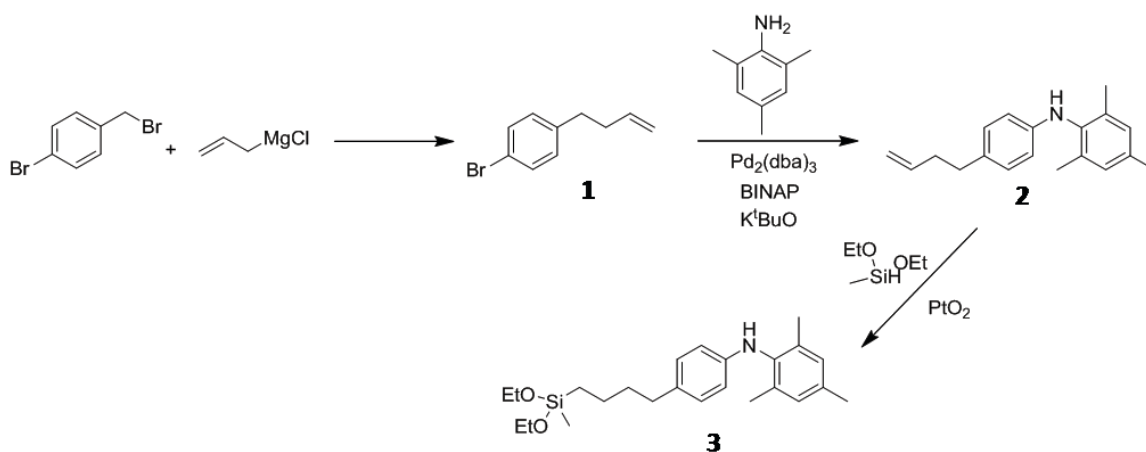


2. Materials and Methods

2.1 Reagents and materials

Organosilanes, which included tetraethyl orthosilicate (TEOS), methyldiethoxysilane, and 3-(pentafluorophenyl)propyl trimethoxysilane (PFP-TMS) were purchased from Gelest, Inc. Other chemical reagents were purchased from Sigma-Aldrich, Inc. All chemicals were used as received without further purification.

2.2 Synthesis of diarylamine organosilane (DAS)



Scheme 3-2 Synthesis of diarylamine-functionalized methyldiethoxo-silane (DAS)

2.2.1 Synthesis of 4-(4-bromophenyl)-1-butene (**1**)

A 250 ml two-necked round-bottom flask, equipped with an addition funnel and condenser, was charged with 4-bromo-benzyl bromide (20.0 g, 80 mmol) in 50 ml dry ether at 0 °C ice bath for 10 min. The allylmagnesium chloride (48.0 ml of a 2.0 M solution in ether, 96 mmol) was added dropwise *via* an addition funnel over a period of 30 min at 0 °C. Subsequently, the mixture was stirred at room temperature for 2 h and refluxed for another 3

h. The reaction was monitored by TLC analysis. After the starting material disappeared, the reaction was quenched by water and transferred to a separation funnel. The organic layer was washed with brine, dried over anhydrous MgSO_4 , and then concentrated under vacuum to yield a yellow crude liquid. The product was purified by Kugelrohr distillation to obtain the final product as a transparent liquid (14.10 g, 83% yield), whose ^1H and ^{13}C NMR spectra matched with the earlier reported literature data.³⁰

2.2.2 Synthesis of *N*-(4-(but-3-en-1-yl)phenyl)-2,4,6-trimethylaniline (2)

A mixture of $\text{Pd}_2(\text{dba})_3$ (517.6 mg, 5 mol% Pd), BINAP (1.06 g, 1.5 eq of Pd), and potassium *tert*-butoxide (3.05 g, 27.13 mmol) in 80 ml toluene was prepared in a round-bottom flask in a glove box. The 4-(4-bromophenyl)-1-butene (5.00 g, 22.6 mmol) and 2,4,6-trimethylaniline (3.80 ml, 27.13 mmol) were added by syringe, and the reaction mixture was stirred in a 80 °C oil bath for 12 h. The mixture was quenched with a saturated $\text{NaHCO}_3(\text{aq})$ solution and then concentrated under reduced pressure. The crude product was purified by column chromatography (t-butyl methyl ether/heptane (v/v) = 3/97, R_f = 0.3) to afford *N*-(4-(but-3-en-1-yl)phenyl)-2,4,6-trimethylaniline (4.83 g, 76.7%). ^1H NMR (300 MHz, CDCl_3): δ 6.95 (m, 4H), 6.44 (s, 1H), 6.42 (s, 1H), 5.87 (m, 1H), 5.01 (m, 2H+NH), 2.60 (t, 2H), 2.30 (s, 1H), 2.17 (s, 6H). ^{13}C NMR (100 MHz, CDCl_3): δ 144.7, 138.8, 135.6, 135.2 (2C), 134.8, 131.5, 129.4 (2C), 129.2 (2C), 114.8, 113.6 (2C), 36.1, 34.8, 21.1, 18.5 (2C). MS (EI): m/z: calc. for $\text{C}_{19}\text{H}_{23}\text{N}$: 265.18; found 265.18.

2.2.3 Synthesis of *N*-(4-(4-(diethoxy(methyl)silyl)butyl)phenyl)-2,4,6-trimethylaniline (3)

Compound **2** (5 g, 18.8 mmol) and 15 ml of methyldiethoxysilane were placed in a Schlenk tube under argon. The platinum oxide, PtO₂ (20 mg, 478 ppm), was added to the mixture, and the tube was sealed and heated at 85 °C for 20 h. After cooling to room temperature, the crude product was diluted with anhydrous ethanol and filtered through activated charcoal to remove PtO₂. The filtrate was concentrated at reduced pressure and purified by column chromatography (ethyl acetate/heptane = 2.5/97.5, R_f = 0.38) to afford the compound **3** (4.82 g, 65.7% yield). ¹H NMR (300 MHz, CDCl₃): δ 7.28 (dd, 2H), 7.26 (s, 2H), 6.94 (dd, 2H), 5.02 (s, NH), 3.74 (t, 4H), 2.49 (t, 3H), 2.30 (s, 3H), 2.16 (s, 6H), 1.57 (m, 2H), 1.41 (m, 2H), 1.21 (t, 6H), 0.64 (t, 2H), 0.10 (s, 3H). ¹³C NMR (100 MHz, CDCl₃): δ 144.6, 136.2, 135.8 (2C), 135.2, 132.4, 129.4 (4C), 113.6 (2C), 58.3 (2C), 35.5, 34.9, 22.8 (2C), 21.1, 18.6 (2C), 13.9 (2C), -4.6. MS (EI): m/z calc. for C₂₄H₃₇NO₂Si: 399.26; found 399.26.

2.3 Synthesis of bifunctionalized PFP/DAT-MSN catalysts

The functionalized MSNs were synthesized *via* our previously reported co-condensation method.¹⁴ Typically, a mixture of CTAB (1.0 g, 2.75 mmol) and 2.0 M of NaOH_(aq) (3.5 ml, 7.0 mmol) in 240 ml H₂O was heated at 80 °C for 30 min. To this clear solution, tetraethoxysilane (5 ml, 22.4 mmol), PFP-TMS (0.44 g, 1.44 mmol), and/or DAS organosilane (0.58 g, 1.44 mmol) were injected rapidly and sequentially to yield an opaque reaction mixture. The resulting reaction mixtures were stirred at 80 °C for 2 h. The as-made MSNs were obtained after hot filtration, followed by washing with copious amount of water and methanol, and drying under vacuum. The surfactant was removed by stirring the solution of as-made materials (1.0 g) and 0.8 ml of concentrated HCl in 100 ml methanol at 60 °C for

6 h. The resulting surfactant-free MSNs were filtered, washed with water and methanol, and dried under vacuum for 24 h.

The trifluoromethanesulfonic acid (TFA) (0.27 ml, 3 mmol) was added to a suspension of the MSN materials (0.2 g) in dry toluene (10 ml, 94.1 mmol), and stirred at room temperature for 6 h. The solid powder was filtered and washed with copious amount of toluene, hexane, ether, and dried under vacuum for 12 h at room temperature. Finally, the resulting powder was heated at 135 °C under the vacuum (< 1 mmHg) for 18 h to remove the excess amount of physisorbed acid remaining on the silica surface. The resulting MSN catalysts were then sealed in scintillation vials and stored in a desiccator.

2.4 Synthesis of TMS/DAT-MSN catalyst

The passivation of silica surface with HMDS (hexamethyldisilazane) has been reported elsewhere.³¹ Typically, a 50 ml round-bottom flask charged with the surfactant-free DAS-MSNs (0.3 g) was pre-dried under vacuum at 90 °C for 6 h to remove the physisorbed moisture. A solution of HMDS (1.25 ml, 6 mmol) in dry toluene (15 ml) was injected into the reaction flask. The reaction was then stirred at 60 °C for 24 h. The solid product was isolated by filtration, followed by washing with 200 ml of toluene and 50 ml of methanol, and dried under high vacuum for 24 h. The acid treatment with TFA of this TMS/DAS-MSN sample was following the same method described in the experimental section. The TMS/DAT MSN exhibited $685 \text{ m}^2 \text{ g}^{-1}$ specific surface area estimated from BET method and 2.2 nm of mean pore diameter. The loading of DAT group in this material, calculated via ^1H DPMAS NMR (see section 4), was 0.16 mmol g^{-1} . The loading of TMS was calculated to be 2.2 mmol g^{-1} .

2.5 Summary of solid-state NMR measurements

2.5.1 Experimental section

^{13}C solid-state NMR was used to confirm the structure of the moieties in mono- and bi-functionalized MSNs. ^{29}Si and ^1H spectra were obtained to determine the loading of these moieties on the surface of the MSN. ^{19}F spectra were measured to determine the conformation of PFP in different environments on the MSN surface. The measurements were performed at 150.8 MHz (^{13}C), 119.1 MHz (^{29}Si), 599.6 MHz (^1H) and 564.2 MHz (^{19}F) on a Varian NMR System 600 spectrometer.

2.5.2 Characterization of functional groups using ^{13}C NMR

^{13}C NMR spectra were acquired with a 1.6 mm FastMASTM probe, using magic angle spinning (MAS) rate $\nu_{\text{R}} = 41.6$ kHz, ^1H - ^{13}C cross-polarization (CP) with the contact time $\tau_{\text{CP}} = 1$ ms, the average magnitude of the tangent ^1H RF field $\nu_{\text{RF}}^{\text{H}} = 65$ kHz, $\nu_{\text{RF}}^{\text{C}}$ during CP = 107 kHz, $\nu_{\text{RF}}^{\text{H}}$ during SPINAL-64 decoupling = 11 kHz, the recycle delay $\tau_{\text{RD}} = 1$ s, and the number of scans NS = 80,000. The ^{13}C CPMAS NMR spectra of samples Cat A, B, C, and D showed that the PFP and DAT functional groups were indeed present on the surface. The spectra of Cat A and Cat C are shown in Figure 3-2 along with the spectral assignments, which are indicated in reference to the molecular structures shown on the top of the figure. The peaks at 12, 23, 25 and 116 ppm in the spectrum of Cat A (marked 1 through 4) represent carbons C1, C2, C3 and C4 in PFP. Indeed, these are the only resonances observed in the spectrum of Cat D (not shown). Their identity was unambiguously established by 2D ^1H - ^{13}C HETCOR NMR in our earlier studies.^{20,32} The aromatic carbons in PFP were identified by 2D ^{19}F - ^{13}C HETCOR spectroscopy.²⁰ The remaining carbon resonances in Cat A, as well as those observed in the spectrum of Cat C, are consistent with the structure of

DAT. These resonances are slightly better resolved in the spectrum of Cat A, which may be due to increased torsional mobility of DAT in the presence of PFP coating on the surface.

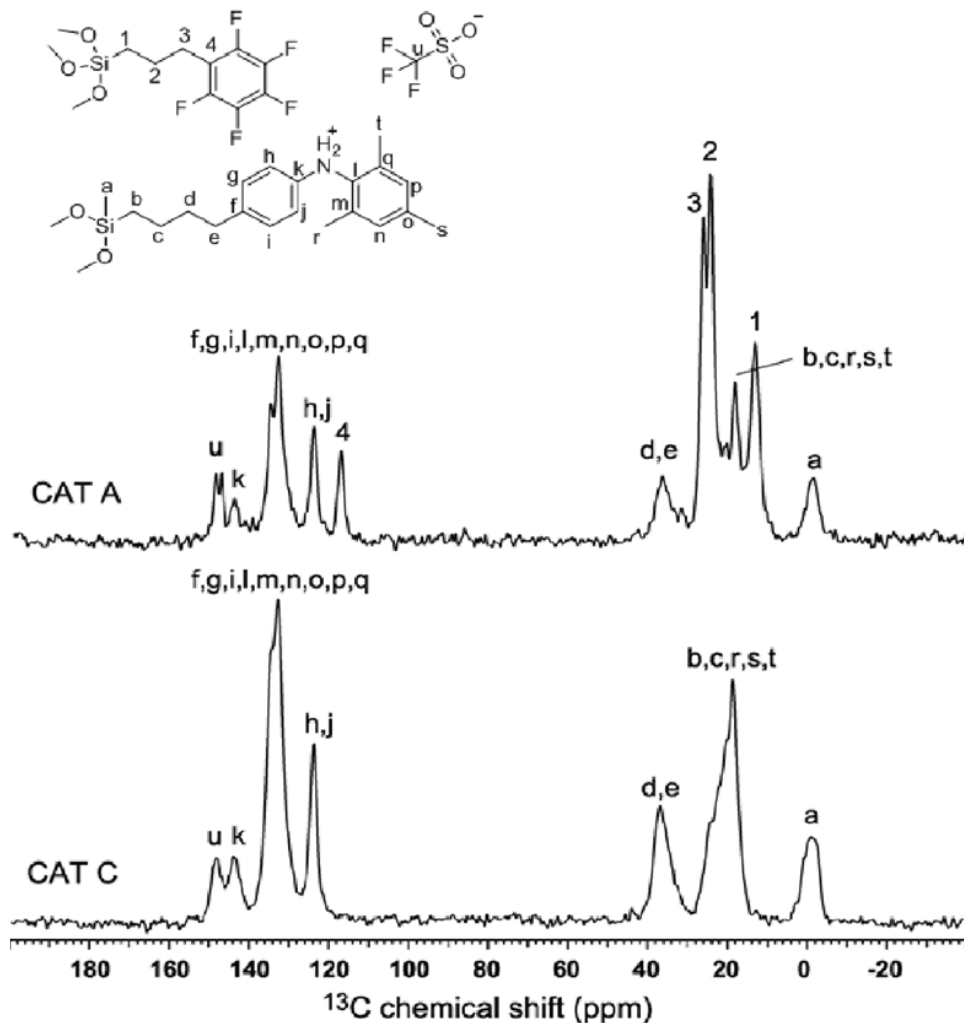


Figure 3-2 ^{13}C CPMAS spectra of Cat A and Cat C acquired under MAS at 41.6 kHz.

2.5.3 Quantification of functional groups using ^{29}Si NMR

The quantification of silicon in bifunctionalized samples (Cat A and B) was carried out by using ^1H - ^{29}Si CPMAS and ^{29}Si direct polarization MAS (DPMAS) experiments, as explained below. The sensitivity of both measurements was enhanced by refocusing the ^{29}Si

magnetization using the Carr-Purcell-Meiboom-Gill (CPMG) train of π pulses.³³ The spectra were acquired with a 3.2 mm MAS probe, using $\nu_R = 20$ kHz, ν_{RF}^{Si} during DPMAS and CPMAS experiments = 100 kHz, average ν_{RF}^H during tangent CP = 80 kHz, $\tau_{CP} = 15$ ms, ν_{RF}^H during high-power SPINAL-64 decoupling = 125 kHz, the recycle delay $\tau_{RD} = 300$ s (DPMAS) or 1 s (CPMAS), and NS = 288 (DPMAS) or 8,000 (CPMAS).

The core of silica walls consists of silicon sites referred to as Q^4 , which are connected to four Si neighbors via siloxane linkages ((SiO)₄Si). In non-functionalized materials, the silica surface is terminated by the silanol groups forming Q^3 sites ((SiO)₃Si(OH)) and Q^2 sites ((SiO)₂Si(OH)₂). In samples Cat A and Cat B these sites are observed at around -113, -104 and -94 ppm, respectively (Figure 3-3). Also observed in these samples are peaks at about -68 and -58 ppm, which are assigned to silicon atoms in positions (SiO)₃SiR and (SiO)₂Si(OH)R, denoted as T^3 and T^2 . These resonances are associated with the covalently bound PFP groups.^{32,33} Finally, the peak at approximately -16 ppm represents the so-called D^2 sites in positions (SiO)₂SiR₁R₂, whose presence is due to the covalently bound DAT species.

Although only the DPMAS measurements can provide strictly quantitative ²⁹Si spectra, we were unable to determine the concentration of D sites using this method due to low signal intensity. Therefore, the DPMAS spectra were only used to quantify the T sites. We then used the CPMAS spectra to determine the $T : D$ (i.e., PFP : DAT) ratio, taking into account the difference in CP dynamics between these sites. This dynamics

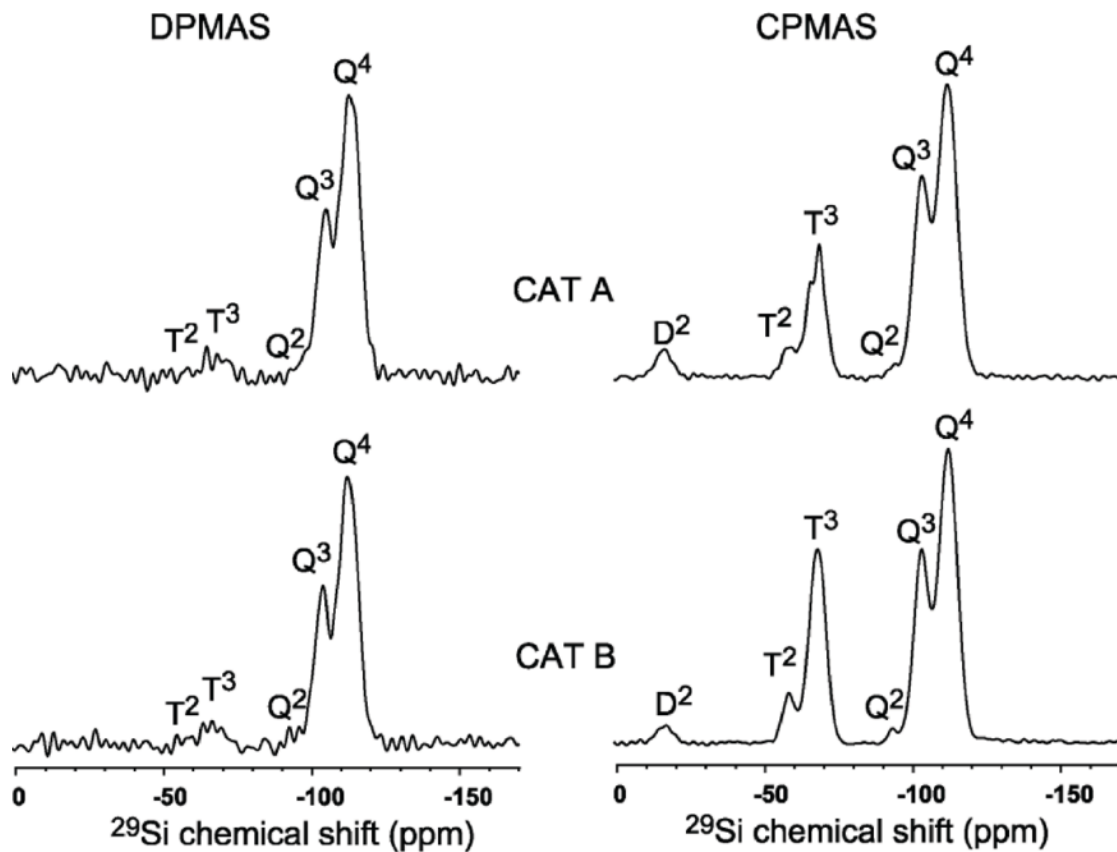


Figure 3-3 ^{29}Si DPMAS and CPMAS spectra of Cat A and Cat B.

turned out to be such that the spectra taken with $\tau_{\text{CP}} = 15$ ms yielded almost identical efficiency for *D* and *T* functionalities (Figure 3-4). By using the *Q* : *T* ratio from the DPMAS spectra and the *T* : *D* ratio from the CPMAS spectra, we were able to evaluate the absolute concentrations of PFP and DAT in each sample. The concentrations of PFP molecules measured by ^{29}Si NMR and the BET surface areas were used to determine the surface coverage of the PFP in molecules/ nm^2 and in % (the latter by assuming that the footprint area of the PFP molecule in prone position is $\sim 0.6 \text{ nm}^2$). The final results are summarized in Table 3-1.

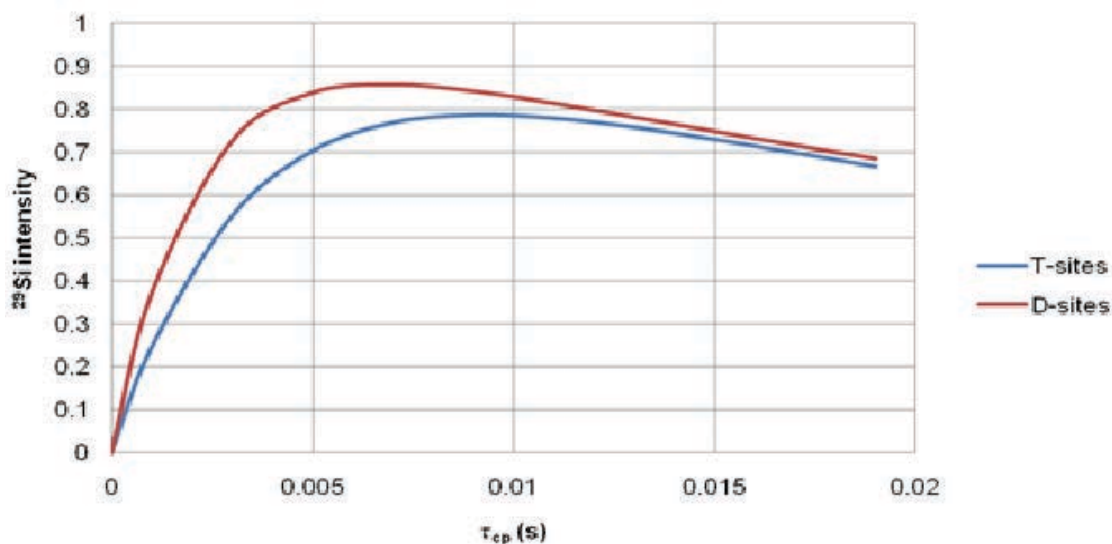


Figure 3-4 Evolution of normalized ^{29}Si CPMAS intensities for *T* sites (blue) and *D* sites (red) in bifunctionalized sample (Cat A) as a function of τ_{CP} . The curves were derived based on the measurements performed for 10 values of τ_{CP} , using the standard phenomenological formula for the behavior of spin magnetization in a diluted system (see equation (37) in reference [33]).

2.5.4 Quantification of functional groups using ^1H NMR

The quantification of DAT groups in Cat C and TMS/DAT-MSN was carried out using ^1H DPMAS spin counting under 40 kHz MAS using 1.6 mm FastMASTM probe. A standard for comparison was made of a Hexamethylbenzene (HMB):sulfur (1:30) which contained 2×10^{19} ^1H spins. The spectra of DAT have well resolved aromatic regions (6 ^1H /molecule) that were used in the quantification. To ensure full relaxation, 4 scans were used with recycle delays of 10 s. The result for Cat C can be seen in Table 3-1, and the TMS/DAT result is above in section 2.4.

2.5.5 Study of PFP conformation by ^{19}F MAS NMR

Based on our earlier study, the conformations of PFP functionalities in a ‘dry’ state (i.e. in the absence of solvent inside the pores) and in the presence of heptane could be

determined by measuring 1D ^{19}F MAS spectra. The experiments were carried out under 40 kHz MAS using 1.6 mm FastMASTM probe. The spectra are shown and discussed in the main paper (Figure 3-1).

2.6 Catalytic esterification reactions

The reactions were carried out using equal amount of catalytic sites in a capped tubular reactor. For example, the reaction mixture consisting of heptanoic acid (49.8 mg, 0.383 mmol), benzyl alcohol (41.4 mg, 0.383 mmol) and catalysts (0.2 mol%) in 1 ml of heptane was heated at 60 °C for 1.5 h. The catalysts were isolated by centrifuge and washed with 10 ml of heptane. Diphenyl ether (ca. 100 mg), was added into the combined heptane solution as an internal standard. The reaction conversion and product yield were determined by gas chromatography using a HP-5 column. The oven temperature was initially set at 40 °C for 4 min, then increased to 250 °C with a ramp rate of 10 °C/min, and kept at 250 °C for 5 min. The peaks corresponding to all reagents and products were separated, and their integrated intensities were calibrated using an internal standard. For the recyclability test, the reaction mixture of 3-phenylpropanoic acid (57.5 mg, 0.383 mmol), benzyl alcohol (41.4 mg, 0.383 mmol), and 0.4 mol% of Cat B in 1 ml of heptane was stirred at 70 °C for 2.5 h. The filtered catalyst was dried under vacuum for 24 h and recharged with the same amount of starting material for each run.

3. Result and Discussion

We first synthesized a diarylamine-functionalized alkoxy silane (DAS), *N*-(4-(4-(diethoxymethylsilyl)butyl)phenyl)-2,4,6-trimethyl-aniline, as a precursor for the synthesis of

the aforementioned bifunctionalized MSN materials as shown in Scheme 3-2. The 4-(4-bromophenyl)-1-butene **1** was coupled with 2,4,6-trimethylaniline through a palladium-mediated amination to yield a diarylamine **2**, followed by a hydrosilylation reaction with methyldiethoxysilane to synthesize the desired DAS compound **3**. Two bifunctionalized MSN catalysts were prepared by introducing DAS and PFP-trimethoxysilane in molar ratios 1:1 (sample A) and 1:4 (sample B), into a NaOH-catalyzed, cetyltrimethylammonium bromide (CTAB)-templated co-condensation reaction of tetraethoxysilane, as detailed in the experimental section 2.3. Additionally, two monofunctionalized MSN catalysts with only the DAS (sample C) and the PFP (sample D) group were synthesized *via* the same method. After the removal of CTAB, these MSN samples were treated with triflic acid to yield the corresponding catalysts, labeled as Cat A, Cat B, Cat C, and Cat D, respectively. The physisorbed triflic acid on the surface was removed under vacuum at elevated temperature, as indicated by the TGA analysis. (Figure 3-5) The synthesized MSN catalysts were then characterized via various techniques. The SEM images showed that all silica particles exhibited an elliptical shape with the aspect ratio of 1.5-2.0 and average length of 350-400 nm, as shown in Figure 3-6. The mesoporous channels were arranged in 2D hexagonal array, as observed by TEM and powder X-ray diffraction (XRD). These studies indicated that the porous structure of these MSN materials remained intact after treatment with triflic acid. (Figure 3-7 and Figure 3-8) The nitrogen sorption analysis of the samples showed a type IV isotherm, which is characteristic of a cylindrical mesoporous structure. The measured BET surface areas of Cat A, B, C, and D were 792, 861, 874 and 837 m² g⁻¹, respectively. The average pore size calculated using the BJH method is 2.6 ± 0.2 nm for all materials. (See Figure 3-S1 and Table 3-S1 in supporting information)³⁴

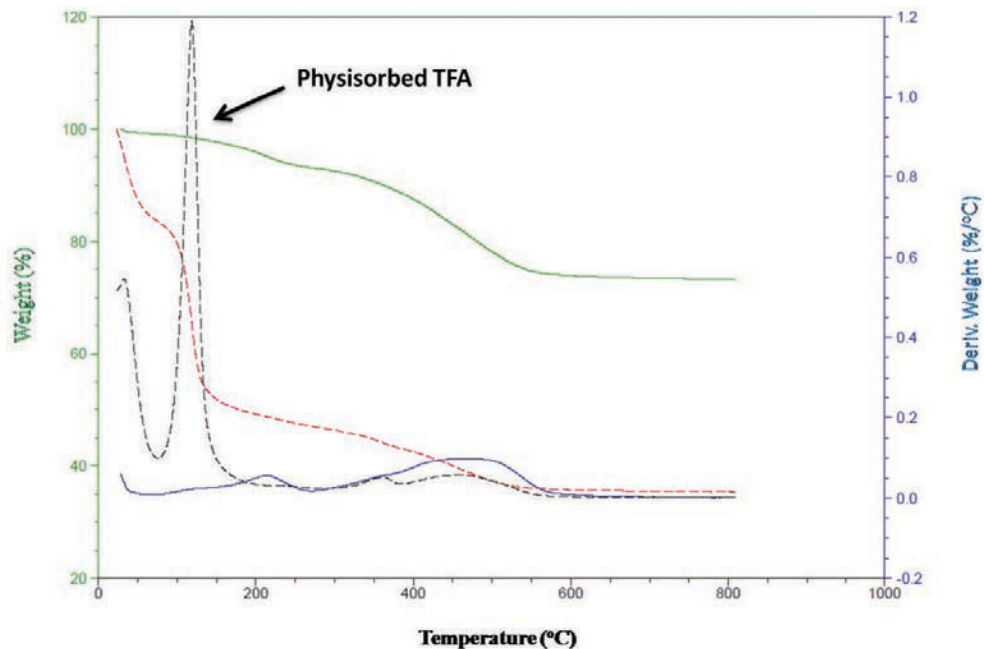


Figure 3-5 TGA weight loss vs. temperature curves for Cat A treated with TFA (red dashed line) and Cat A after the removal of physically adsorbed TFA (green solid line), along with their first derivatives (black dashed and blue solid lines, respectively). The analysis was performed in air between 25°C and 800°C with a ramp rate of 2 °C/min.

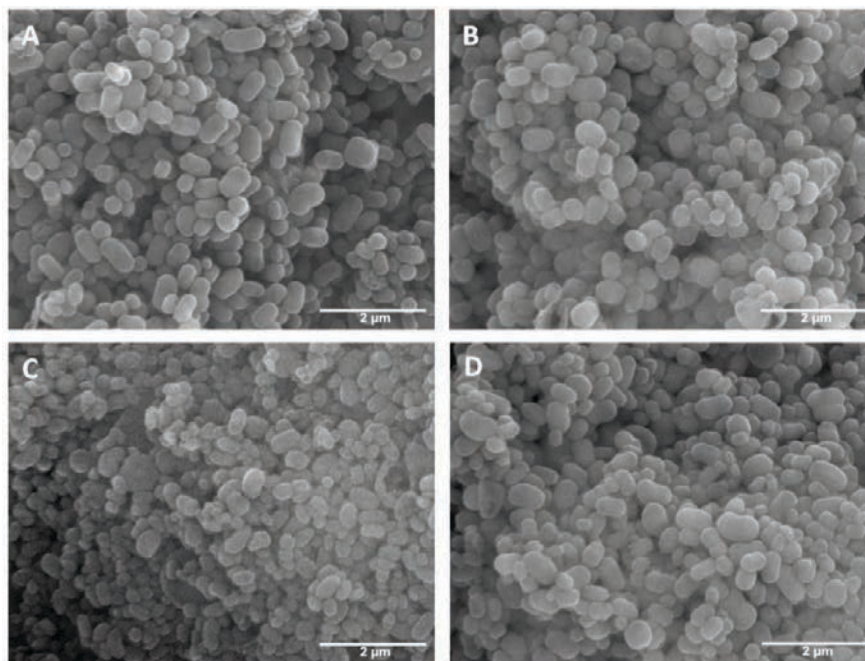


Figure 3-6 SEM images of (A) Cat A (PFP/DAT = 6/1), (B) Cat B (PFP/DAT = 15/1), (C) Cat C (DAT only), and (D) Cat D (PFP only).

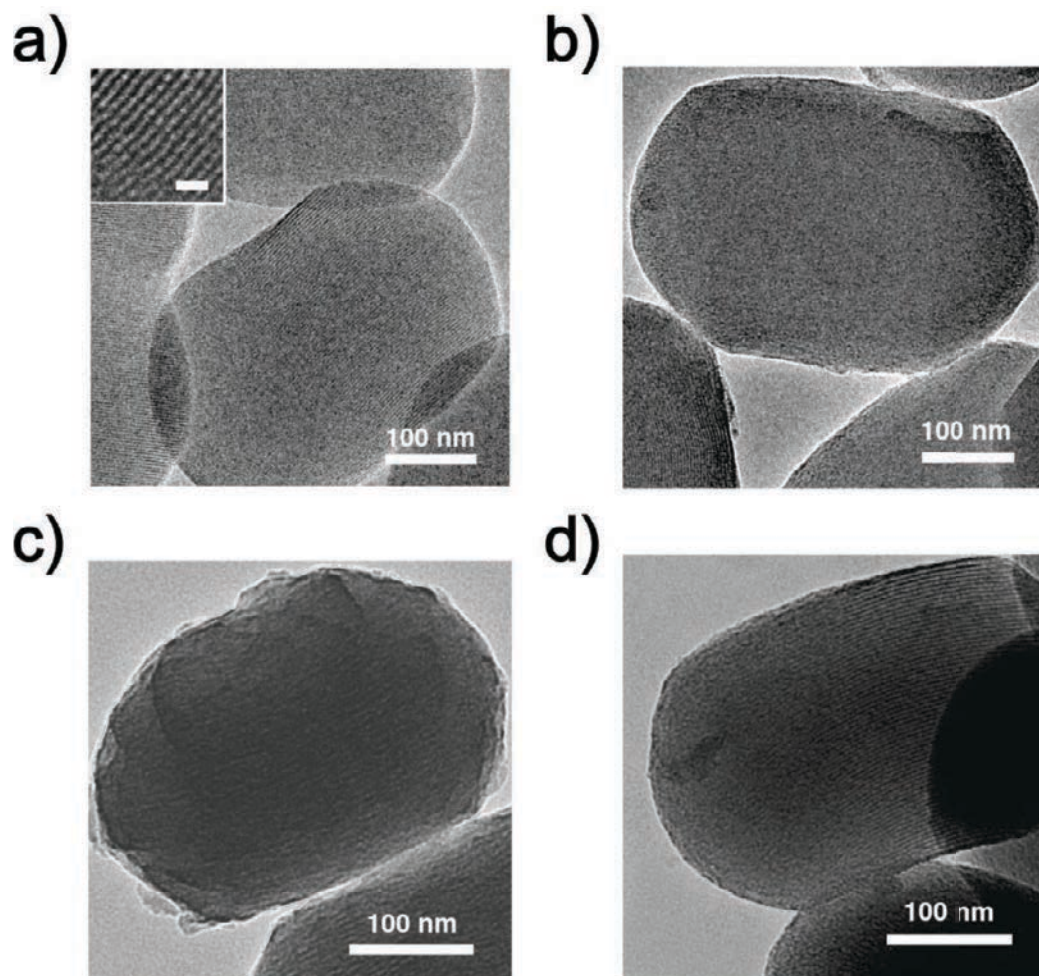


Figure 3-7 TEM images of Cat A (a), Cat B (b), Cat C (c), and Cat D (d). Scale bars are 100 nm. The inset in (a) represents parallel mesoporous channels of Cat A. Scale bar = 10 nm.

The total concentration of covalently bound surface organic functionalities was evaluated by solid-state ^{29}Si NMR, based on the relative intensities of resonances representing Q^n , T^n , and D^n sites, as detailed in the section 2.5 and summarized in Table 3-1. In addition, the concentrations of DAT groups were quantified using ^1H MAS NMR spectra, in which the resonances representing aromatic protons were clearly resolved. The ^{13}C CPMAS NMR spectra were measured to confirm the covalent immobilization of all functional groups and the integrity of their chemical structures. (Figure 3-2)

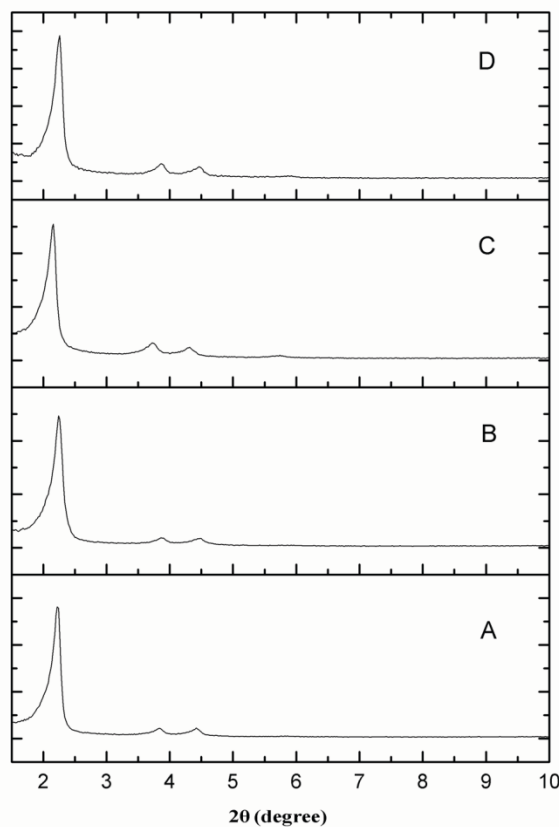


Figure 3-8 XRD patterns of (A) Cat A, (B) Cat B, (C) Cat C, and (D) Cat D.

Table 3-1. Loading and relative ratio of organic functional groups in the MSN catalysts based on quantitative solid-state ^{29}Si MAS NMR.

Sample	PFP (mmol g ⁻¹) ^[a]	DAT (mmol g ⁻¹) ^[a]	PFP:DAT ratio
Cat A	0.70 (35%) ^[b]	0.12	6:1
Cat B	0.76 (35%) ^[b]	0.05	15:1
Cat C	0	0.15	NA
Cat D	0.62 (30%) ^[b]	0	NA

[a] The loading in mmol g⁻¹ was measured with an error of $\pm 8\%$ for PFP and $\pm 15\%$ for DAT. [b] The surface coverage of PFP was calculated assuming that the inner pore surface area in MSNs constitutes 90% of the total surface, and the footprint area of the PFP compound is $\sim 0.6 \text{ nm}^2$. The DAT groups were not included.

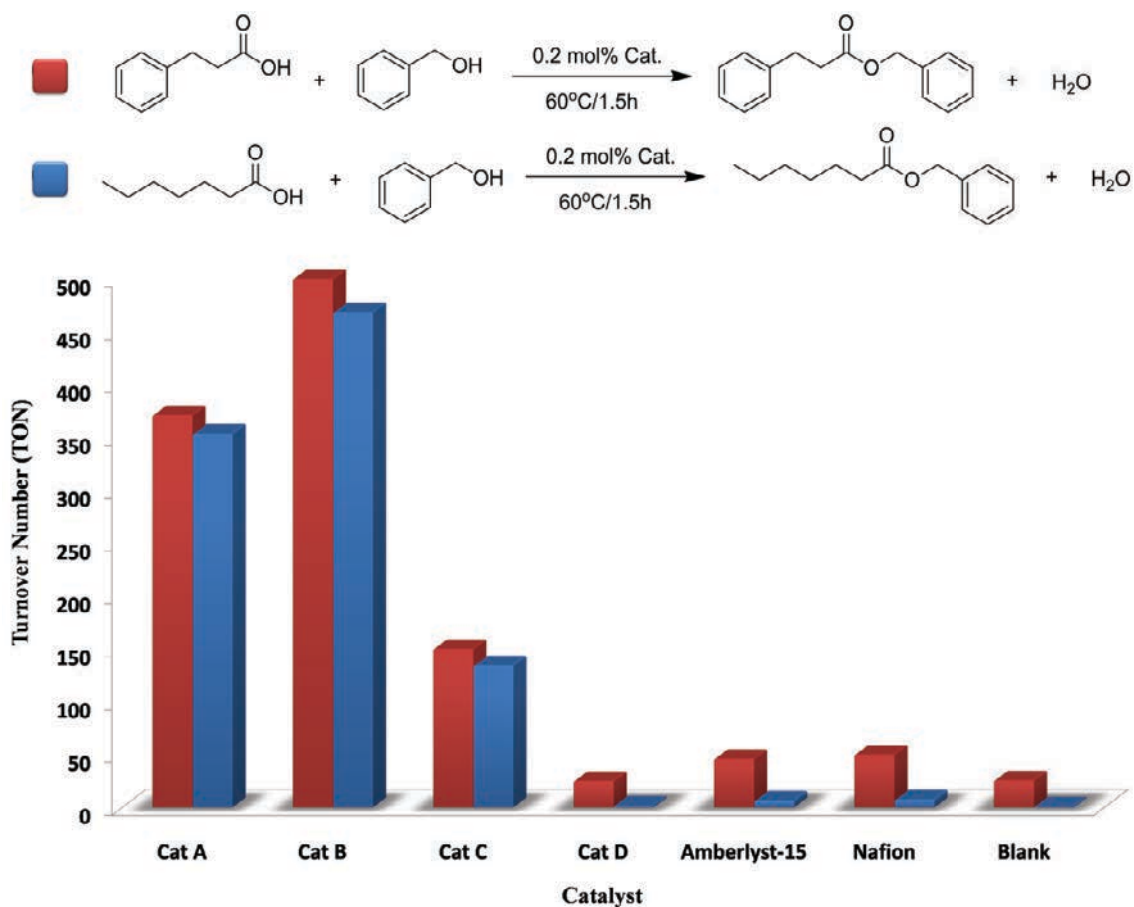


Figure 3-9 Esterification reactions of 3-phenylpropionic acid (red) and heptanoic acid (blue) with benzyl alcohol catalyzed by various heterogeneous acid catalysts.

To examine the effect of PFP groups on the catalytic performance of DAT, catalysts A-D were tested in the esterification reactions of 3-phenylpropionic acid or heptanoic acid with benzyl alcohol in heptane. As illustrated in Figure 3-9, the bifunctionalized PFP/DAT MSNs (Cat A and Cat B) exhibit the best reactivity among all catalysts. The turnover frequency (TOF, measured after 1.5 h of reaction time) of Cat B is higher than that of Cat A, which may be attributed to the higher relative concentration of PFP. The TOF of Cat C is considerably lower than those of Cat A and Cat B, which shows that the DAT groups alone are less

efficient in both esterifications. Cat D exhibits negligible activity, indicating that PFP groups do not catalyze these reactions.

To compare the effect of PFP with other commonly used hydrophobic groups, the surface of Cat C was further passivated with a TMS group to make the TMS/DAT MSN material. The esterification reaction yield of methyl 3-phenylpropionate catalyzed by TMS/DAT MSN (57%, corresponding to TOF = 190 h⁻¹) was slightly higher than that of Cat C, but proved to be lower than observed in Cat A and Cat B. We also note that the reaction of 3-phenylpropionic acid and benzyl alcohol catalyzed by homogeneous triflic acid under the same conditions only gave 18.3% of yield (TOF = 61.3 h⁻¹). Given the low reactivity and high acidity (pKa = -14) of triflic acid, this result indicates that the acid strength of the catalyst is not the only factor affecting the equilibrium of this reaction.³⁵

The enhancement of catalytic properties observed in bifunctional catalysts Cat A and Cat B is attributed to the aforementioned formation of a surface-bound layer of PFP molecules, whose prone orientation in the presence of heptane prevents direct interaction between water and the surface silanol groups. It appears that in spite of the incomplete PFP coverage (see Table 3-1), the catalyst surface became sufficiently hydrophobic to effectively reduce the concentration of water inside the mesopores and thereby drive the chemical equilibrium toward the completion of the esterification reaction. Indeed, following the reaction the amount of water byproduct observed on the walls of reaction tubes containing Cat A and Cat B was much higher than for Cat C and TMS/DAT MSN. Cat D did not produce any water due to its negligible activity.

The bifunctional PFP/DAT MSNs and DAT-MSN proved to be recyclable at least five times with identical yields, as illustrated in Figure 3-10, indicating that the reactivity difference between bi- and mono-functional catalysts is not due to the decomposition of DAT groups. We also note that the pKa values of all relevant chemical species in our

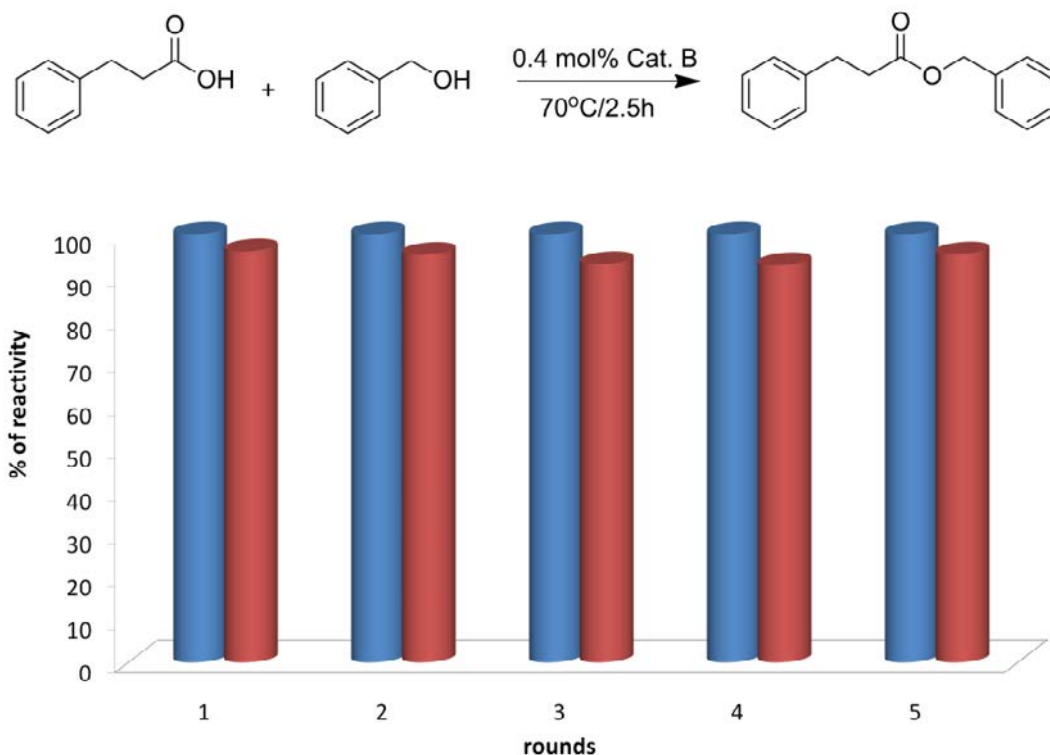


Figure 3-10 Recyclability of Cat B in five successive runs of esterification. The blue and red bars represent the reaction conversion and yield, respectively. Reaction condition: [acid] = [alcohol] = 0.38 M in heptane, 0.4 mol % Cat B, 70 °C for 2.5 h.

catalytic system do not favor the proton transfer from these groups. The pKa values of triflic acid, protonated carboxylic acid, protonated alcohol and DAT salt are -14, -6 to -7, -2 and 1, respectively.³⁶ The surface diphenylamine (DAS) group treated with triflic acid resulted in proton transfer to form the diphenylammonium (DAT) salt quantitatively. Thus, only limited amount of protons could have been transferred from DAT groups to acids and alcohols in the

catalysts studied in this work. Finally, all studied DAT-MSNs showed higher reactivity than the commercial polymeric solid acid catalysts, Amberlyst-15 and Nafion NR-50[®], under the examined reaction conditions. It is noted, however, that Amberlyst-15 and Nafion NR-50[®] use a different functionality (sulfonic acid), for which the conditions used in our tests were not optimized. Although these resin-based catalysts bear high density of acid sites,³⁷ they often require the use of swelling solvents to enhance the accessibility of reactants to these sites.³⁸

4. Conclusion

We have reported on a bifunctional MSN catalytic system with a superior reactivity in the equilibrium reaction, whose improved yield is the result of a nanoenvironment designed to efficiently remove the byproduct (water) through incorporation of the secondary functional group. This study integrated a novel synthetic approach with state-of-the-art characterization and theory,²⁰ which served as predictive tools in the design of an efficient new catalyst for the esterification reaction. We expect that similar principles can be used in designing new heterogeneous acid catalysts for other important reactions involving dehydration.

Acknowledgement

This research was inspired by Professor Victor Lin and carried out under his guidance just before his untimely death. His presence at Iowa State University and Ames Laboratory is greatly missed. It was supported by the U.S. Department of Energy, Office of Basic Energy Sciences under Contract No. DE-AC02-07CH11358 (at Ames Laboratory) and under Award

Number DE-SC0001298 (as part of the Center for Catalytic Hydrocarbon Functionalization, an Energy Frontier Research Center).

Reference

- (1) Wight, A. P.; Davis, M. E. *Chem. Rev.* **2002**, *102*, 3589.
- (2) Corma, A.; Garcia, H. *Chem. Rev.* **2003**, *103*, 4307.
- (3) Hoffmann, F.; Cornelius, M.; Morell, J.; Froba, M. *Angew. Chem. Int. Ed.* **2006**, *45*, 3216.
- (4) Melero, J. A.; Van Grieken, R.; Morales, G. *Chem. Rev.* **2006**, *106*, 3790.
- (5) Margelefsky, E. L.; Zeidan, R. K.; Davis, M. E. *Chem. Soc. Rev.* **2008**, *37*, 1118.
- (6) Thomas, J. M.; Raja, R. *Acc. Chem. Res.* **2008**, *41*, 708.
- (7) Raja, R.; Thomas, J. M.; Jones, M. D.; Johnson, B. F. G.; Vaughan, D. E. W. *J. Am. Chem. Soc.* **2003**, *125*, 14982.
- (8) McKittrick, M. W.; Jones, C. W. *J. Am. Chem. Soc.* **2004**, *126*, 3052.
- (9) Mihalcik, D. J.; Lin, W. *Angew. Chem., Int. Ed.* **2008**, *47*, 6229.
- (10) Alvaro, M.; Corma, A.; Das, D.; Fornes, V.; Garcia, H. *Chem. Commun.* **2004**, 956.
- (11) Ngo, H. L.; Zafiropoulos, N. A.; Foglia, T. A.; Samulski, E. T.; Lin, W. *Energy Fuels* **2008**, *22*, 626.
- (12) Chen, H.-T.; Huh, S.; Wiench, J. W.; Pruski, M.; Lin, V. S. Y. *J. Am. Chem. Soc.* **2005**, *127*, 13305.
- (13) Schlossbauer, A.; Schaffert, D.; Kecht, J.; Wagner, E.; Bein, T. *J. Am. Chem. Soc.* **2008**, *130*, 12558.

- (14) Huh, S.; Chen, H.-T.; Wiench, J. W.; Pruski, M.; Lin, V. S. Y. *J. Am. Chem. Soc.* **2004**, *126*, 1010.
- (15) Huh, S.; Chen, H.-T.; Wiench, J. W.; Pruski, M.; Lin, V. S. Y. *Angew. Chem. Int. Ed.* **2005**, *44*, 1826.
- (16) Margelefsky, E. L.; Zeidan, R. K.; Dufaud, V.; Davis, M. E. *J. Am. Chem. Soc.* **2007**, *129*, 13691.
- (17) Sharma, K. K.; Asefa, T. *Angew. Chem., Int. Ed.* **2007**, *46*, 2879.
- (18) Kuschel, A.; Polarz, S. *J. Am. Chem. Soc.* **2010**, *132*, 6558.
- (19) Shylesh, S.; Wagener, A.; Seifert, A.; Ernst, S.; Thiel, W. R. *Angew. Chem. Int. Ed.* **2010**, *49*, 184.
- (20) Mao, K.; Kobayashi, T.; Wiench, J. W.; Chen, H.-T.; Tsai, C.-H.; Lin, V. S. Y.; Pruski, M. *J. Am. Chem. Soc.* **2010**, *132*, 12452.
- (21) Howard, J. A. K.; Hoy, V. J.; O'Hagan, D.; Smith, G. T. *Tetrahedron* **1996**, *52*, 12613.
- (22) Danten, Y.; Tassaing, T.; Besnard, M. *J. Phys. Chem. A* **1999**, *103*, 3530.
- (23) Wakasugi, K.; Misaki, T.; Yamada, K.; Tanabe, Y. *Tetrahedron Lett.* **2000**, *41*, 5249.
- (24) Funatomi, T.; Wakasugi, K.; Misaki, T.; Tanabe, Y. *Green Chem.* **2006**, *8*, 1022.
- (25) Sakakura, A.; Nakagawa, S.; Ishihara, K. *Nature Protocols* **2007**, *2*, 1746.
- (26) Lei, M.; Wu, D.-D.; Wei, H.-G.; Wang, Y.-G. *Synth. Commun.* **2009**, *39*, 475.
- (27) Diaz, I.; Marquez-Alvarez, C.; Mohino, F.; Perez-Pariente, J.; Sastre, E. *J. Catal.* **2000**, *193*, 295.
- (28) Mbaraka, I. K.; Shanks, B. H. *J. Catal.* **2005**, *229*, 365.

- (29) Dacquin, J.-P.; Cross, H. E.; Brown, D. R.; Dueren, T.; Williams, J. J.; Lee, A. F.; Wilson, K. *Green Chem.* **2010**, *12*, 1383.
- (30) Srivastava, R. R.; Singhaus, R. R.; Kabalka, G. W. *J. Org. Chem.* **1999**, *64*, 8495.
- (31) Anwander, R.; Nagl, I.; Widenmeyer, M.; Engelhardt, G.; Groeger, O.; Palm, C.; Roeser, T. *J. Phys. Chem. B* **2000**, *104*, 3532.
- (32) Kumar, R.; Chen, H.-T.; Escoto, J. L. V.; Lin, V. S. Y.; Pruski, M. *Chem. Mater.* **2006**, *18*, 4319.
- (33) Wiench, J. W.; Lin, V. S. Y.; Pruski, M. *Journal of Magnetic Resonance* **2008**, *193*, 233.
- (34) See supporting information for details.
- (35) Ishihara, K.; Nakagawa, S.; Sakakura, A. *J. Am. Chem. Soc.* **2005**, *127*, 4168.
- (36) Smith, M. B.; March, J. *March's Advanced Organic Chemistry*; 6th ed.; Wiley-interscience, 2007.
- (37) Kunin, R.; Meitzner, E. F.; Oline, J. A.; Fisher, S. A.; Frisch, N. W. *Ind. Eng. Chem. Prod. Res. Dev.* **1962**, *1*, 140.
- (38) Gebel, G.; Aldebert, P.; Pineri, M. *Polymer* **1993**, *34*, 333.

Supporting Information

1. Nitrogen sorption isotherm results

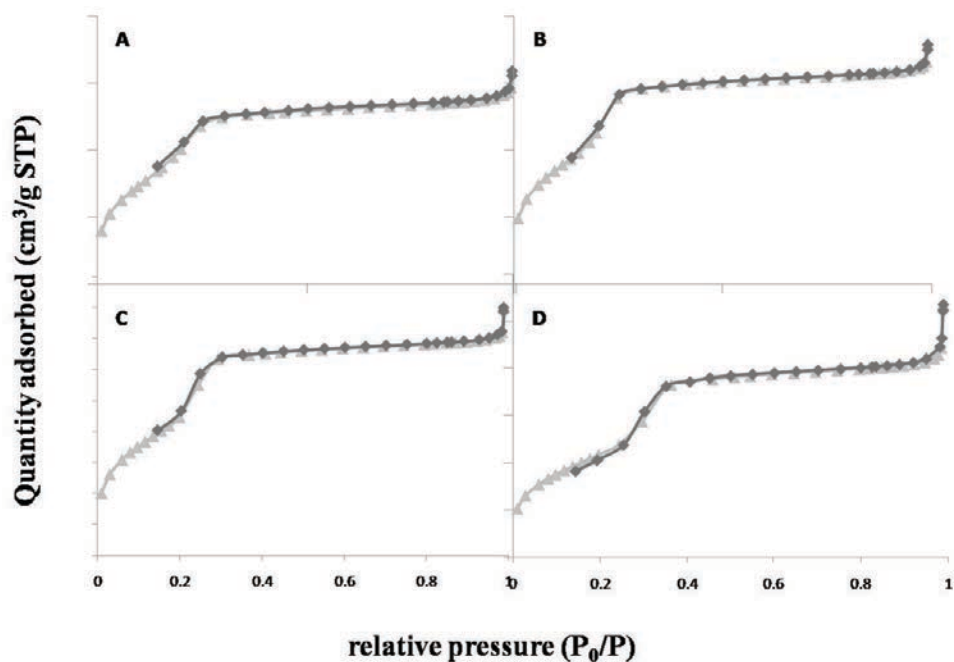


Figure 3-S1 Nitrogen adsorption isotherms of (A) Cat A, (B) Cat B, (C) Cat C, and (D) Cat D.

Table S1. Textural properties of MSN catalysts prepared in this study.

Sample	Surface area ($\text{m}^2 \text{g}^{-1}$) ^a	Average pore diameter (nm) ^b
Cat A	792.1	2.6
Cat B	861.3	2.4
Cat C	874.4	2.8
Cat D	837.4	2.4

^a. The specific surface area is calculated using the BET method. ^b.

The average pore diameter is measured by the BJH method.

CHAPTER 4. AEROBIC OXIDATIVE ESTERIFICATION OF PRIMARY ALCOHOLS OVER Pd-Au BIMETALLIC CATALYSTS SUPPORTED ON MESOPOROUS SILICA NANOPARTICLES

A manuscript in preparation and to be submitted to *ACS Catalysis*

Chih-Hsiang Tsai, Wei Huang, Hung-Ting Chen and Brian Trewyn

Abstract

We have prepared a series of mesoporous silica nanoparticle (MSN) supported Pd-Au bimetallic catalysts using a newly developed sequential impregnation method. These catalysts were fully characterized by various techniques including nitrogen sorption, powder X-ray, inductively coupled plasma mass spectrometry (ICP-MS), transmission electron microscopy (TEM) and the high angle annular dark-field scanning transmission electron microscopy (HAADF-STEM). By using this synthetic approach we observed metal nanoparticles (1-2 nm) homogeneously distributed within the mesopores of MSN. The catalytic performance of these MSN supported metal NPs was tested by aerobic oxidative esterification. In a tandem reaction primary alcohols are oxidized to their corresponding aldehydes and further to esters. We found that Pd NPs are very efficient in the first step of oxidation; however stagnant in the subsequent oxidation. On the contrary, Au NPs show slow reactivity in converting alcohols to aldehydes, but extraordinarily efficient in the oxidation of aldehydes to esters. All bimetallic catalysts exhibit better reactivity toward a variety of primary alcohols than the corresponding monometallic catalysts. In addition, we also found

that the bimetallic Pd-Au@MSN catalysts can be recycled three times without a significant loss in activity.

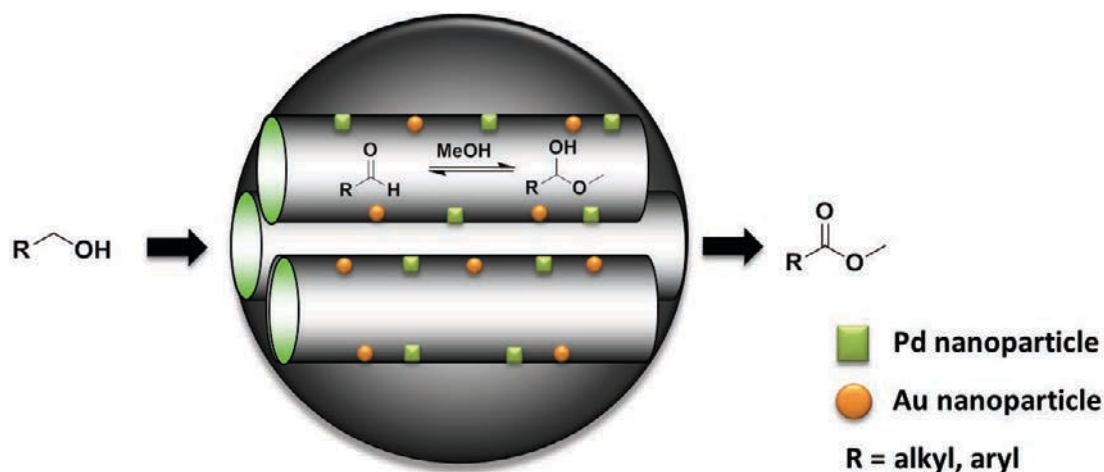
1. Introduction

Selective oxidation of alcohols to the corresponding carbonyl compounds is a primary topic of interest in organic synthesis.¹⁻⁶ The resulting aldehyde, ketone, ester and acid products are valuable intermediates to fine chemical, pharmaceutical and agrochemical industries.^{5,7,8} Typically this type of reaction is carried out in high yield using stoichiometric amounts of strong reagents such as transition metal oxidants or halo-oxoacids.⁹ However, with emerging environmental and economic concerns increased effort has been focused on the development of new types of catalysts to enhance catalytic reactivity and reduce chemical waste. Using molecular oxygen as an oxidant, aerobic oxidation of alcohols catalyzed by transition-metal catalysts including organometallic complexes and metal nanoparticles has recently attracted the attention of researchers worldwide.¹⁰⁻¹³ Among these catalysts, supported metal-nanoparticle catalysts show very interesting features and promising catalytic activities.^{1,10,14-16} Not only can these heterogeneous catalysts be easily separated and recyclable several times, but they also exhibit extremely high reactivity and selectivity even under mild reaction conditions. For example, Clark and coworkers have reported the synthesis of palladium nanoparticles supported on SBA-15 type materials that demonstrate very efficient and selective aerobic oxidation of various alcohols.^{14,17} A quantitative yield can be reached even with a relatively-inert alkyl substrate under ambient conditions. In addition, Hutchings *et al.* developed a TiO₂ supported Au-Pd catalyst which shows extremely high

catalytic activity in aerobic oxidation of alcohols to aldehydes.³ Very recently, they demonstrated that this bimetallic catalyst can also efficiently oxidize toluene under 10 bar of oxygen to yield benzyl benzoate.¹⁸

Functionalized mesoporous silica materials represent ideal inorganic supports for immobilizing catalysts due to their high surface area ($>700 \text{ m}^2 \text{ g}^{-1}$), defined pore structure, tunable pore diameter (2-10 nm) and narrow pore size distribution. It has been reported that the confined mesochannels can effectively control the agglomeration of metal nanoparticles.^{15,19-21} Furthermore, the surface-bound ligands/functionalities can be used to stabilize the metal NPs, whose high surface energy frequently leads to the aggregation of nanoparticles.^{17,22-27} Several studies involved in supporting metal nanoparticles on the mesoporous silica materials, such as Pd, Pt, Au, Rh, Ir and Ru on MCM/SBA-type materials, have revealed superior catalytic performances on many types of chemical transformations.^{15,16,28-32} The synergistic effect has also been observed in some bimetallic systems.^{1,17,33} For example, Chen and coworkers recently reported a Pd/Au bimetallic catalyst system exhibiting enhanced reactivity and selectivity toward the solvent-free aerobic oxidation of alcohols, where the Pd and Au complexes were coordinated onto the amine-functionalized SBA-16 silica support prior to their reduction to nanoparticles.²⁷

Herein, we report the synthesis of a series of mono- and bimetallic Pd/Au catalysts supported on mesoporous silica nanoparticles (MSNs) through a sequential impregnation method. This synthetic approach has shown to be effective in producing homogeneously distributed metal NPs inside the MSN support. We compared the catalytic performance of our MSN catalysts with several commercially available Au and Pd catalysts, such as



Scheme 4-1 Schematic representation of Pd-Au bimetallic MSN catalyzed aerobic oxidative esterification of alcohols in methanol.

Au@TiO₂, Au@Al₂O₃ and Pd/C, in the aerobic oxidative esterification of benzyl alcohol in methanol. Interestingly, monometallic Pd@MSN catalyst exhibited high reaction conversion but poor selectivity, leading to benzaldehyde as the major product. On the contrary, catalysts containing Au showed superior selectivity to ester product but suffered from sluggish reactivity. Compared to their monometallic counterparts, the bimetallic Pd-Au@MSN catalyst was more efficient in both reactivity and selectivity. An in depth study of different substrates was also performed with the most efficient Pd-Au bimetallic MSN catalyst. We also tested the recyclability of the bimetallic Pd-Au@MSN catalyst with the aerobic oxidation of benzyl alcohol and did not observe a decrease in activity in until after three repeated cycles. However, the result showed that the reactivity started declining after three cycles. TEM images suggested that the deactivation of catalyst may be attributed to the agglomeration of metal nanoparticles, as well as the deformation of MSN support.

2. Materials and Methods

2.1 Reagents and materials

All chemicals were used as received without further purification. Tetraethoxysilane (TEOS) was purchased from Gelest, Inc. Au/TiO₂ (1 wt% Au) and Au/Al₂O₃ (1wt% Au) were purchased from Strem Chemicals, Inc. Other chemical reagents were purchased from Sigma-Aldrich, Inc.

2.2 Synthesis of mesoporous silica nanoparticle (MSN)

The MSN material was synthesized via our previously reported co-condensation method.^{34,35} Typically, a mixture of cetyltrimethylammonium bromide (CTAB, 2.0 g, 5.5 mmol) and 2.0 M of NaOH_(aq) (7.0 ml, 14 mmol) in 480 ml of de-ionized water was heated at 80 °C for 30 min. To this solution, tetraethoxysilane (TEOS, 10.0 ml, 44.8 mmol) was injected rapidly. A milky solution was formed within 2 min after the injection. The resulting reaction mixtures were stirred at 80 °C for 2 h. The solid product was then filtered, washed by copious amount of de-ionized water and methanol and dried overnight under high vacuum. A hydrothermal treatment of the as-made MSN material was performed by soaking MSN material (3.0 g) in 20 ml of DI water. The reaction mixture was incubated in 100 °C convection oven for 6 h. The solid product was filtered and dried under high vacuum for 24 h. To remove the surfactant molecules, a solution of MSN materials (2.0 g) and 2.0 ml of concentrated HCl in 200 ml of methanol was stirred at 60 °C for 6 h. The resulting surfactant-free MSNs were filtered, washed with water and methanol, and dried under vacuum for 24 h.

2.3 Synthesis of $Au(en)_2Cl_3$

The synthetic procedure of this Au complex precursor has been reported in the literature.²⁵ Typically, ethylenediamine (0.45 ml, 6.7 mmol) was slowly added into 10 ml of aqueous solution of $HAuCl_4 \cdot 3H_2O$ (1.0 g, 2.54 mmol) until the solution turned transparent. This solution was stirred for 30 min at room temperature. Anhydrous ethanol (70 ml) was then added into the solution and a precipitate formed immediately. The solid product was filtered, followed by washing with ethanol and drying overnight under high vacuum.

2.4 Synthesis of monometallic $Pd@MSN$

A 50 ml round-bottom flask charged with 500 mg surfactant-free MSNs was pre-dried under vacuum at 90 °C for 6 h to remove physisorbed water molecules. To this reaction flask a solution of $Pd(OAc)_2$ (28 mg, 0.125 mmol) in 15 ml dry toluene was injected. The reaction was then stirred at 35 °C for 3 h, followed by filtration and washing with 300 ml of toluene and 100 ml of methanol, and dried under vacuum for 24 h to obtain a brownish solid product denoted as Pd-Complex-MSNs. The Pd-Complex-MSNs were then reduced by flowing H_2 at a rate of 30 ml min^{-1} at 250 °C for 3 h to yield the grayish final product.

2.5 Synthesis of monometallic $Au@MSN$

Typically, $Au(en)_2Cl_3$ (36 mg, 0.085 mmol) was dissolved in 60 ml of DI water. The pH value of this solution was adjusted by adding 1.0 M NaOH solution to reach a pH of 10.0. Subsequently, 1.0 g of surfactant-free MSNs were added. The pH value of this solution dropped to around 6 immediately due to the intrinsic acidity of silica material. By adding 1.0 M NaOH solution, the final pH value of the reaction mixture was tuned to 9.5. The mixture was stirred for an additional 2 h at room temperature, followed by filtration and washing with 300 ml of water and 100 ml of methanol, and dried under vacuum for 24 h to obtain a

yellowish solid product denoted as Au-Complex-MSN. The reduction of the Au-Complex-MSNs was carried out by the previously described method to yield a purplish final product.

2.6 Synthesis of bimetallic Pd-Au@MSNs

A sequential impregnation method was applied to synthesize the bimetallic MSNs. Typically, the pre-synthesized Au-Complex-MSN (500 mg) was dried at 90 °C for 6 h to remove the physisorbed water molecules. A solution of Pd(OAc)₂ (17.7 mg, 0.079 mmol) in dry toluene (25 ml) was then added. The mixed solution was stirred at 35 °C for 3 h, followed by filtration and washing with copious amount of toluene and methanol, and dried under vacuum for 24 h. The reduction procedure was the same as previously described. By tuning the introducing molar ratio of Pd and Au, three bimetallic Pd-Au@MSNs-x (where x indicates Pd/Au molar ratio) catalysts were synthesized.

2.7 Aerobic oxidative esterification of Benzyl alcohol for comparison of catalysts

A mixture of benzyl alcohol (108 mg, 1 mmol), K₂CO₃ (138 mg, 1 mmol), and catalysts (0.005 mmol, 0.5 mol% metal) in dry methanol (2 ml) was prepared in a reaction tube at room temperature. The reactor was then purged and filled with pure oxygen (balloon filled). The resulting mixture was then stirred at 60 °C under an oxygen atmosphere (balloon) for 1 h. After completion of the reaction, the solid catalyst was filtered off and washed with methanol (2 ml x 3). The filtrate was combined and analyzed by GC (Hewlett-Packard 5890 GC equipped with HP-5 column) using anisole as the internal standard.

2.8 Aerobic oxidative esterification of alcohols catalyzed by Pd-Au@MSN-1.8

The reaction procedure is the same as previously described but with varied reaction time. The result was analyzed by GC (Hewlett-Packard 5890 GC equipped with HP-5 column), GC-MS (model).

2.9 Test of recyclability of Pd-Au@MSN-1.8

A mixture of benzyl alcohol (324 mg, 3 mmol), K_2CO_3 (414 mg, 3 mmol), and Pd-Au@MSN-1.8 catalyst (66 mg, 0.5 mol% metal) in dry methanol (6 ml) was prepared in a reaction flask at room temperature. The reaction mixture was then purged and filled with pure oxygen (balloon filled). The resulting mixture was then stirred at 60 °C under an oxygen atmosphere (balloon) for 1 h. After completion of reaction, the solid catalyst was filtered off and washed with methanol (2 ml x 3). The filtrate was combined and analyzed by GC using anisole as the internal standard. The catalyst was then recovered by washing with water (10 ml x 3) and methanol (10 ml x 3), and drying under vacuum for 24 h. The recovered catalyst was then used for the next run.

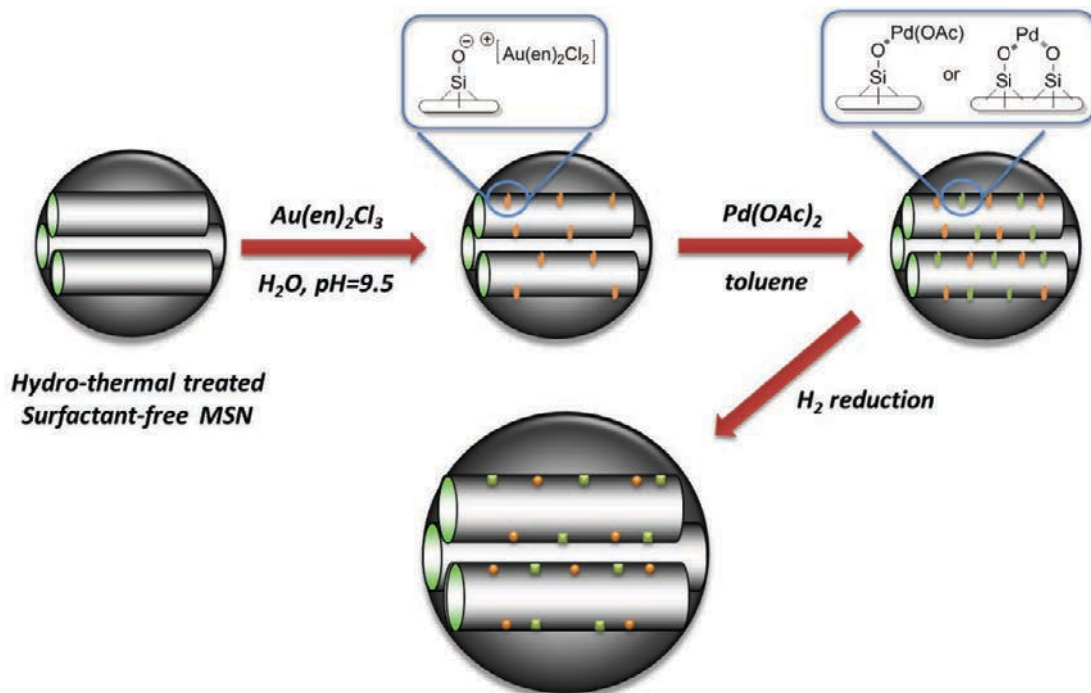
2.10 Characterization methods

Surface analysis of these MSN catalysts was performed by nitrogen sorption isotherms at 77 K with a Micromeritics ASAP 2020 surface area and porosity analyzer. The surface area and median pore diameter were evaluated by BET and BJH methods, respectively. The powder diffraction patterns of these catalysts were measured by Rigaku Ultima IV X-Ray Diffractometer using a $Cu K\alpha$ radiation source. Low angle diffraction with a 2θ range of 1.5 to 10 degrees was used to investigate the long range order of the materials. High angle diffraction with a 2θ range from 10 to 90 degrees was used to determine the degree of crystallinity of metals inside the mesopores of MSN catalysts. Tecnai G² F20 transmission electron microscopy (TEM) operated at 200 kV was used to examine the mesostructure of materials. The metal content of these MSN catalysts was quantified by Hewlett-Packard 4500 ICP-MS.

3. Results and Discussion

3.1 Material synthesis

As illustrated in Scheme 4-2, the Pd-Au bimetallic MSN catalysts (Pd-Au@MSNs) were synthesized via a sequential impregnation method. Gold was introduced into the MSN support in an aqueous solution through a deposition-precipitation method developed by Dai et al.,²⁵ where $\text{Au}(\text{en})_2\text{Cl}_3$ was used as the precursor. By fine tuning the pH value, positively charged Au complexes can be well-distributed over the negatively charged silica surface due to their strong electrostatic interaction. Subsequently, $\text{Pd}(\text{OAc})_2$ was impregnated into the gold-containing MSN (Au-Complex-MSN) in toluene, followed by moderate hydrogen reduction to form metal nanoparticles inside the MSN support. With this method, metal precursors can be efficiently loaded onto the MSN surface without the assistance of chelating ligands, such as amine groups, resulting in a homogeneous distribution of metal nanoparticles. Several studies have disclosed that using strong ligands to bind the metal complexes could efficiently control the distribution and the size of metal nanoparticles.^{17,22-27} However, it has also been reported that the ligand-assisted strategy would sometimes lead to inferior catalytic performance due to strong interactions between chelating ligands and the metal surface.²² In addition, it is also plausible that some organic ligands would participate in the reaction resulting in complicated systems, e.g. amine groups may be oxidized to imine or enamine under



Scheme 4-2 Schematic representation of synthesis of bimetallic Pd-Au@MSN catalyst.

metal nanoparticles catalyzed oxidation reaction.³⁶ In general, the silanol groups on the silica surface are not strong ligands for coordinating Pd metal. Thus, the efficiency of Pd impregnation on pure silica surface was usually low.³⁶⁻³⁸ However, after base-treatment the deprotonated silanol groups would become electron-rich and be able to effectively coordinate with the electron-deficient Pd metal center. As a result, we found that the molar ratio of Pd and Au elements can be easily controlled by using our synthetic method due to the fact that the determined actual loading of metals is very close to the amount of metal precursors we initially introduced. Monometallic Pd- and Au@MSN catalysts were also synthesized via the same procedure for comparison of catalytic reactivity.

3.2 Characterization of MSN catalysts

These mono- and bi-metallic MSN catalysts were fully characterized by various techniques. As shown in Figure 4-1, the high angle annular dark-field scanning transmission electron microscopy (HAADF-STEM) images clearly show that Pd and Au nanoclusters are well distributed within the mesoporous channel of all MSN catalysts. The size of metal particles was estimated around 2 nm by visual analysis of these images. In addition, there are no apparent aggregates of metals observed in any of these samples. EDX was also applied to determine the elemental composition of Pd-Au@MSN catalyst, as shown in Figure 4-S1. Both metal elements are clearly detected in the case of bimetallic Pd-Au@MSN catalysts; however, it is still difficult to confirm if a Pd-Au alloy, core shell or well-separated metal clusters were formed inside the Pd-Au@MSN

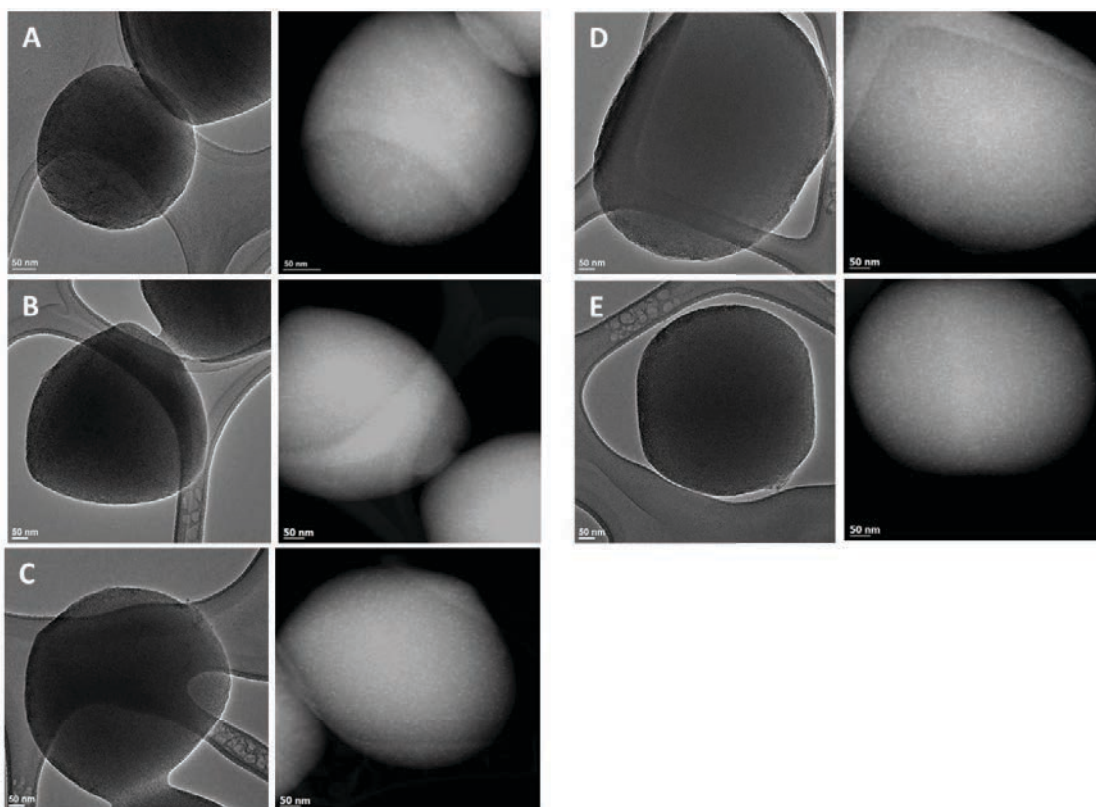


Figure 4-1 TEM images of bimetallic MSN catalysts. Bright field (left) and dark field (right). A). Pd@MSN; B). Au@MSN; C). Pd-Au@MSN-1.8; D). Pd-Au@MSN-1.0; E). Pd-Au@MSN-0.55.

catalyst due to the limits on resolution. Figure 4-2 and Figure 4-3 show the powder X-ray diffraction patterns of these MSN catalysts. As illustrated in Figure 4-2, at low angle range ($2\theta = 1.5\sim 10$ degree) three distinct peaks are observed which correspond to 2D-hexagonal patterns in all samples, indicating that the mesoporous structure of these MSN catalysts remained intact after the impregnation and reduction processes. On the other hand, at high angle range there is only one small peak at around $2\theta = 40^\circ$ which is diffracted from Au[111] and/or Pd[111] phase besides the characteristic broad peak of pure amorphous silica at around $2\theta = 22^\circ$ (Figure 4-3).^{39,40} This result implies that the sizes of the metal clusters are relatively small and no large crystalline domain exists, which is in a full agreement with TEM images.

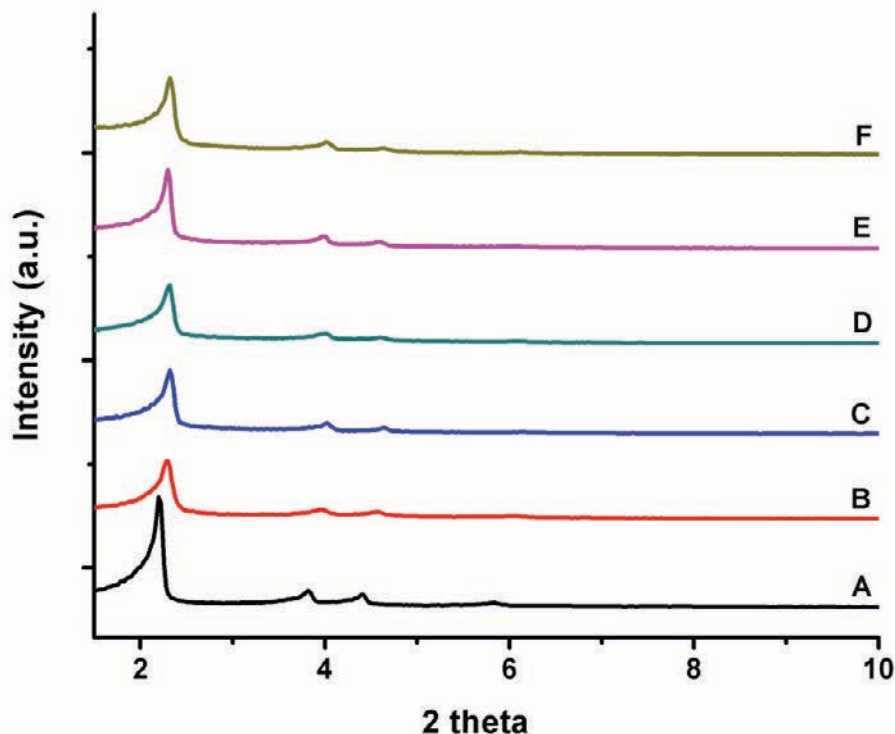


Figure 4-2 Low angle powder X-ray diffraction of MSN catalysts. A). MSN; B). Pd@MSN; C). Au@MSN; D). Pd-Au@MSN-1.8; E). Pd-Au@MSN-1; F). Pd-Au@MSN-0.55

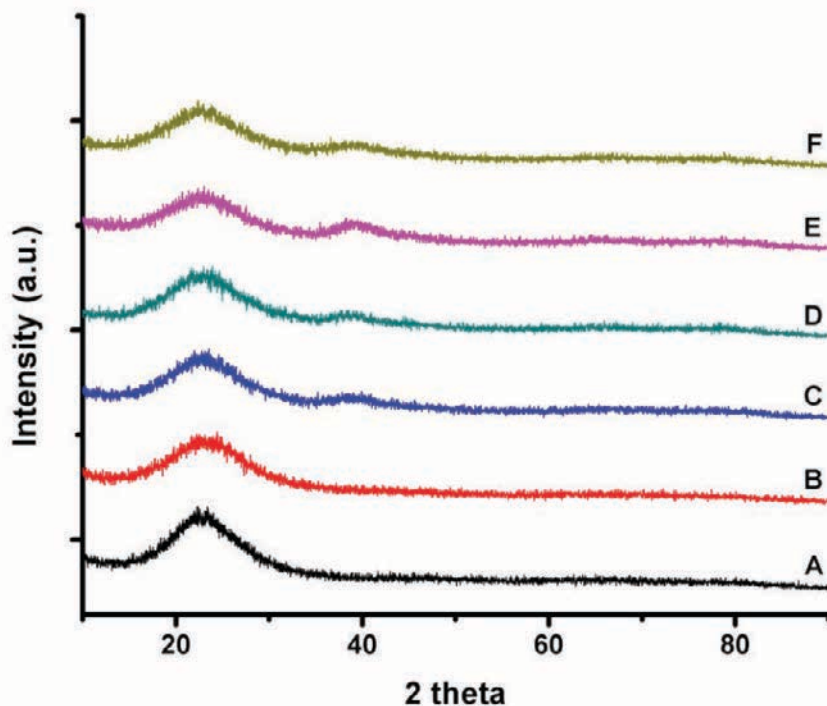


Figure 4-3 High angle powder X-ray diffraction of MSN catalysts. A). MSN; B). Pd@MSN; C). Au@MSN; D). Pd-Au@MSN-1.8; E). Pd-Au@MSN-1; F). Pd-Au@MSN-0.55

Complemented to XRD results, nitrogen sorption isotherm analysis provided the bulk-average information of the mesoporous materials. As shown in Figure 4-S2, the plots obtained are typical type IV isotherms without hysteresis loops for all MSN catalysts. In addition, as summarized in Table 4-1 the synthesized catalysts exhibited an approximate BET surface area of $900 \text{ m}^2 \text{ g}^{-1}$, and a narrow size distribution at around 2.7 nm, which both are slightly reduced if when compared to the plain MSN (Table 4-1, Entry 1).

These results also suggest that the formed Pd and Au nanoparticles do not block the mesoporous channel of MSN catalysts, assuring the accessibility of the catalytic metal nanoparticles inside the mesopores. The actual loading of metal content of these MSN catalysts was determined by ICP-MS analysis and the results were summarized in Table 4-1. Surprisingly, the measured actual loading is very close to the amount introduced, indicating

this sequential impregnation method is very efficient and easy to control the molar ratio of Pd and Au.

Table 4-1 Summary of physical properties of catalysts.

Entry	Catalyst	Pd (wt%) ^a	Au (wt%) ^a	Mole ratio ^b	Surface Area (m ² /g) ^c	Pore Size (nm) ^c	Pore Volume (cm ³ /g) ^c
1	MSN	----	----	----	1038	3.1	1.01
2	Pd@MSN	1.36	NA	----	938	2.8	0.79
3	Au@MSN	NA	1.63	----	878	2.7	0.76
4	Pd-Au@MSN-1.8	1.57	1.59	1.824	865	2.7	0.77
5	Pd-Au@MSN-1	1.15	2.17	0.978	873	2.7	0.81
6	Pd-Au@MSN-0.55	0.84	2.89	0.541	883	2.7	0.80
7 ^d	Au@TiO ₂	NA	1	----	40-50	NA	----
8 ^d	Au@Al ₂ O ₃	NA	1	----	200-260	NA	----
9 ^d	Pd/C (5%)	5	NA	----	868	NA	0.54

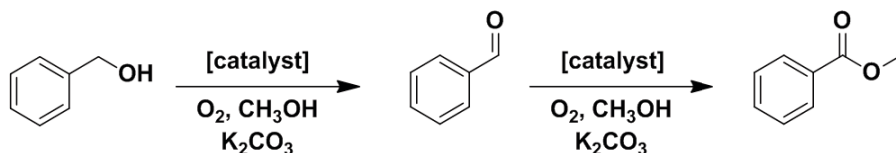
^a The metal content was determined by ICP-MS analysis. ^b Pd to Au molar ratio ^c Specific surface area (S_{BET}) and mean pore diameter (W_{BJH}) were obtained from nitrogen sorption analysis. The specific surface area was calculated by BET method and the mean pore diameter was calculated by BJH method. ^d Information acquired from manufacturers' websites.

3.3 Catalytic results

To compare catalytic performance of the mono- and bi-metallic MSN catalysts with commercially available solid supported gold and palladium catalysts, the aerobic oxidative esterification of benzyl alcohol was carried out in methanol at 60 °C with 0.5 mol% catalyst and one equivalent amount of K₂CO₃. As shown in Table 4-2, the bi-metallic Pd-Au@MSN-1.8 catalyst exhibits the highest catalytic reactivity among all catalysts tested here, which results in a full conversion of benzyl alcohol to yield the ester product quantitatively in one hour. It is interesting to note that all Pd-containing catalysts (Table 4-2, Entry 1-6) show

higher benzyl alcohol conversion than mono-metallic Au catalysts (Table 4-2, Entry 1, 7-8). However, mono-metallic Pd catalysts (Entry 1-2) suffer from poor selectivity with a yield of only 50% methyl benzoate. On the contrary, reactions catalyzed by Au-containing catalysts exhibit better selectivity to the ester product. The major byproduct is benzaldehyde which is the intermediate of this tandem oxidative reaction. These results directly suggest that Pd catalysts can effectively catalyze the oxidation of benzyl alcohol to form benzaldehyde but

Table 4-2 Comparison of catalytic performance of catalysts on aerobic oxidative esterification of benzyl alcohol.

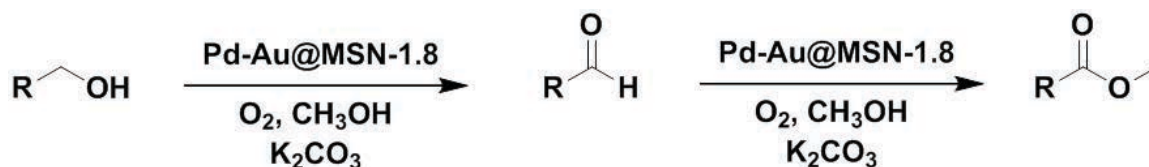


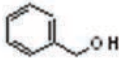
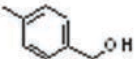
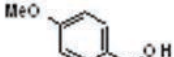



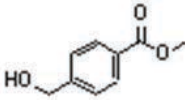

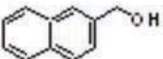
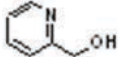
Entry	Catalyst	Conversion (%) ^b	Yield (% ester) ^c	Selectivity ^d
1	Pd/C	88	49	55.7
2	Pd@MSN	89	43	48.3
3	Au@MSN	38	37	97.3
4	Pd-Au@MSN-1.8	100	100	100
5	Pd-Au@MSN-1	85	83	97.6
6	Pd-Au@MSN-0.55	61	60	98.4
7	Au@TiO ₂	31	30	96.7
8	Au@Al ₂ O ₃	39	39	100

^a Reaction condition is detailed in experimental section. Reactivity results were determined by GC-FID using anisole as the internal standard. ^b Percent conversion of benzyl alcohol. ^c Percent yield of benzyl benzoate. ^d yield/conversion x 100%.

they are retarded in converting benzaldehyde to methyl benzoate. Compared to palladium, supported Au catalysts are very selective toward this reaction. The high selectivity of Au catalyst can be attributed to its high catalytic efficiency on the oxidative esterification of aldehyde, while the *in-situ* generated benzaldehyde would be rapidly converted to methyl benzoate.⁴¹⁻⁴³ The rate determining step (RDS) of gold catalyzed aerobic oxidation reaction of alcohol has been reported to be the dehydrogenation of the alcohol to form its corresponding aldehyde.⁴¹ Therefore, the slow RDS at the first step of the oxidation reaction limits the overall catalytic performance of mono-metallic supported Au catalysts. Comparing the catalytic performance of three bi-metallic MSN catalysts, we can clearly observe a trend that catalysts with higher Pd to Au ratio lead to higher reactivity. In addition, the bimetallic Pd-Au@MSN-1.8 catalyst appears to be more efficient than mono-metallic Pd catalysts (Entry 4-6) in terms of benzyl alcohol conversion, suggesting a synergistic effect which has been reported previously.^{1,17,33}

It is also interesting to note that Au@MSN shows comparable reactivity with Au@Al₂O₃ and Au@TiO₂ since SiO₂ has been reported to be poorer support than Al₂O₃ and TiO₂ in the case of oxidation of benzyl alcohol.⁴⁴⁻⁴⁷ This may be attributed to the large surface area of MSN, around 4 and 10 times higher than Al₂O₃ and TiO₂, respectively, providing better diffusion of substrates and accessibility to the catalyst. Based on the abovementioned results, we have demonstrated the bi-metallic Pd-Au@MSN catalytic system can significantly enhance the reactivity of the aerobic oxidative esterification of benzyl alcohol. Further interests on metal-metal interaction, metal-support interaction and metal size effect in determining the catalytic performance are still under investigation.

Table 4-3 Catalytic performance of Pd-Au@MSN-1.8 in the oxidation of various alcohols ^a.

Entry	Substrate	Conversion (%) ^b	Yield (% ester) ^c	Selectivity ^d
1		100	100	100
2		100	100	100
3		100	100	100
4 ^e		81	11	13.5
5		93	65	70
6		100	76	76
7 ^f		100	86	86
8 ^g		72	72	100
9 ^g	CH ₃ (CH ₂) ₁₁ OH	56	56	100
10 ^h		98	92	93.8
11 ^h		100	100	100

^a Reactions were carried out at 60 °C for 4 h with 0.5 mol% Pd-Au@MSN-1.8 and 0.5 M substrate concentration in methanol. Reactivity results were determined by GC-MS using anisole as an internal standard.

^b Percent conversion of benzyl alcohol. ^c Percent yield of benzyl benzoate. ^d yield/conversion x 100%. ^e Methyl benzoate is the major product. ^f Methyl 4-methylbenzoate is the major byproduct. ^g 20 h reaction time.

^h Reactivity determined by NMR with *p*-xylene as internal standard.

Several examples of aerobic oxidative esterification catalyzed by Pd-Au@MSN-1.8 are summarized in Table 4-3. Most aromatic alcohols containing both electron-donating and -withdrawing groups in the *para*-position were converted to the corresponding methyl esters in high yields (entry 1-3, 5, 7 and 10). Heteroaromatic 2-pyridyl methanol and cinnamyl alcohol were also oxidized to the corresponding methyl ester in decent yields. On the contrary, the oxidation of aliphatic alcohols needed extended reaction time to achieve moderate yields (entry 8-9). The poor reactivity of aliphatic alcohols could be due to slow oxidation of the first step of the reaction since we did not observe the formation of the intermediate aldehyde after the reaction. It is noteworthy that *p*-chlorobenzyl alcohol was not oxidized to its corresponding ester or aldehyde (entry 4). Instead, the major product was methyl benzoate (63% yield). This result implies that an oxidative insertion reaction followed by a reductive elimination occurred along with the aerobic oxidative esterification reaction of the alcohol. It has been well documented that Pd nanoparticle catalysts can efficiently catalyze Suzuki coupling reactions.⁴⁸⁻⁵⁰ However, this phenomenon is not usually seen in most of aerobic oxidation reaction conditions. Therefore, this result suggests that our Pd-Au@MSN catalyst may have potential in catalyzing oxidative coupling reactions. In most cases the major byproducts are the corresponding aldehydes. However, in the case of methyl 4-(hydroxymethyl)benzoate (Entry 7) the only byproduct we observed is methyl 4-methylbenzoate instead of its aldehyde intermediate, which may result from a dehydroxylation reaction. This observation also proves the reaction mechanism proposed by Prof. Hutching *et al.*, in which hydrides were generated *in situ* on the metal surface even under reaction condition with oxygen atmosphere.⁵¹

The fidelity of heterogeneous catalysis in the case of Pd NPs catalyzed reaction is still in debate. It has been suggested that palladium nanoparticles would serve as reservoirs which release the Pd atoms to the solution and catalyze the reaction homogeneously.⁵² In addition, catalyst leaching has always been a concern of supported metal catalysts. To rule out the contribution of homogeneous catalysis, the reaction with benzyl alcohol was conducted in the presence of Pd-Au@MSN-1.8 for 30 min to obtain a conversion of 78% and a yield of 63%. The solid catalyst was then hot-filtered and the reaction solution was transferred to another reaction tube containing K_2CO_3 . The catalyst-free solution was then stirred at 60 °C under O_2 atmosphere for additional 24 hours, but no further reaction took place. In addition, the reaction solution was subsequently analyzed by ICP-MS and no metal (Pd and Au) species were detected within the detection limit. Hence, these results suggested that the supported Pd and Au nanoparticles were indeed securely confined inside the mesopores of MSN material and would not leak to the solution during the course of the reaction.

To test the recyclability of this bimetallic MSN catalyst, an aerobic oxidative esterification with benzyl alcohol was performed in the presence of Pd-Au@MSN-1.8 catalyst. Figure 4-4 shows the recyclability of the MSN catalyst for four cycles. It is noteworthy that both conversion and selectivity started dropping during the third run and declined significantly for the next cycle. To investigate the catalyst deactivation, the MSN catalyst was examined by TEM after the third cycle. As shown in Figure 4-S3, the mesostructure of MSN is less defined and its original 2d-hexagonal mesopores has been reshaped to a wormlike structure. This deformation of MSN support would likely reduce the accessibility of catalytic sites inside the MSN, causing the decline in reactivity. Another STEM mode image, also shown in Figure 4-S3, shows that the metal nanoparticles are

mostly confined within the mesopores after three runs of reactions even though some small agglomerates are sporadically observed. This is also evident that mesoporous silica is a good solid support, preventing the supported metal clusters from agglomeration due to its confined mesoporosity.

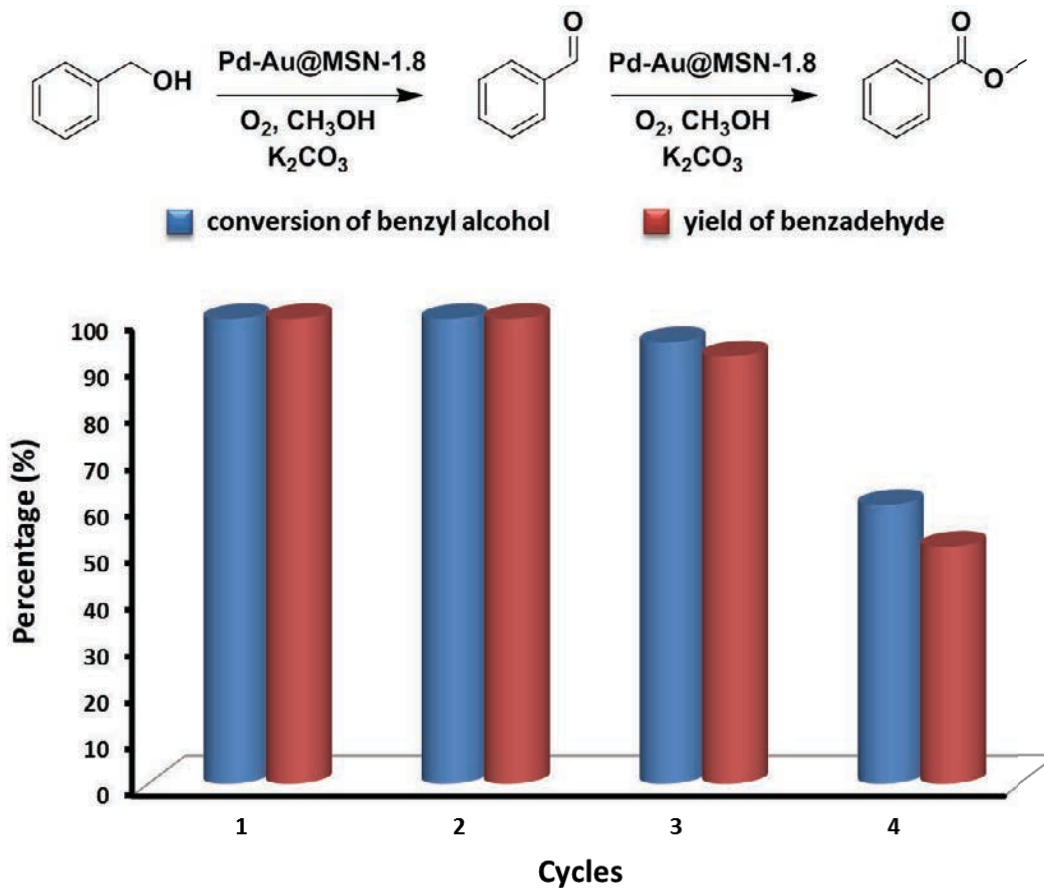


Figure 4-4 Recyclability test of Pd-Au@MSN-1.8. Reactions were carried out under 60°C for 1h with 0.5 mol% Pd-Au@MSN-1.8.

4. Conclusions

A series of MSN supported Pd-Au bimetallic NPs as catalysts for aerobic oxidative esterification has been synthesized through a sequential impregnation method. We have

shown that samples prepared by this approach exhibit homogeneously distributed metal nanoparticles within the mesopores. The Pd-Au bimetallic catalyst reveals the superior catalytic reactivity and selectivity over all of monometallic catalysts including commercial available Pd/C, Au@TiO₂ and Au@Al₂O₃. The reaction kinetics and mechanism were also discussed. In addition, a great scope of primary alcohols has been tested, and shown quantitative yields in most cases, indicating a general application of our Pd-Au@MSN catalyst. For recyclability, we have found that these MSN catalysts can be reused three times without losing activity.

Acknowledgement

This research was inspired by Professor Victor Lin and carried out under his guidance just before his untimely death. His presence at Iowa State University and Ames Laboratory is greatly missed. It was supported by the U.S. Department of Energy, Office of Basic Energy Sciences under Contract No. DE-AC02-07CH11358 (at Ames Laboratory) and under Award Number DE-SC0001298 (as part of the Center for Catalytic Hydrocarbon Functionalization, an Energy Frontier Research Center).

Reference

- (1) Abad, A.; Concepcion, P.; Corma, A.; Garcia, H. *Angewandte Chemie, International Edition* **2005**, *44*, 4066.
- (2) Edwards, J. K.; Solsona, B. E.; Landon, P.; Carley, A. F.; Herzing, A.; Kiely, C. J.; Hutchings, G. J. *Journal of Catalysis* **2005**, *236*, 69.

- (3) Enache, D. I.; Edwards, J. K.; Landon, P.; Solsona-Espriu, B.; Carley, A. F.; Herzing, A. A.; Watanabe, M.; Kiely, C. J.; Knight, D. W.; Hutchings, G. J. *Science (Washington, DC, United States)* **2006**, *311*, 362.
- (4) Sheldon, R. A.; Arends, I. W. C. E.; ten Brink, G.-J.; Dijkstra, A. *Accounts of Chemical Research* **2002**, *35*, 774.
- (5) Sheldon, R. A.; Kochi, J. K. *Metal-Catalyzed Oxidation of Organic Compounds*; Academic Press: New York, 1981.
- (6) ten Brink, G.-j.; Arends, I. W. C. E.; Sheldon, R. A. *Science (Washington, D. C.)* **2000**, *287*, 1636.
- (7) Hudlicky, M. *Oxidations in Organic Chemistry*; American Chemical Society: Washington, DC, 1990.
- (8) Pillai, U. R.; Sahle-Demessie, E. *Applied Catalysis, A: General* **2003**, *245*, 103.
- (9) Smith, M. B.; March, J. *March's Advanced Organic Chemistry*; 6th ed.; Wiley-interscience, 2007.
- (10) Mallat, T.; Baiker, A. *Chemical Reviews (Washington, DC, United States)* **2004**, *104*, 3037.
- (11) Punniyamurthy, T.; Velusamy, S.; Iqbal, J. *Chemical Reviews (Washington, DC, United States)* **2005**, *105*, 2329.
- (12) Schultz, M. J.; Sigman, M. S. *Tetrahedron* **2006**, *62*, 8227.
- (13) Miyamura, H.; Matsubara, R.; Miyazaki, Y.; Kobayashi, S. *Angewandte Chemie, International Edition* **2007**, *46*, 4151.
- (14) Karimi, B.; Zamani, A.; Abedi, S.; Clark, J. H. *Green Chemistry* **2009**, *11*, 109.

- (15) White, R. J.; Luque, R.; Budarin, V. L.; Clark, J. H.; MacQuarrie, D. J. *Chemical Society Reviews* **2009**, *38*, 481.
- (16) Corma, A.; Garcia, H. *Chemical Society Reviews* **2008**, *37*, 2096.
- (17) Karimi, B.; Abedi, S.; Clark, J. H.; Budarin, V. *Angewandte Chemie, International Edition* **2006**, *45*, 4776.
- (18) Kesavan, L.; Tiruvalam, R.; Ab Rahim, M. H.; bin Saiman, M. I.; Enache, D. I.; Jenkins, R. L.; Dimitratos, N.; Lopez-Sanchez, J. A.; Taylor, S. H.; Knight, D. W.; Kiely, C. J.; Hutchings, G. J. *Science (Washington, DC, United States)* **2011**, *331*, 195.
- (19) Sun, J.; Bao, X. *Chemistry--A European Journal* **2008**, *14*, 7478.
- (20) Lee, B.; Ma, Z.; Zhang, Z.; Park, C.; Dai, S. *Microporous and Mesoporous Materials* **2009**, *122*, 160.
- (21) Perez-Cabero, M.; El Haskouri, J.; Solsona, B.; Vazquez, I.; Dejoz, A.; Garcia, T.; Alvarez-Rodriguez, J.; Beltran, A.; Beltran, D.; Amoros, P. *Journal of Materials Chemistry* **2010**, *20*, 6780.
- (22) Chi, Y.-S.; Lin, H.-P.; Mou, C.-Y. *Applied Catalysis, A: General* **2005**, *284*, 199.
- (23) Yang, C.-m.; Liu, P.-h.; Ho, Y.-f.; Chiu, C.-y.; Chao, K.-j. *Chemistry of Materials* **2003**, *15*, 275.
- (24) Yang, C.-M.; Zibrowius, B.; Schueth, F. *Chemical Communications (Cambridge, United Kingdom)* **2003**, 1772.
- (25) Zhu, H.; Liang, C.; Yan, W.; Overbury, S. H.; Dai, S. *Journal of Physical Chemistry B* **2006**, *110*, 10842.

- (26) Yang, C.-M.; Lin, H.-A.; Zibrowius, B.; Spliethoff, B.; Schueth, F.; Liou, S.-C.; Chu, M.-W.; Chen, C.-H. *Chemistry of Materials* **2007**, *19*, 3205.
- (27) Chen, Y.; Lim, H.; Tang, Q.; Gao, Y.; Sun, T.; Yan, Q.; Yang, Y. *Applied Catalysis, A: General* **2010**, *380*, 55.
- (28) Jacquin, M.; Jones, D. J.; Roziere, J.; Albertazzi, S.; Vaccari, A.; Lenarda, M.; Storaro, L.; Ganzerla, R. *Applied Catalysis, A: General* **2003**, *251*, 131.
- (29) Whilton, N. T.; Berton, B.; Bronstein, L.; Hentze, H.-P.; Antonietti, M. *Advanced Materials (Weinheim, Germany)* **1999**, *11*, 1014.
- (30) Harada, T.; Ikeda, S.; Ng, Y. H.; Sakata, T.; Mori, H.; Torimoto, T.; Matsumura, M. *Advanced Functional Materials* **2008**, *18*, 2190.
- (31) Huang, W.; Kuhn, J. N.; Tsung, C.-K.; Zhang, Y.; Habas, S. E.; Yang, P.; Somorjai, G. A. *Nano Letters* **2008**, *8*, 2027.
- (32) Niederer, J. P. M.; Arnold, A. B. J.; Holderich, W. F.; Spliethof, B.; Tesche, B.; Reetz, M.; Bonnemann, H. *Topics in Catalysis* **2002**, *18*, 265.
- (33) Hutchings, G. J. *Chemical Communications (Cambridge, United Kingdom)* **2008**, 1148.
- (34) Huh, S.; Chen, H.-T.; Wiench, J. W.; Pruski, M.; Lin, V. S. Y. *Journal of the American Chemical Society* **2004**, *126*, 1010.
- (35) Tsai, C.-H.; Chen, H.-T.; Althaus, S. M.; Mao, K.; Kobayashi, T.; Pruski, M.; Lin, V. S. Y. *ACS Catalysis* **2011**, *1*, 729.
- (36) Zhu, B.; Lazar, M.; Trewyn, B. G.; Angelici, R. J. *Journal of Catalysis* **2008**, *260*, 1.
- (37) Beck, A.; Horvath, A.; Szucs, A.; Schay, Z.; Horvath, Z. E.; Zsoldos, Z.; Dekany, I.; Gucci, L. *Catalysis Letters* **2000**, *65*, 33.

- (38) Papp, S.; Szucs, A.; Dekany, I. *Applied Clay Science* **2001**, *19*, 155.
- (39) Gao, S.; Zhang, H.; Wang, X.; Mai, W.; Peng, C.; Ge, L. *Nanotechnology* **2005**, *16*, 1234.
- (40) Yan, W.; Petkov, V.; Mahurin, S. M.; Overbury, S. H.; Dai, S. *Catalysis Communications* **2005**, *6*, 404.
- (41) Marsden, C.; Taarning, E.; Hansen, D.; Johansen, L.; Klitgaard, S. K.; Egeblad, K.; Christensen, C. H. *Green Chemistry* **2008**, *10*, 168.
- (42) Taarning, E.; Madsen, A. T.; Marchetti, J. M.; Egeblad, K.; Christensen, C. H. *Green Chemistry* **2008**, *10*, 408.
- (43) Kaizuka, K.; Miyamura, H.; Kobayashi, S. *Journal of the American Chemical Society* **2010**, *132*, 15096.
- (44) Schubert, M. M.; Hackenberg, S.; van Veen, A. C.; Muhler, M.; Plzak, V.; Behm, R. *J. Journal of Catalysis* **2001**, *197*, 113.
- (45) Haruta, M.; Date, M. *Applied Catalysis, A: General* **2001**, *222*, 427.
- (46) Wolf, A.; Schuth, F. *Applied Catalysis, A: General* **2002**, *226*, 1.
- (47) Chen, M. S.; Goodman, D. W. *Catalysis Today* **2006**, *111*, 22.
- (48) Das, D. D.; Sayari, A. *Journal of Catalysis* **2007**, *246*, 60.
- (49) Fihri, A.; Bouhrara, M.; Nekoueshahraki, B.; Basset, J.-M.; Polshettiwar, V. *Chemical Society Reviews* **2011**, *40*, 5181.
- (50) Mondal, J.; Modak, A.; Bhaumik, A. *Journal of Molecular Catalysis A: Chemical* **2011**, *350*, 40.

- (51) Dimitratos, N.; Lopez-Sanchez, J. A.; Morgan, D.; Carley, A. F.; Tiruvalam, R.; Kiely, C. J.; Bethell, D.; Hutchings, G. J. *Physical Chemistry Chemical Physics* **2009**, *11*, 5142.
- (52) Davies, I. W.; Matty, L.; Hughes, D. L.; Reider, P. J. *Journal of the American Chemical Society* **2001**, *123*, 10139.

Supporting Information

1. EDX analysis of Pd-Au-MSN-1.8

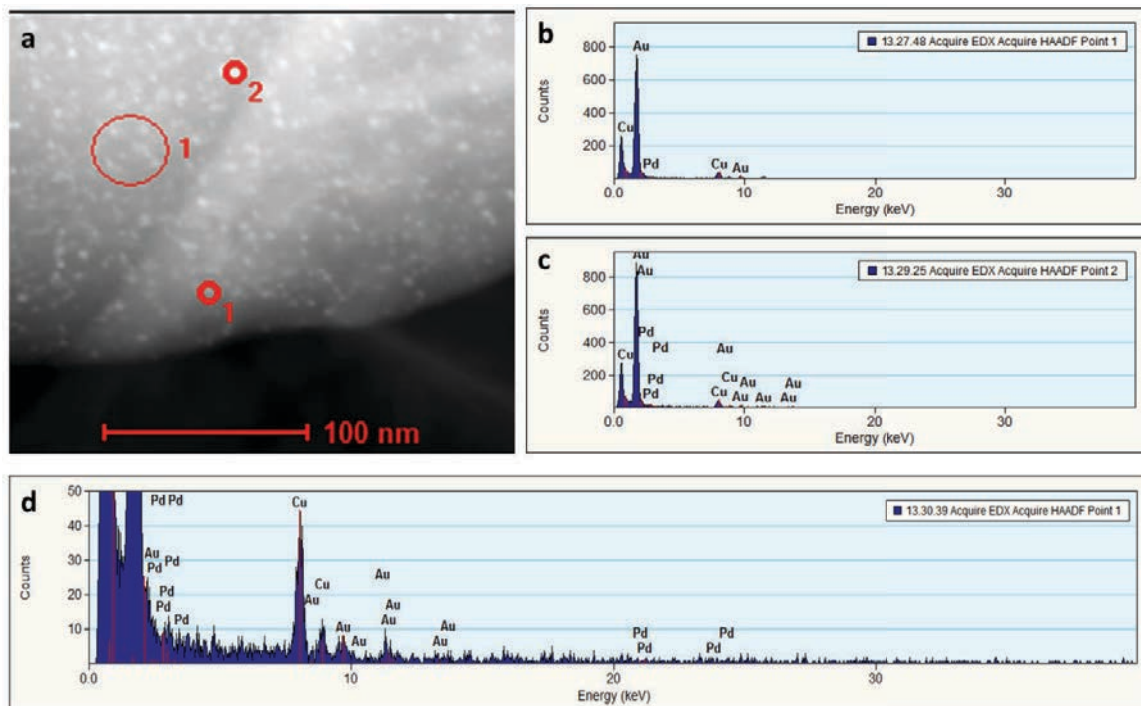


Figure 4-S1 Selective area of EDX analysis of Pd-Au@MSN-1.8. a). dark-field TEM images of Pd-Au@MSN-1.8; b). element analysis of point 1; c). element analysis of point 2; d). element analysis of area 1.

2. Nitrogen sorption analysis of MSN catalysts

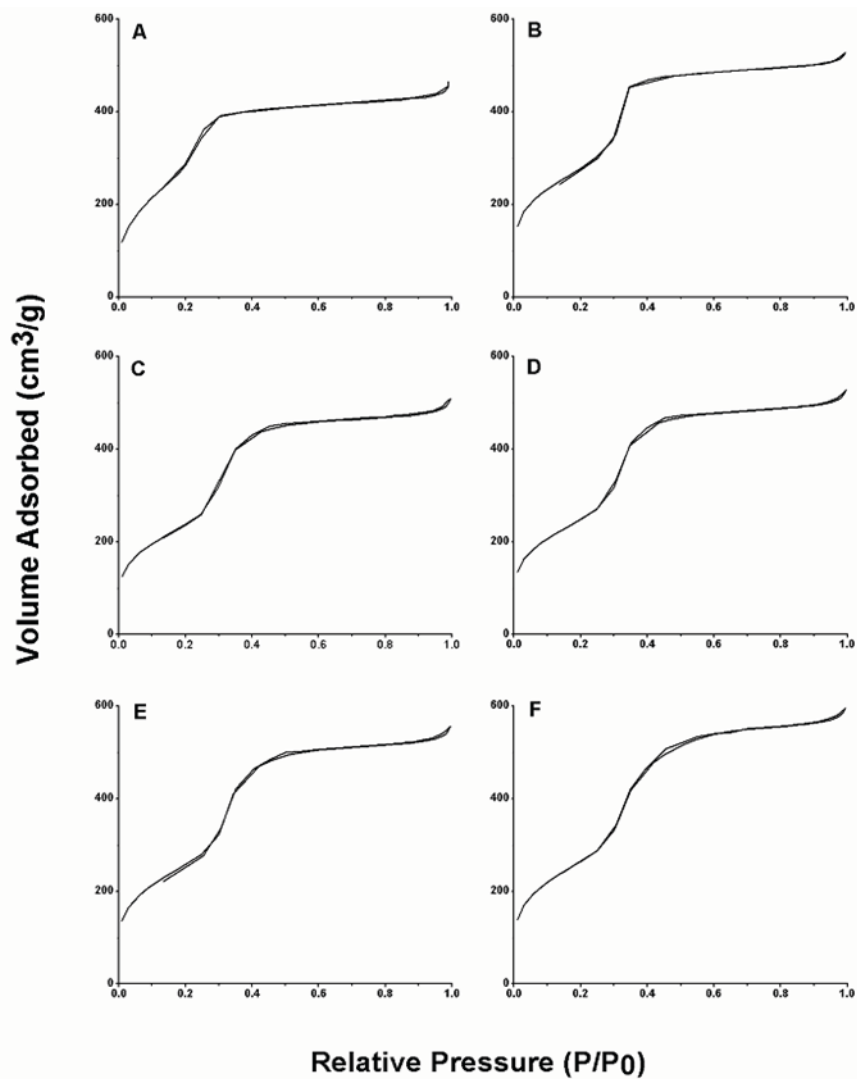


Figure 4-S2a Nitrogen sorption isotherm of MSN catalysts A). MSN; B). Pd@MSN; C). Au@MSN; D). Pd-Au@MSN-1.8; E). Pd-Au@MSN-1; F). Pd-Au@MSN-0.55

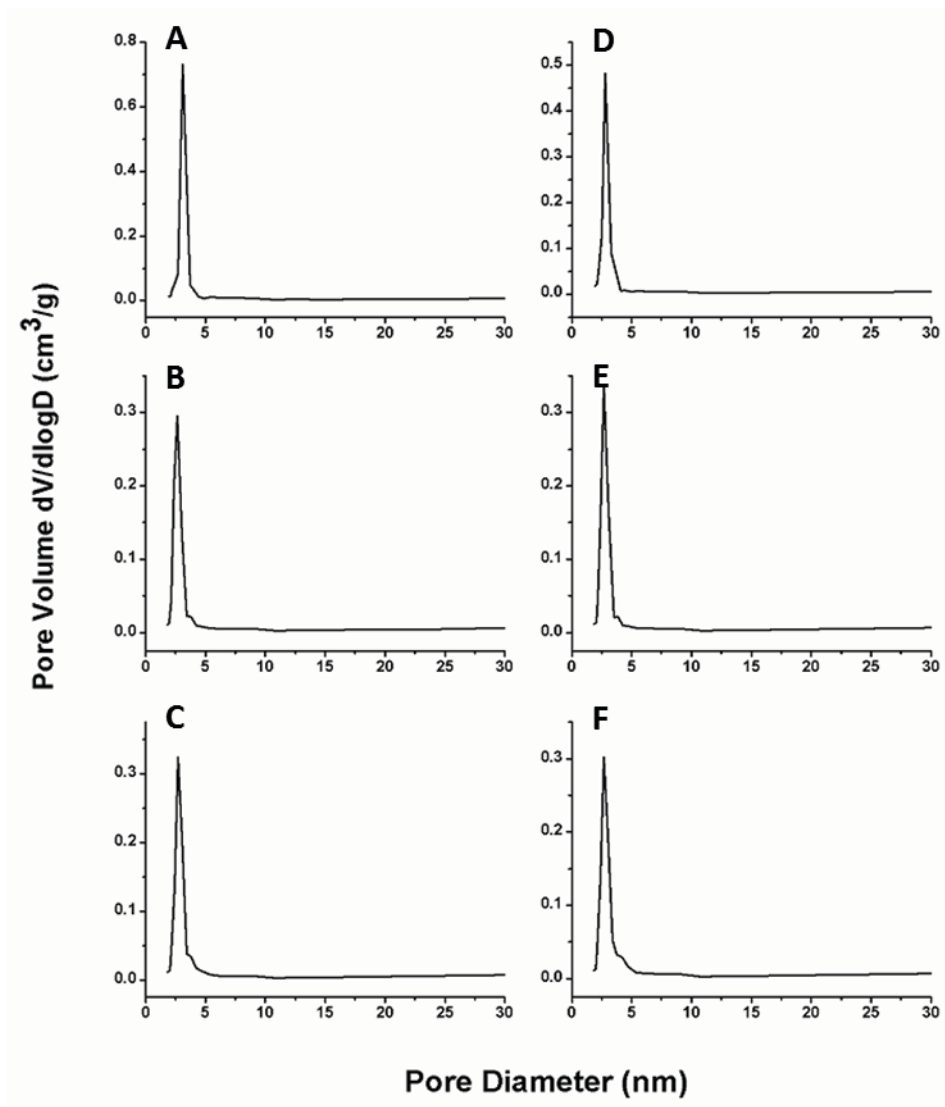


Figure 4-S2b BJH pore size distribution of MSN catalysts A). MSN; B). Pd@MSN; C). Au@MSN; D). Pd-Au@MSN-1.8; E). Pd-Au@MSN-1; F). Pd-Au@MSN-0.55

3. Investigation of deactivation of Pd-Au@MSN-1.8 after recycled three times

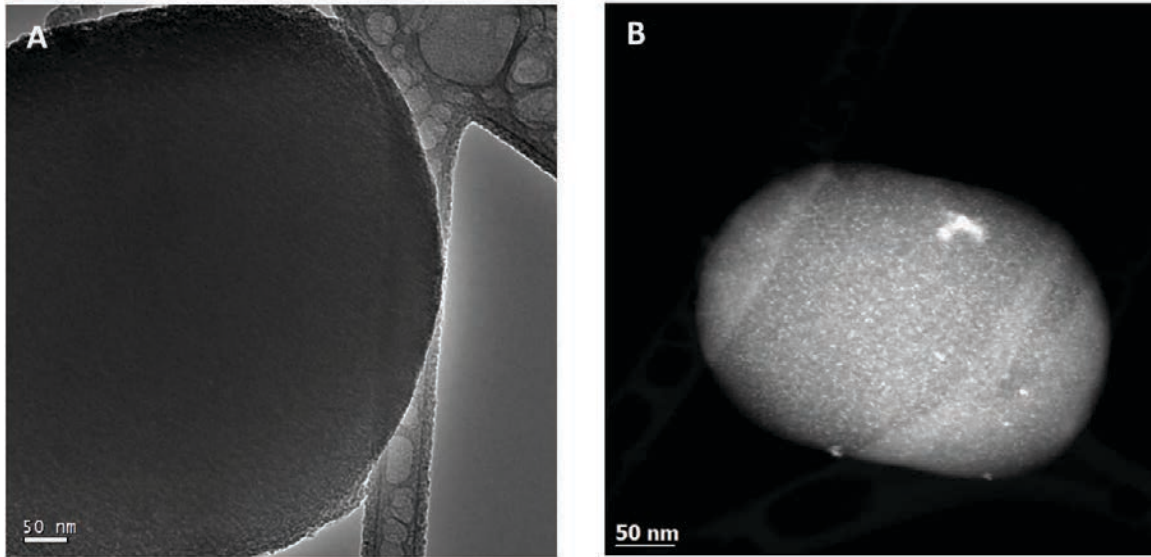


Figure 4-S3 TEM images of recycled Pd-Au@MSN-1.8 after three runs. A). Bright field image; B). Dark-field image

CHAPTER 5. GENERAL CONCLUSION

Great advance on the development of functionalized mesoporous silica nanoparticles (MSNs) has attracted much attention in recent years. According to Sci-Finder, there are more 22,000 of publications related to the concept of “mesoporous” and “silica” up to date, and the number is still rapidly growing. Indeed, these types of materials, featuring assorted patterns of mesostructure, controllable particle size and shape, tunable pore size, great biocompatibility and robust inorganic framework, are intriguing for scientists in both material science and applied chemistry. Our lab has extensively studied the application of MSNs on the fields of drug delivery and heterogeneous catalysis. This dissertation presented my primary work during my Ph.D. study in Iowa State Univ.

The early stage of my research mainly focused on the development of new strategy for hydrophobic drug delivery using MSNs as platforms. As demonstrated in Chapter 2, we first synthesized a biocompatible phosphate monoester surfactant as the structure directing agent for synthesizing mesoporous silica materials. To synthesize the “anionic surfactant-templated” MSNs, we applied a “co-structure directing method (CSDA)” using aminopropyltrimethoxysilane (APTMS) as the co-structure directing agent. By fine tuning the molar ratio of APTMS to PMES, we successfully synthesized a series PMES-MSNs with well-separated spherical shape and radially aligned mesostructure. A clear trend of phase transition has been observed along with the increase of APTMS to PMES ratio. In addition, particle sizes and shapes can also be controlled by the same factor. For the particle formation mechanism, our observation agreed with the “aggregate-growth”

mechanism proposed by Rankin *et al.* To further study the intrinsic structure of the fascinating radial mesostructure, we carried out a carbon replication using PMES-MSNs as the template. However, the resulting carbon replica did not present an expected-to-be urchin-like mesostructure under transmission electron microscopy; instead, still a radially-aligned pattern. For biological application, we loaded a hydrophobic drug, resveratrol, into the surfactant-containing PMES-MSNs using a conventional impregnation method. We found that the loading amount of surfactant-containing PMES-MSNs was almost 4 times higher than that of surfactant-free MSNs. In addition, with the assistance of PMES, a steady release of resveratrol up to 90 % of loaded drugs has been observed. These results strongly indicate that this surfactant-assistant strategy can efficiently promote the amount of loading of hydrophobic drugs and its release efficiency using MSNs as delivery vectors. We also found that these PMES-MSNs can effectively escape from endosomes after endocytosed by HeLa cells. Last but not least, we investigated stimuli-responsive release system using Ca^{2+} as stimuli. Due to strong interaction between Ca^{2+} and PMES, we observed a responsive release pattern when $[\text{Ca}^{2+}]$ was increased.

In addition to the investigation of MSNs in biological application, we also aim to develop new type of heterogeneous catalyst base on MSNs. First, we developed a series of bifunctionalized MSNs catalysts, containing different ratio of diarylammonium triflate (DAT) groups as Brønsted acid sites and pentafluorophenyl propyl (PFP) groups. According to our solid-state NMR study, PFP groups are in prone position inside the silica matrix when MSNs were wetted with solvents. This finding inspired us to design a new catalytic system, in which the PFP groups are coated on the silica surface providing

extremely hydrophobic effect to accelerate catalytic dehydration reaction. These bifunctionalized DAT/PFP-MSN catalysts were well characterized by cutting-edge techniques including ssNMR. We tested these catalysts on esterification of benzyl alcohol, and found that the reactivity is proportional to the ratio of PFP to DAT. This result confirms our assumption that the PFP groups can help expel the water (byproduct of esterification) out of the mesopores due to strong hydrophobic effect, so as to enhance the reactivity. In addition, we also found that PFP groups provided stronger effect than traditional TMS and phenyl groups. Furthermore, compared to commercially available acid catalysts amberlyst-15 and Nafion-50, our bifunctionalized MSN exhibit much efficient reactivity under our examined condition. Last, the recyclability result showed these catalysts can be reused at least five times without losing any activity.

Another common application of MSNs is metal nanoparticle supported solid catalyst. As depicted in Chapter 4, we developed a new sequential impregnation method to prepare a series of bimetallic Pd-Au@MSN catalysts. TEM images indicated that both Pd and Au nanoparticles with sizes around 1-2 nm are homogeneously distributed inside the MSNs. These catalysts were used to catalyze aerobic oxidative esterification reactions. Our results suggested that the Pd-rich bimetallic catalyst exhibits highest reactivity and selectivity among all catalysts tested. In addition, we also found that Pd nanoparticles are efficient on the first step of oxidation, in which alcohols are converted to aldehydes. On the other hand, Au is very active toward the second step of oxidation, where aldehydes are oxidized to esters. For the study of substrate scope, we found our bimetallic Pd-Au@MSNs catalyst has great tolerance to most of common functional groups. Also, most of aromatic alcohols can be quantitatively converted to desired esters.

Very recently, we developed a supported Bpy-PtPh₂ catalyst showing very interesting results in hydroarylation reactions. The heterogeneous solid catalyst not only increases reactivity but also enhance the thermal stability compared to its counter homogeneous complex. In addition, by changing the tethering groups, the product selectivity can be tuned. These preliminary results indicated that the nature of MSNs as solid supports provides great potential on the development of new type of heterogeneous catalyst.